An ASTER Digital Elevation Model (DEM) for the Darwin-Hatherton Glacial System, Antarctica.

A thesis submitted in partial fulfillment
of the requirements for the Degree
of
Master of Science in Geography
in the
University of Canterbury
by
Nita Jane Smith

University of Canterbury

2007

Abstract

The Darwin-Hatherton glacial system is an outlet glacial system in the Transantarctic Mountains, Antarctica, which drains ice from the East Antarctic Ice Sheet into the Ross Ice Shelf. This research provides remotely sensed data that can be used in modeling research for the Darwin-Hatherton glacial system, which in turn can be used in mass balance research for the West Antarctic Ice Sheet.

Two improved digital elevation models (DEM) are produced to cover the lower Darwin Glacier and to cover the upper Darwin and Hatherton Glaciers. The new improved DEMs are generated from Advanced Spaceborne Thermal Emission and Reflection Radiometer (ASTER) satellite data, with a resolution of 45 m. To produce the two final DEMs, multiple DEMs are firstly adjusted to remove systematic errors and are then stacked and averaged to increase the accuracy and produce the final two DEMs. For the lower Darwin Glacier, 5 DEMs were averaged and in the upper Darwin and Hatherton Glaciers, 6 DEMs were averaged. The accuracy is quantified by a remaining error of $\pm$ 9 m for the lower Darwin Glacier DEM and $\pm$ 37 m for the upper Darwin and Hatherton Glaciers DEM. This is a significant improvement from the existing 200 m resolution Radarsat Antarctic mapping project (RAMPv2) DEM which has a remaining error of $\pm$ 138 m over the lower Darwin Glacier and $\pm$ 152 m over the upper Darwin and Hatherton Glaciers. The accuracy is assessed by comparing the ASTER and RAMPv2 DEMs to highly accurate ice, cloud and land elevation satellite (ICESat) laser altimetry data.

A 15 m resolution, true colour, orthorectified image is provided for the entire Darwin-Hatherton glacial system from ASTER satellite imagery. The DEMs used to orthorectify the ASTER satellite imagery are the two new 45 m resolution ASTER DEMs.

Lastly feature tracking was explored as a method for measuring surface ice velocity. This research shows that feature tracking is unsuitable for the Darwin-Hatherton glacial system if using 15 m resolution satellite imagery over a 1 to 4 year time period.

Contents

List of figures

List of tables

Table

Chapter 1: Introduction, aims and rationale of thesis

1.1 Introduction

The Darwin-Hatherton glacial system (Figure 1.1) is an outlet glacial system in the Transantarctic Mountains, Antarctica which drains ice from the East Antarctic Ice Sheet into the Ross Ice Shelf. This research creates a new digital elevation model (DEM) and orthorectified satellite image for the Darwin-Hatherton glacial system and investigates whether feature tracking is suitable for measuring surface ice flow. The methodology is entirely remote sensing based using Advanced Spaceborne Thermal Emission and Reflection Radiometer (ASTER) satellite images.

It is important to understand the mass balance of the Ross Embayment ice drainage system (Figure 1.1) in order to make predictions as to how the West Antarctic Ice Sheet (WAIS) may change in the future due to climate change (Bindschadler, 1998). The WAIS grounding line has been retreating since the last glacial maximum (LGM), (Conway et al., 1999), and has blocked and dammed the Darwin-Hatherton glacial system for part of this time (Bockheim et al., 1989). Understanding the lowering of the Darwin-Hatherton glacial system after the grounding ice retreated past and unblocked the outlet, allows information to be combined with other research to investigate the retreat of the WAIS. The Darwin-Hatherton glacial system is focused on as it has rarely preserved LGM glacial drifts for outlet glaciers in the southern Transantarctic Mountains (Bockheim et al., 1989). Modeling has been undertaken to investigate the LGM profile of the Darwin-Hatherton glacial system (Anderson et al., 2004), with more accurate data being required to increase the certainty of the model. Therefore this research provides a new higher quality DEM for the Darwin-Hatherton glacial system which can be used for various glaciological applications. The DEM is validated to give a reliable indication of the accuracy of the new DEM product.

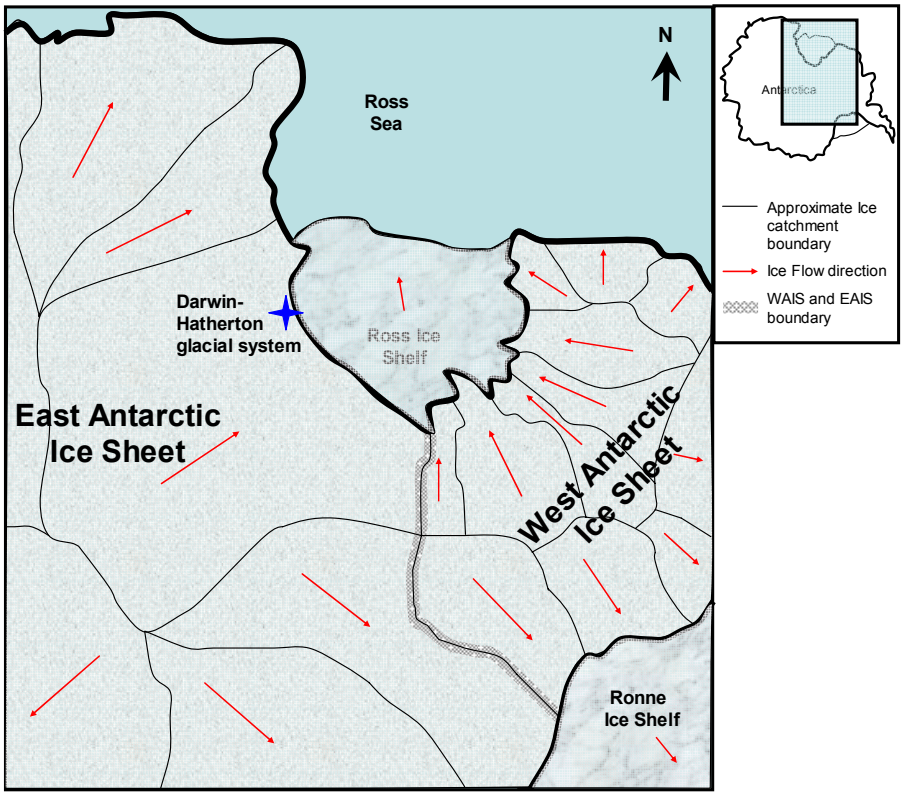

Figure 1.1: The Ross ice drainage system draining ice from the WAIS and EAIS into the Ross Ice Shelf.

1.2 Thesis aim and rationale

The primary aim of this thesis is to use remote sensing techniques to develop a high quality digital elevation model (DEM) for the Darwin-Hatherton glacial system, Antarctica. Specific aims are to:

1) Construct a high resolution DEM of the Darwin-Hatherton glacial system to be used for remote sensing applications.
2) Validate the accuracy of the DEM using independently measured, high accuracy laser altimetry elevation data.
3) Construct a high resolution satellite image of the entire Darwin-Hatherton glacial system.
4) Assess feature tracking as a technique to measure surface ice velocity on the Darwin-Hatherton Glacier.

The rationale for this research is to provide glacial ice surface measurements in the form of DEMs and satellite maps for the Darwin-Hatherton glacial system (Figure 3.1) so that these measurements can be used in other research to model the last glacial maximum ice thickness profile for the Darwin-Hatherton Glacier. Currently a 200 m resolution DEM of Antarctica covers the study area (www.nsidc.org, 2007). However a resolution of 200 m is too low for localised outlet glacier scale applications and has significant error (Bamber and Bindschadler, 1997). The motivation in producing a DEM with higher resolution and greater accuracy that can be used to assist in establishing the LGM profile for the Darwin-Hatherton glacial system (Figure 3.3 and 3.5), is that this glacier has a well preserved sequence of glacial drifts which can be used to validate the model used by Anderson et al., (2004). From Ross Island south along the Transantarctic Mountains there are very few ice free areas, and the extent of the Darwin-Hatherton Glacier glacial drifts is not seen elsewhere in this area. LGM profiles of outlet glaciers along the Transantarctic Mountains are used to help determine the retreat of the WAIS, using the grounding line as a marker. The grounded ice of the WAIS dammed the outlet glaciers, causing the ice profile to be much thicker at the outlet glacier terminus. When the grounding line retreated past each outlet glacier, the dam ceased and the outlet glacier thinned at the terminus. By being able to model the Darwin-Hatherton Glacier's profile change, an age can be given for the retreat of the WAIS grounding line as it passed the Darwin-Hatherton Glacier.

The Ross Ice Shelf (Figure 2.1) is the most prominent remaining ice filled marine basin on earth (Bindschadler, 1998) and it is important to understand the mass balance of the Ross Embayment ice drainage system in order to make predictions as to how the WAIS and EAIS may change in the future due to climate change.

1.3 Thesis approach and structure

The overall approach for this thesis involves the development of a DEM using high resolution ASTER satellite data and testing of the accuracy of this DEM. Secondary aims are achieved by using the constructed DEM for further remote sensing applications. The remote sensing techniques used are driven by the availability of suitable data for the Darwin-Hatherton glacial system area. ASTER imagery is the data type available which allows stereoscopy to be the DEM method and feature tracking to be the ice velocity method. The DEM accuracy is assessed from independently measured ice, cloud and land elevation satellite (ICESat) data. Feature tracking has been used on glaciers covered in features e.g. Byrd Glacier (Stearns and Hamilton, 2005). Therefore feature tracking is assessed as a method to measure ice velocity on the relatively feature free Darwin-Hatherton glacial system. Feature tracking requires an orthorectified image generated using the resulting DEM. Finally a mosaic of all orthorectified images is constructed and a satellite map of the Darwin-Hatherton glacial system is generated. Below is an outline of the thesis structure based on the chapters in the thesis.

Chapter 2 sets the context to where this thesis fits into Antarctic science and glaciology, by presenting two research themes that underpin this research. These are are; remote sensing of outlet glaciers, and climate change and its glaciological effects on the Ross Embayment.

Chapter 3 describes the Darwin-Hatherton glacial system and outlines relevant research that has been done at this location.

Chapter 4 outlines the remote sensing methodology and data including; generation and accuracy validation of the DEM, generation of a satellite map, and attempting to use feature tracking to establish ice velocity.

Chapter 5 presents the results and discussion. The raw DEMs are presented, adjusted, and used to generate two stacked and averaged ASTER DEMs to cover the Darwin-Hatherton glacial system. The new DEM accuracy is validating against independent ICESat elevation data and compared to an existing RAMPv2 DEM to show the improvements the new product provides. A 15 m orthorectified true colour satellite map is presented for the Darwin-Hatherton glacial system.

Chapter 6 concludes this thesis by outlining the applications for this data and recommends future research for DEM generation and ice velocity measurement for the Darwin-Hatherton glacial system. Lastly a conclusion of thesis findings is made.

Chapter 2: Background and themes

2.1 Remote sensing of outlet glaciers

Remote sensing of outlet glaciers is the key theme of this research. The methodological approach undertaken to achieve the aims is entirely remote sensing based. Remote sensing techniques have been successfully used in many aspects of glaciology (Table 2.1). Therefore it is important to outline remote sensing techniques used in glaciology as well as to describe the previous research and methods used for DEM generation and measuring ice flow.

Table 2.1: Summary of ice sheet parameters that can be measured/monitored by satellite sensors. (r) indicates parameter still in research and development (adapted from Massom and Lubin, 2006).

Satellite Sensor	**Passive micro-wave**	**Synthetic aperture radar (SAR)**	**Visible and thermal infrared**		**Active microwave (except synthetic aperture radar)**		
Ice sheet parameter			Low resolution	High resolution	Scatter-ometer	Radar Altimeter	Laser Altimeter
Ice velocity		☺	☺	☺			
Grounding line detection		☺		☺		☺	☺
Tidal motion		☺				☺	☺
Strain rate		☺		☺			
Topography/elevation change		☺	☺	☺		☺	☺
Balance velocity and flux		☺	☺			☺	☺
Surge behaviour		☺		☺			
Ice discharge flux		☺		☺		☺	☺
Ice Sheet facies	☺	☺	☺	☺	☺	☺	☺
Melt/refreeze cycle and extent	☺	☺			☺	☺	☺
Ice Sheet margin change		☺	☺	☺		☺	☺
Iceberg detection/tracking	☺	☺	☺	☺	☺		
Iceberg thickness – freeboard height						☺ (large icebergs & ice shelf)	☺
Accumulation	☺ **(r)**	☺ **(r)**			☺ **(r)**		
Ice shelf basal melt/refreeze		☺				☺	☺
Surface/near surface temp	☺		☺	☺			
Surface albedo			☺	☺			☺
Snow-grain size	☺ **(r)**		☺	☺	☺		☺
Snow layering/volume	☺ **(r)**	☺ **(r)**			☺ **(r)**	☺ **(r)**	
Snow impurity content			☺				☺
Surface roughness		☺	☺	☺	☺	☺	☺
Proxy wind patterns					☺		

2.1.1 Digital elevation model extraction using remote sensing

DEMs are essential in earth science remote sensing research and are used in most applications that either represent and/or analyse changes in the topography (San and Suzen, 2005). Within glaciology, DEMs are used to measure volume change which is used in understanding mass balance and ice surface deformation. DEMs of outlet glaciers and ice streams that flow into ice shelves can be used to detect the grounding line and analyse tidal dynamics (Baek et al., 2005). DEMs are also required in order to remove topographic distortion as part of pre-processing when orthorectifing raw satellite images. The resolution and accuracy of the DEM determines the application of the DEM. For example, in the interior of Antarctica a DEM with a horizontal resolution in the kilometre scale is useful for ice sheet scale applications (Bamber and Gomez-Dans, 2005), but a DEM at much higher resolution is needed for outlet glacier and ice stream scale applications. A high vertical accuracy is critical for all applications, but this is especially true for any change detection of surface height (Schenk et al., 2005).

DEMs can be created by stereoscopy, photoclinometry, synthetic aperture radar (SAR) or laser and radar altimetry methods. Stereoscopy requires two images of the same area that are slightly different in viewing angle. The binocular disparity or parallax is the difference between these two images and the convergence angle between the two images determines the degree of disparity (Toutin, 2001). Clinometry uses shadows to derive elevation for specific objects, such as mountain peaks and seracs etc. This method has been applied to aerial photos and visible infra-red (VIR) satellite images (Toutin, 2001). Laser and radar altimetry and synthetic aperture radar determines surface elevation by transmitting electromagnetic radiation and measuring the reflected energy (Massom and Lubin, 2006). Laser altimetry has often been used to validate the accuracy of DEMs created by other methods (Bamber and Gomez-Dans 2005, Baek et al. 2005, Bamber et al. 2001, Bhang et al. 2007).

Currently there are three DEMs that cover most of Antarctica; the Antarctic DEM from ERS-1 altimetry, the RADARSat Antarctic mapping project volume 2 (RAMPv2) DEM, and the ICESat DEM (www.nsidc.org, 2007). The Antarctic DEM from ERS-1 altimetry was derived from radar altimetry during 1994 and 1995. This DEM has a resolution of 5 km and does not provide elevation data south of 81.5º S (Bamber and Bindschalder, 1997). The

RAMPv2 DEM was constructed from a variety of sources including synthetic and airborne radar altimetry and topographic maps from the United States Geological Survey (USGS) and the Australian Antarctic Division. This DEM covers the entire Antarctic continent with variable horizontal and vertical resolution and is sampled on a 200 m grid (www.nsidc.org, 2007). Both DEMs vertical accuracy has been assessed by independent laser altimetry measurements. Large errors greater than 100 m occur in areas where data was acquired terrestrially rather than remotely. In other areas a systematic error was found. In the Antarctic DEM this error increases in a monotonic trend with slope, while in the RAMPv2 DEM this error is more complex and less predictable (Bamber and Gomez-Dans, 2005). The ICESat DEM is constructed from laser altimetry measurements from February 2003 to June 2005 and covers the Antarctic continent north of 86º S. The measurements are acquired with an along track spacing of 172 m and are interpolated to give a DEM with a resolution of 500 m DEM (www.nsidc.org, 2007).

ASTER satellite imagery has been used to generate DEMs in many locations, worldwide for example Toutin 2001, Toutin and Cheng 2001, Toutin and Cheng 2002, Kaab 2001. ASTER DEM accuracy has been tested by Kaab, (2005) by comparing a 30 m resolution ASTER DEM against a 25 m resolution reference DEM generated from aerial photogrammetry for the Gruben area in the Swiss Alps (Kaab, 2001). This is an area of rough terrain, with elevations ranging from 1500 m to 4000 m, which is similar to the Darwin-Hatherton glacial system. Severe vertical errors of up to 500 m occurred in areas where steep north facing slopes existed (Kaab, 2005). These severe errors were a function of the look angle of the satellite obscuring and distorting northern faces combined with north facing slopes also being in shadow. The residual error for the ASTER DEM resulted in $\pm$ 78 m standard deviation with maximum and minimum elevation differences between -220 m and 630 m. A 60 m resolution ASTER DEM was also generated and the residual error between the 30 m and 60 m resolution DEMs were compared. For elevation differences less than 100 m (approximately 90 % of sample) the 30 m DEM had greater accuracy than the 60 m DEM. However for elevation differences greater than 100 m (remaining 10 % of sample), this is reversed with the 60 m DEM having greater accuracy than the 30 m DEM (Kaab, 2005). A 30 m resolution DEM generated for an area of smoother terrain over the Gries Glacier in the Swiss Alps was also validated. The severe errors were similar but the residual error was considerably smaller with an error of $\pm$ 35 m standard deviation (Kaab, 2005).

2.1.2 Ice velocity measurements using remote sensing

Ice velocity can be remotely sensed by either feature tracking or synthetic aperture radar interferometry (InSAR), (Table 2.2). Each method has different strengths as well as limitations.

InSAR techniques use active coherent microwave radiation to illuminate the earth surface. By measuring the differences in the phase of the return radar signal from two slightly different positions twice over a short time period, both surface topography and slight changes in the surface such as ice flow can be mapped (Massom and Lubin, 2006). InSAR has a high temporal resolution in dependence of the satellite system (Massom and Lubin, 2006) . The use of microwave illumination means that cloud cover and darkness are not an issue. However, the interferogram used to establish ice velocity is limited by phase unwrapping due to phase noise and surface discontinuities such as crevasses. Excessive change in the surface over the image pair acquisition time is also a limitation as well as tropospheric and ionospheric decorrelation (Massom and Lubin, 2006).

Feature tracking uses high resolution images by applying a cross correlation algorithm to identify the displacement of patterns of pixels over surface features between two images. The image time separation is determined by estimated ice velocity, image resolution, and potential surface feature distortion. Optical images have to be cloud free and the sun illumination angle has to be as similar as possible between images so that features can be consistantly identified. In addition the features must not be distorted beyond recognition. Automated feature tracking for ice flow was developed in 1991 by Bindschadler and Scambos. The main drive for this method was to allow remotely sensed velocity measurements to be undertaken in areas that have little to no bedrock exposed that could be used to co-register images such as Ice Stream E (Binschadler and Scambos, 1991). Feature tracking has been used in a number of glaciological applications around the world (Table 2.2).

Table 2.2: Selected applications of feature tracking on glaciers around the world.

Glacier	Authors	Period	Satellite type	Other information
Ice Stream E, West Antarctica	Bindschadler and Scambos, (1991)	Jan - Dec 1988	Landsat 5 TM	Co-registration using surface undulations relating to subglacial topography
Larsen Ice Shelf, Antarctic Peninsular	Rack et al., (1999)	1986-1989, 1992-1997	Landsat, ERS SAR	Compared to velocity measurements at stake profiles
Byrd Glacier, Transantarctic Mountains	Stearns and Hamilton, (2005)	Dec 2000 and Nov 2001	ASTER	Compared to previous photogrammety velocity measurements (Bretcher, 1982)
Mertz Glacier, East Antarctica	Berthier et al., (2003)	Jan 1989, Jan 2000 and Dec 2001	Landsat 5 TM, Landsat 7 ETM+	
Daugaard Jensen Gletscher, Greenland	Stearns et al., (2005)	Aug 2000 and July 2001	ASTER	Compared to ground velocity survey (Olsen and Reeh, 1969)
Baltoro Glacier, Pakistan	Mayer et al., (2006)	1999, 2000 and 2001	Landsat, ASTER	Compared to short term GPS velocity measurements of a stake network

2.2 Climate change and its glaciological effects on the Ross Embayment

Climate change and its glaciological effects on the Ross Embayment is a secondary theme of this research and underpins why research is being done in the Darwin-Hatherton glacial system within the Ross Embayment. The rationale (Section 1.2) outlines the importance of this research and how it fits into the Ross Embayment, while this section describes the Ross Embayment and previous research in more detail and outlines the significance of the Ross Embayment in terms of climate change.

2.2.1 Ross Embayment

The Ross Embayment is an ice filled marine basin in Antarctica. Presently the Ross Ice Shelf covers approximately two thirds of the embayment and the remaining area varies seasonally between sea ice and open water (Figure 1.1). The Ross ice drainage system is a large complex glacial system that drains ice from approximately a quarter of Antarctica's ice sheet surface (Denton and Hughes, 2000). Within this system ice accumulates in both the WAIS and the EAIS (Figure 1.1). The ice sheet ice flows slowly until it becomes funneled into valley type glaciers. Ice from the WAIS reaches a series of ice streams and ice from the EAIS reaches a series of outlet glaciers that flow seaward through the Transantarctic Mountains. At the point where the ice reaches the Ross Ice Shelf, the ice loses its grounding with the bedrock and becomes a floating ice shelf.

2.2.2 Ross Embayment glacial retreat and evidence from the Transantarctic Mountains

The grounding line of the WAIS has been retreating southward since the LGM, but with most of the recession occurring in the middle to late Holocene (Conway et al., 1999). The grounding line was north of Cape Ross 7600 years before present and retreat has occurred in a "swinging gate" style (Figure 2.1). This implies that the southward retreat was not uniform across the Ross Embayment, but was hinged just north of Roosevelt Island. At this hinged point the slowest rate of retreat occurred, and the greatest rate of retreat occurred along the Transantarctic Mountains. In the last 7500 years the average retreat equates to 120 my^{-1} with similar rates still occurring e.g. the grounding line of Ice Stream C is retreating at 30 my^{-1} and Ice Stream B at 450 my^{-1} (Whillams and Bindschadler, 1988). This retreat was pre-determined by major climate change at the LGM. Equilibrium has not yet been reached (Conway et al., 1999).

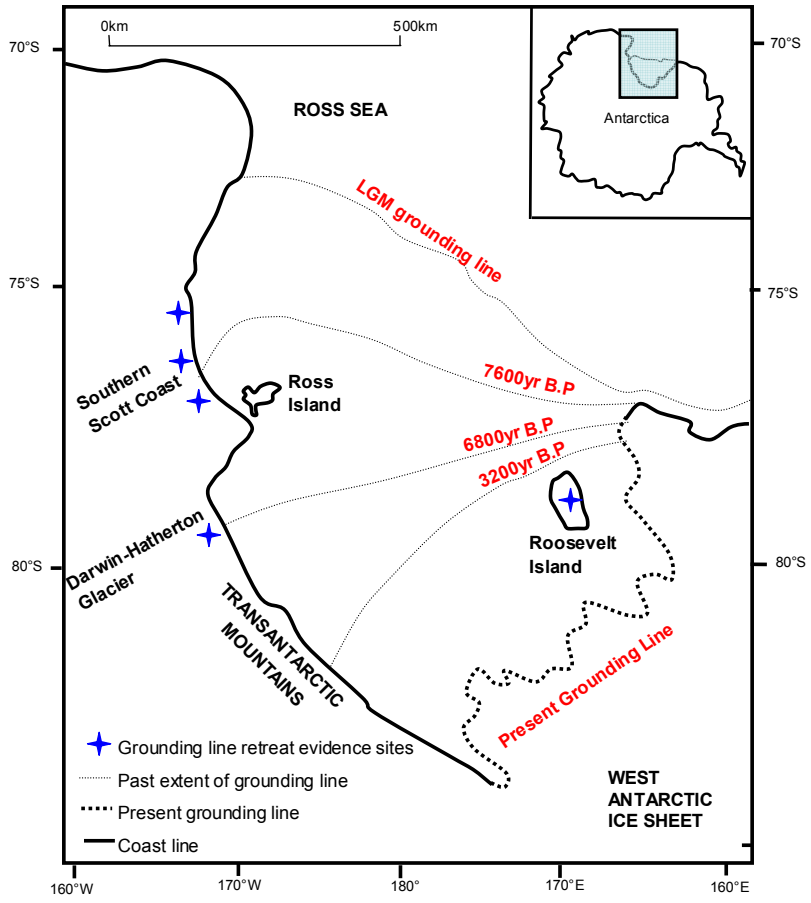

Figure 2.1: Swinging gate model for Ross Embayment grounding line retreat since the LGM with evidence from the Scott Coast, Darwin-Hatherton Glacier and Roosevelt Island (Conway et al., 1999)

Evidence for this retreat has been found at three main sites. These include the Scott Coast, the Darwin-Hatherton glacial system and at Roosevelt Island.

The Dry Valleys of the southern Scott Coast are an area where the Ross Ice Shelf terminated on land rather than into the ocean. Due to the landward flow of ice, proglacial lakes from the Ross Ice Sheet were dammed in the Dry Valleys. Lacustrine algae from the Dry Valleys and marine shells and seal skin from the Southern Scott Coast have been C^{14} dated, showing that the ice was at its approximate LGM position from at least 27,820 to 12,880 years before present, that the grounding line was still north of McMurdo Sound at 9420 years before present (Conway et al., 1999), and that open water was present at 7550 years before present. Therefore the Ross Ice Shelf must have retreated past the Southern Scott Coast between 9420 and 7550 years before present (Figure 2.1), (Conway et al., 1999).

Further south along the Transantarctic Mountains the outlet glaciers' longitudinal profiles have been controlled by WAIS grounded ice. Modeling and extrapolation of glacial drifts in the Darwin-Hatherton glacial system show that the LGM ice profile was between 800 m (Anderson et al., 2004) and 1100 m (Bockheim et al., 1989) thicker than the present ice thickness near the confluence into the Ross Ice Shelf and this LGM profile thickness thinned with distance from the confluence with the WAIS (Section 3.2.2 and 3.2.3). Algal samples from dammed lakes close to the glacier's present level suggest that the grounding line of the Ross Ice Shelf had retreated past the outlet between 6020 and 9429 years before present (Bockheim et al., 1989), (Figure 2.1). The Darwin-Hatherton glacial system is the focus of this research.

Roosevelt Island is a grounded dome of ice with the grounding line approximately 200 m below sea level surrounded by the floating ice of the Ross Ice Shelf. Research investigating bump-amplitude profiles within the ice stratigraphy are combined with ice flow models and show that divide flow first started 3200 years before present (Conway et al., 1999). It is suspected that divide flow began before the ice was fully ungrounded suggesting that the grounding line was still north of Roosevelt Island at 3200 years before present (Conway et al., 1999), (Figure 2.1).

2.2.3 Significance of the Ross Embayment in terms of climate change

Glaciers and ice sheets provide one of the most visible indications of the effects of climate change, as the mass balance of the system is determined by climatic controls (IPCC, 2007). It is important to have accurate measurements for the mass balance of the WAIS, EAIS and the total Antarctic Ice Sheet to help understand climate change. By understanding the link between climate change and mass balance we can help predict the effects that climate change may have on the ice sheets in the future. Currently estimates of Antarctic mass balance vary (Table 2.3).

Table 2.3. Mass balance of the EAIS and WAIS (Modified from Shepherd and Wingham, 2007).

Study	Survey period	Survey type	Survey area $10^6 km^2$	EAIS MB Gt $year^{-1}$	WAIS MB Gt $year^{-1}$
Wingham et al., 1998	1992-1996	Altimetry	7.6	-1 $\pm$ 53	-59 $\pm$ 50
Rignot and Thomas, 2002	1995-2000	Mass Budget	7.2	22 $\pm$ 23	-48 $\pm$14
Davis et al., 2005	1992-2003	Altimetry	7.1	45 $\pm$ 7	
Velicogna and Whar, 2005	2002-2004	Gravimetry	1.7		
Zwally et al., 2005	1992-2002	Altimetry	11.1	16 $\pm$ 11	-47 $\pm$ 4
Velicogna and Whar, 2006	2002-2005	Gravimetry	12.4	0 $\pm$ 51	-136 $\pm$ 19
Ramillien et al., 2006	2002-2005	Gravimetry	14.1	67 $\pm$ 28	-107 $\pm$23
Wingham et al., 2006	1992-2003	Altimetry	8.5		
Range				-1 to 67	-136 to -47

There are two main reasons for this variation. First, there are three main methodological approaches which have different systematic method errors (Shepherd and Wingham, 2007). Secondly, there is uncertainty associated with the lack of complete data for remote locations which causes best estimates to be used in modeling. Currently in Antarctica there are very little glaciological data specifically for outlet glaciers along the southern Transantarctic Mountains.

The need to quantify and understand the mass balance of ice sheets has become increasingly important. This need is due to increased understanding of the impacts of anthropogenic enhanced climate change. The most recent report produced by the IPCC states that the global atmospheric concentrations of carbon dioxide, methane and nitrous oxide (Figure 2.2) have increased markedly as a result of human activities since 1750 and now far exceed pre-industrial values with a radiative forcing of + 1.6 Wm^{-2} (+0.6 to +2.4) (IPCC, 2007).

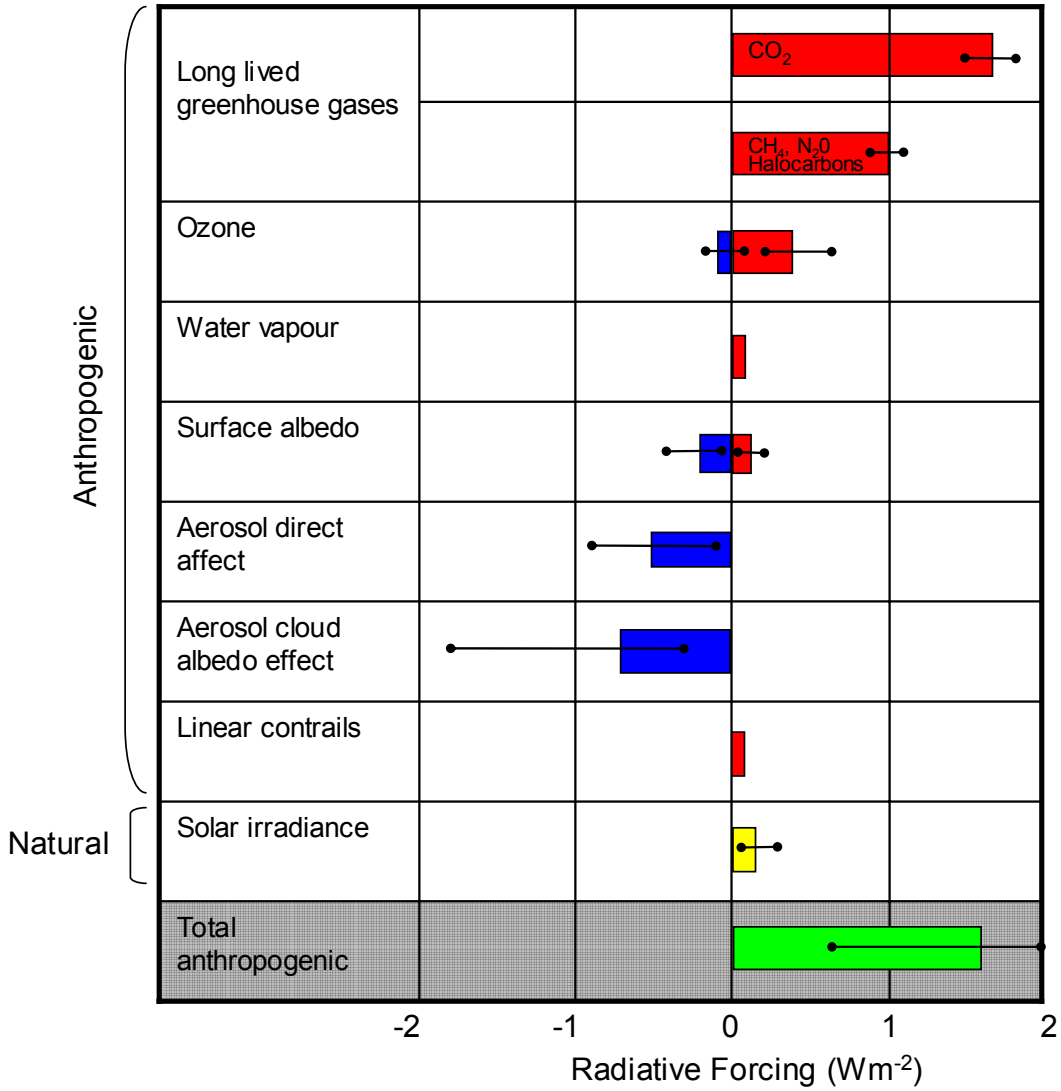

Figure 2.2: Radiative forcing components of climate change (modified from IPCC, 2007)

Some of the direct observations of this positive radiative forcing are: an increased surface temperature of 0.76 ºC with uncertainty of 0.57º to 0.95 ºC since 1850, an increased troposphere temperature, an increased water vapor, a decrease in the size of the Arctic sea ice, a decrease in mountain glaciers/snow, a 7 % loss of northern hemisphere permafrost since 1900, regional changes in precipitation, and an average sea level rise of 1.8 $mmyr^{-1}$ (uncertainty of 1.3 - 2.3$mmyr^{-1}$) since 1961 (IPCC, 2007). The IPCC also states that this change may cause "a probable decrease in the ice sheets of Greenland and Antarctica" and "Current global model studies project that the Antarctic Ice Sheet will remain too cold for widespread surface melting and is expected to gain in mass due to increased snowfall. However, net loss of ice mass could occur if dynamic ice discharge dominates the ice sheet mass balance" (pg 17, Fourth assessment report of the IPCC, 2007). Despite the uncertainty there is concern about the stability of the WAIS. Theoretical analysis suggests that ice-filled marine basins are unstable and current predictions show continued grounding line retreat and loss of volume. Two different retreat models, a linear retreat, and an accelerated retreat predict that the grounding line would reach the West Antarctic ice divide by 7000/4000 years respectively with 0.8/1.3 $mmyr^{-1}$ sea level rise respectively (Bindschadler, 1998a). Therefore further research needs to be undertaken in order to provide mass balance measurements with less uncertainty so that they can be used to validate the WAIS retreat models.

Chapter 3: Darwin-Hatherton glacial system

3.1 Glaciology of the Darwin-Hatherton glacial system

The Darwin-Hatherton glacial system is an Antarctic outlet glacial system located within the Transantarctic Mountains between 155º and 161 ºE longitude, and between 79º and 80 ºS latitude (Figure 3.1).

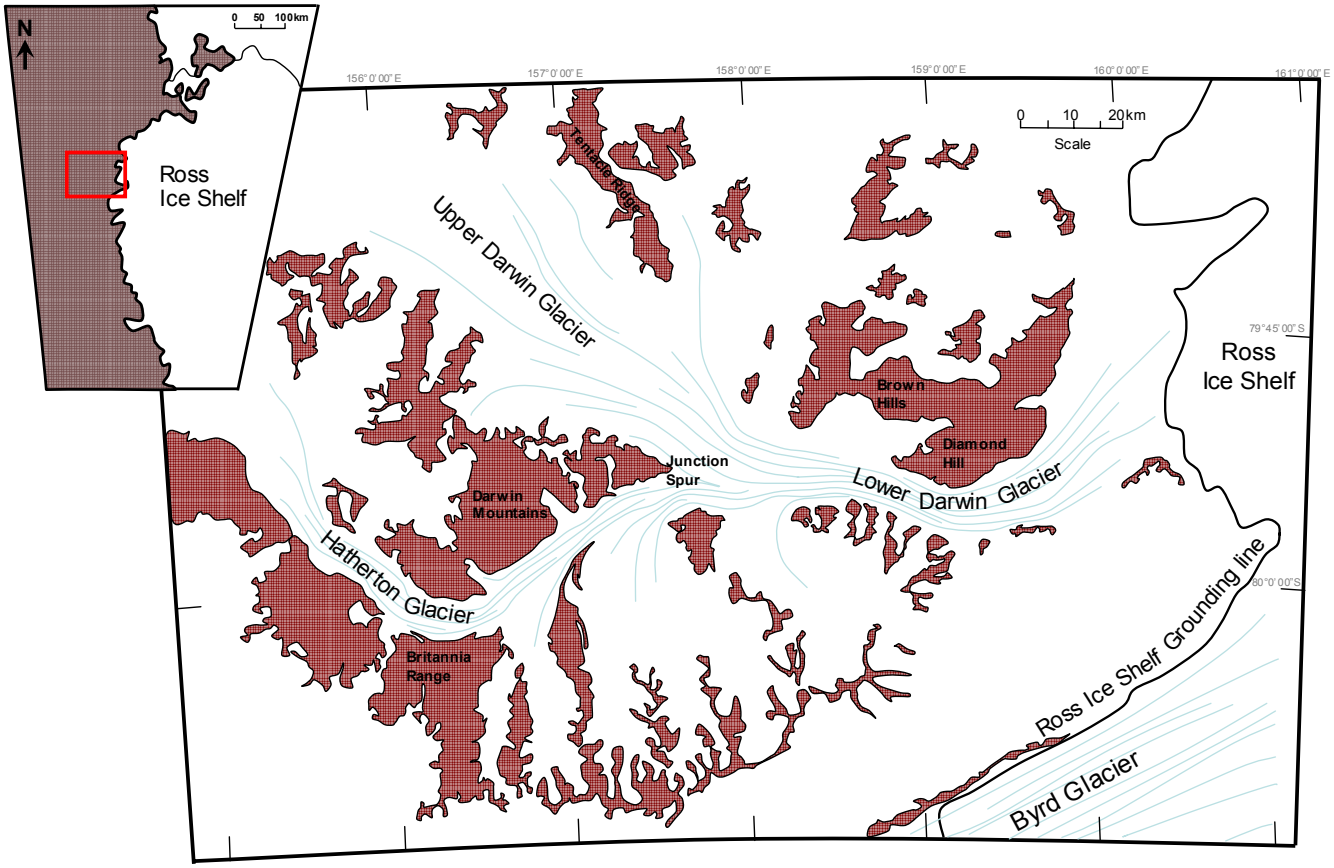

Figure 3.1: Darwin-Hatherton Glacier, Transantarctic Mountains, Antarctica. Light blue lines show glacier flow and brown areas are ice free areas (modified from ST 57-60/13* map, Antarctica 1:250,000 Reconnaissance Series, USGS, 1963.

The geomorphology of the Transantarctic Mountains in this area is a function of mountain uplifting processes through a pre-existing ice sheet (Denton, 1979). As the mountains were uplifted ice carved out valleys, isolating nunataks. Over time valleys with geologic weaknesses became the predominant drainage valleys for the interior EAIS leaving other transverse valleys to have glaciers that were smaller and slower moving. The smaller and slower glaciers are widespread along the Transantarctic Mountains and make up a significant

part of the EAIS drainage system in the Transantarctic Mountains. The Darwin-Hatherton glacial system is an example of a smaller, slower moving glacier. The bed profile of the Darwin-Hatherton glacial system is currently unknown.

The Darwin-Hatherton glacial system has two main accumulation areas; the upper Darwin Glacier and the upper Hatherton Glacier (Figure 3.1). Four other smaller catchments provide ice to the system, three of which drain from the Britannia Range, and a fourth that is separated from the upper Darwin Glacier by Tentacle Ridge. Most of the glacier surface comprises pf "blue ice". The features on the ice surface include: supra-glacial melt water ponds and channels on the lower Darwin Glacier, medial moraines and flow bands in the upper Hatherton and lower Darwin glaciers, and crevasse fields in the upper Darwin Glacier and pockets of supra-glacial moraine in the upper Hatherton Glacier. The Darwin-Hatherton glacial system is grounded and the Ross Ice Shelf is floating. Therefore as the glacier flows out onto the ice shelf the glacier becomes ungrounded. Hughes and Fastook (1981) inferred the position of the grounding line for the neighbouring Byrd Glacier from a break in elevation and velocity in the glacier at approximately 200 m above sea level. Tidal response was also measured, and supports this inference (Hughes and Fastook, 1981). Because of the close proximity it can be inferred that the Darwin-Hatherton Glacier grounding line will be similar in elevation to the Byrd Glacier. Surface ice velocity measurements have been measured once by field surveying in 1981 by Hughes and Fastook (Section 3.2.1). Theoretical calculations of the basal temperature using the Quadrature method (Hindmarsh, 1999) for the Darwin-Hatherton glacial system were conducted for the purpose of modeling (Anderson et al., 2004). These calculations established that part of the base may be above the pressure melting point. The mass balance for the Darwin-Hatherton glacial system is currently only estimated from hypothetical modeling (Section 3.2.3), verified by sparse field measurements (Section 3.2.1). Until velocity data, volume data and input/output data are measured the mass balance can not be calculated accurately. There are currently very sparse meterological data available for this area but estimates of accumulation in the Polar Plateau and Ross Ice Shelf are 0.10 to 0.15 $gcm^{-2}y^{-1}$ and 20 $gcm^{-2}y^{-1}$ respectively and annual average temperatures of -35º to -40 ºC and -30 ºC respectively (Bockheim et al., 1989). The microclimate of the Darwin Glacier and the Hatherton Glacier are different with the Polar Plateau winds affecting the Hatherton Glacier more than the Darwin Glacier (Bockheim et al., 1989).

3.2 Previous research on the Darwin-Hatherton glacial system

The Darwin-Hatherton glacial system is a remote, bordering deep field location of Antarctica (Figure 3.1) and there has been limited research done at this location. This section reviews all glaciological and glacial geomorphological research undertaken in the Darwin-Hatherton glacial system to date.

3.2.1 Ice dynamics research

Velocity has been sparsely measured by Hughes and Fastook (1981), (Figure 3.2). However this research was predominantly based on the neighbouring Byrd Glacier where ice flow research was undertaken initially by field measurements (Hughes and Fastook, 1981), and then subsequently aerial photograph sets were used to undertake a photogrammetry ice flow study (Brecher, 1982) validated by the initial field measurements. The aim of this research was to provide data that could be used to create a finite-element analysis of the Byrd-Ross Ice Shelf interaction. 65 markers were surveyed on the Byrd Glacier and 6 on the Darwin-Hatherton glacial system. The velocities of the Darwin-Hatherton Glacier ranged from approximately 75 my^{-1} above Junction Spur (Figure 3.2) to between 75 my^{-1} and 200 my^{-1} on the lower Darwin-Hatherton glacial system (Figure 3.2).

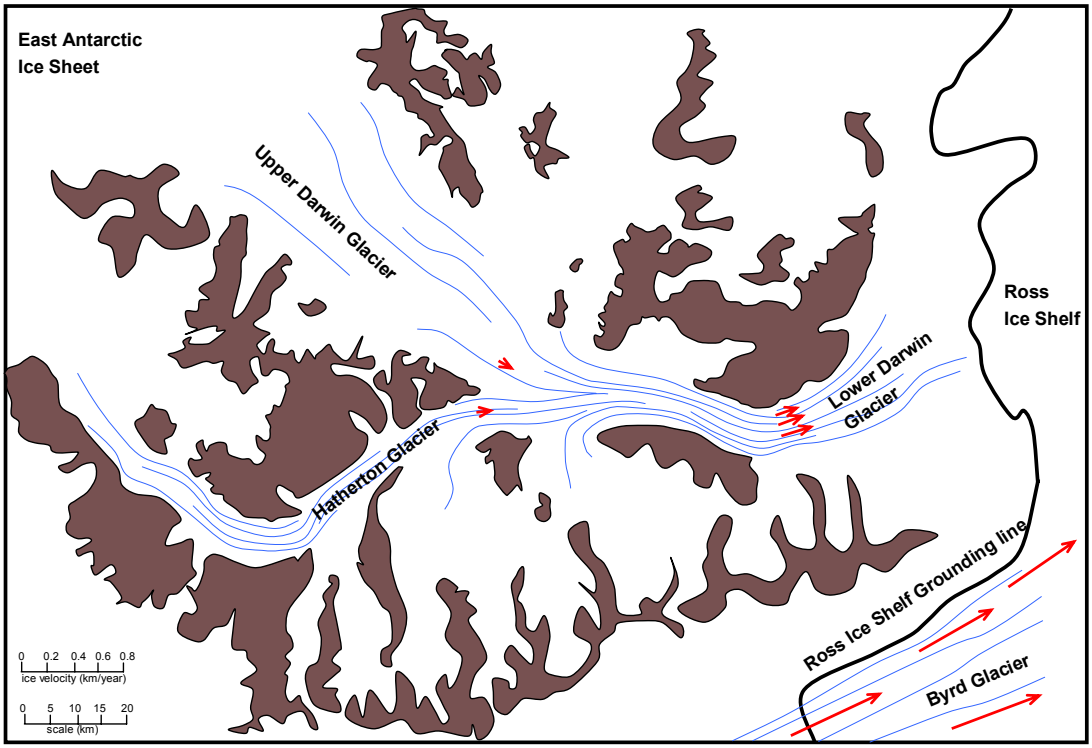

Figure 3.2: Field measurements of ice velocity determined from ground surveys.
(modified from Hughes and Fastook, 1981)

3.2.2 Glacial geomorphology research

Geomorphological research has been undertaken in the Hatherton glacier area (Bockheim and Wilson 1979, and Bockheim et al. 1989), based on the well preserved glacial lateral drifts that are remnants of past glacial regimes in the area. Soil properties were used as relative age indicators and stratigraphic markers to separate out the different lateral drifts and compare to McMurdo Sound sequences (Bockheim and Wilson, 1979). Longitudinal ice surface profiles were constructed for each of the different drifts (Bockheim et al., 1989). The LGM profile is well constrained in the Hatherton Valley but is extrapolated downstream of Junction Spur due to lack of distinct boundaries. The Britannia drift shows that at the Last Glacial Maximum the ice thickened above the present level by (Figure 3.3) by 100 m at the inland extremity, 450 m mid glacier, and by 1100m at the confluence of the glacier to the Ross Ice Shelf (from extrapolated data).

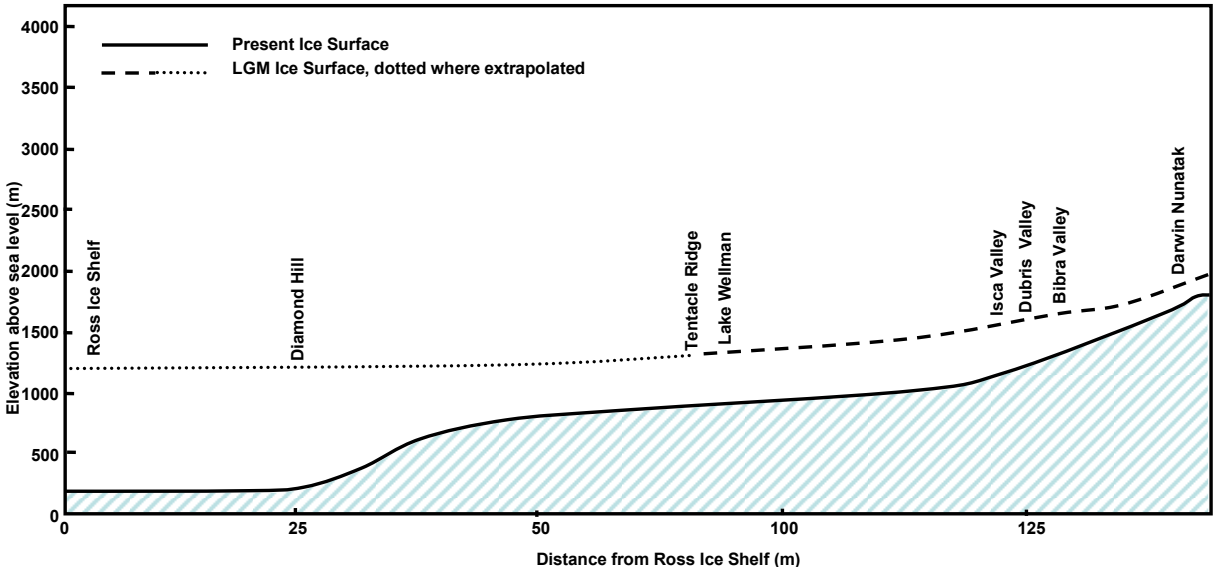

Figure 3.3: Profile of the Darwin-Hatherton Glacial System showing the present ice surface and ice surfaces from the past (Bockheim et al., 1989)

C^{14} dating techniques were used to give a basic age control on ice recession. Algae from former kettle and glacier dammed lakes were used to give a minimum age for recession. The Britannia/LGM drift is dated to between 9420 years and 10,250 years before present and the ice surface was close to its present level between 5740 years and 6020 years before present (Bockheim et al., 1989), indicating that the grounding line of the WAIS retreated past the Darwin-Hatherton glacial system between 6020 years and 9420 years before present

3.2.3 Glacial modeling research

By using the geomorphological research as validation (Chapter 3.2b), modeling research was used to a) model the elevation of ice at the Darwin Glacier/Ross Ice Shelf confluence at the LGM and, b) model the time for the Darwin-Hatherton glacial system to respond to the retreat of the WAIS grounding line (Anderson et al., 2004). The model is a simple one-dimensional flow line model where an average ice velocity is passed through a trapezium transverse valley cross-section (no longitudinal stresses taken into account).

Some of the parameters used in the model are taken from sparse measured data and others are based on glacial theories (Table 3.1).

Table 3.1: Parameters used in glacial model (from Anderson et al., 2004)

Model parameter	Type of data
Surface topography	USGS 1:250 000 map. Ground measured profile in Hatherton valley (Bockheim et al., 1989)
Bedrock topography	Trapezium geometry
Grounding Line	USGS 1:250 000 map and Landsat imagery
Basal temperature	Calculated using Quadrature method (Hindmarsh, 1999)
Mass balance	Accumulation rates from Polar Plateau and Ross Ice Sheet (Bockheim et al. 1989)
Scenario 1	Linear change of accumulation with elevation.
Scenario 2	Same as 1, plus blue ice ablation rates based on measurements from Taylor Glacier (Robinson, 1984).
Scenario 3	Same as 2, but assumes ablation rates from Taylor Glacier are too high due to latitude differences and reduces ablation to fit.
Average cross-section ice velocity	Calculated from local driving stress calculation. Validated from 6 ground measurements (Hughes and Fastook, 1981)

The modeled velocity was validated against 5 velocity measurements (Hughes and Fastook, 1981). The values used in calculating the cross section ice velocity (Table 3.1) were not well established and were used as tuning parameters. The modeled ice velocity matches the measured ice velocity reasonably well with a difference in values of between 10-20 ma^{-1} (Figure 3.4)

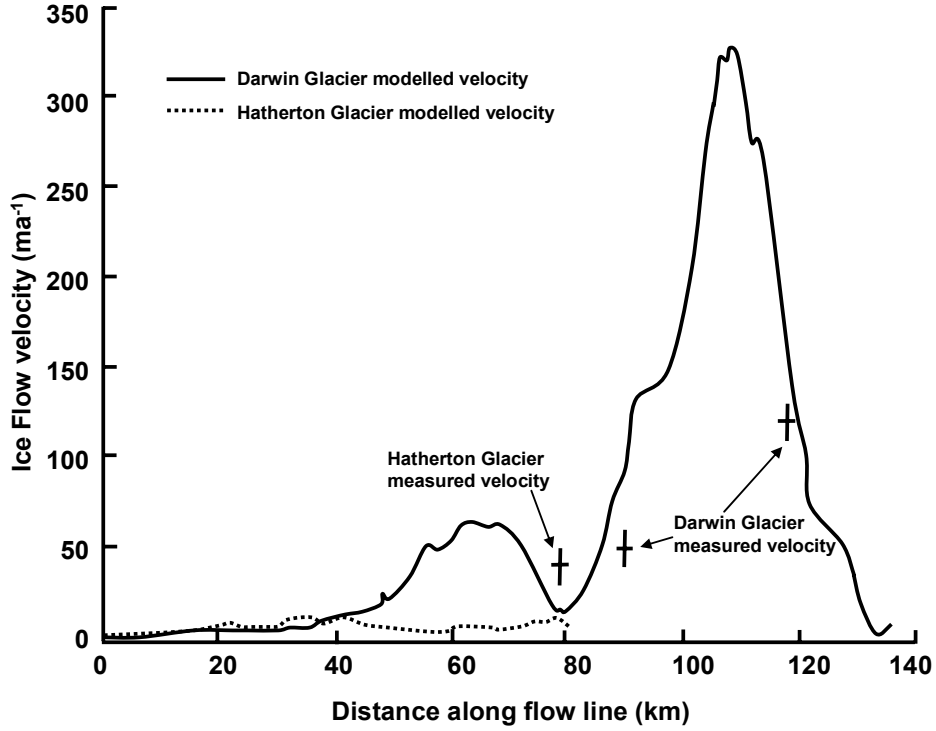

Figure 3.4: A comparison between modeled and measured velocities from the Darwin-Hatherton glacial system (Anderson et al., 2004).

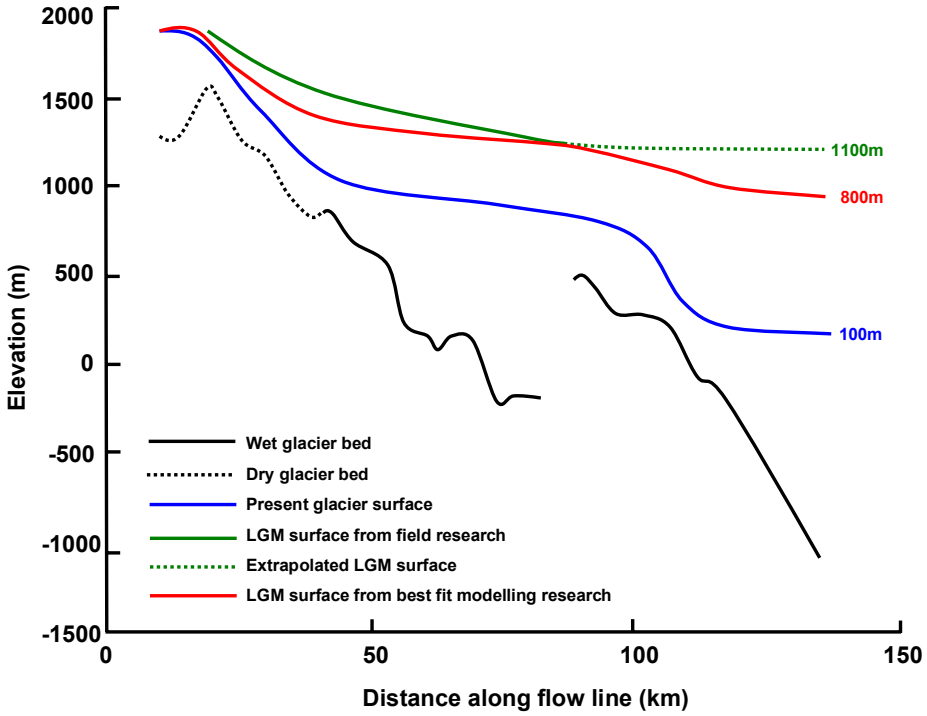

Figure 3.5: Equilibrium profiles of the Darwin-Hatherton Glacier showing present day profile, as well as modeled and measured LGM profiles (modified from Anderson et al., 2004)

The model equilibrium profiles were validated against the LGM profile (Bockheim et al., 1989). The best fit model suggests a LGM outlet profile elevation of 800 m above the present Ross Ice Shelf. The extrapolated LGM profile suggests an 1100 m elevation above the present Ross Ice Shelf (Figure 3.5). Therefore there is a 300 m discrepancy between the two different methods. However the two profiles match well at the junction of the Darwin and Hatherton Glaciers.

The response time between the retreat of the WAIS grounding line and the Darwin-Hatherton glacial system reaching equilibrium was modeled as a linear retreat and as a stepwise with a response time of 300 years and 1100 years respectively. Geomorphological research gives a window of 3400 years (Bockheim et al., 1989) for this to have happened, so both modeled scenarios fit within this window. Due to the lack of measured data that were fed into this model there have been many assumptions made and the potential uncertainty is high. Currently surface velocity, bedrock profiles, atmospheric parameters and paleo-thickness measurements are being studied further. These can then be used to place greater certainty on this model.

Chapter 4: Remote sensing for digital elevation model generation, map generation, and ice velocity

4.1 Outline of the methodology

The aims of this thesis were achieved in four main stages (Figure 4.1).

1) Suitable satellite data and ground control points (GCPs) were chosen and acquired; ASTER satellite imagery, ICESat satellite elevation data and GPS and topographic ground control points (Section 4.2).
2) Individual DEMs were generated for each ASTER image, systematic errors were removed and the precision of the DEMs was increased by stacking and averaging individual DEMs. ICESat elevation data were used to assess the DEM accuracy (Section 4.3).
3) Orthorectification using the DEM and the raw ASTER images and further pre-processing were used to generated a true colour, 15 m resolution satellite map of the Darwin-Hatherton glacial system (Section 4.4).
4) The individual orthorectified ASTER images were further processed and feature tracking techniques were applied in an attempt to establish whether feature tracking using ASTER data could be used to measure the ice surface velocity of the Darwin-Hatherton glacial system (Section 4.5).

Table 4.1: Summary of all data and computer programs used in this thesis

Data source	**Use**
ASTER image data	Create DEM and satellite map
Ground control points	Assist in DEM creation
ICESat data	Validate ASTER DEM
Computer Program	**Use**
ERDAS Imagine Lieca Photogrammetry Suite	• DEM generation. • File conversion
ENVI 4.3	• Orthorectification. • Co-registration. • Sub-setting. • Averaging DEMs. • Mosaicing
ArcGIS	• Gain ground control point data from USGS topographic maps. • Extracting ICESat data • Presenting maps
IMCORR	• Feature tracking

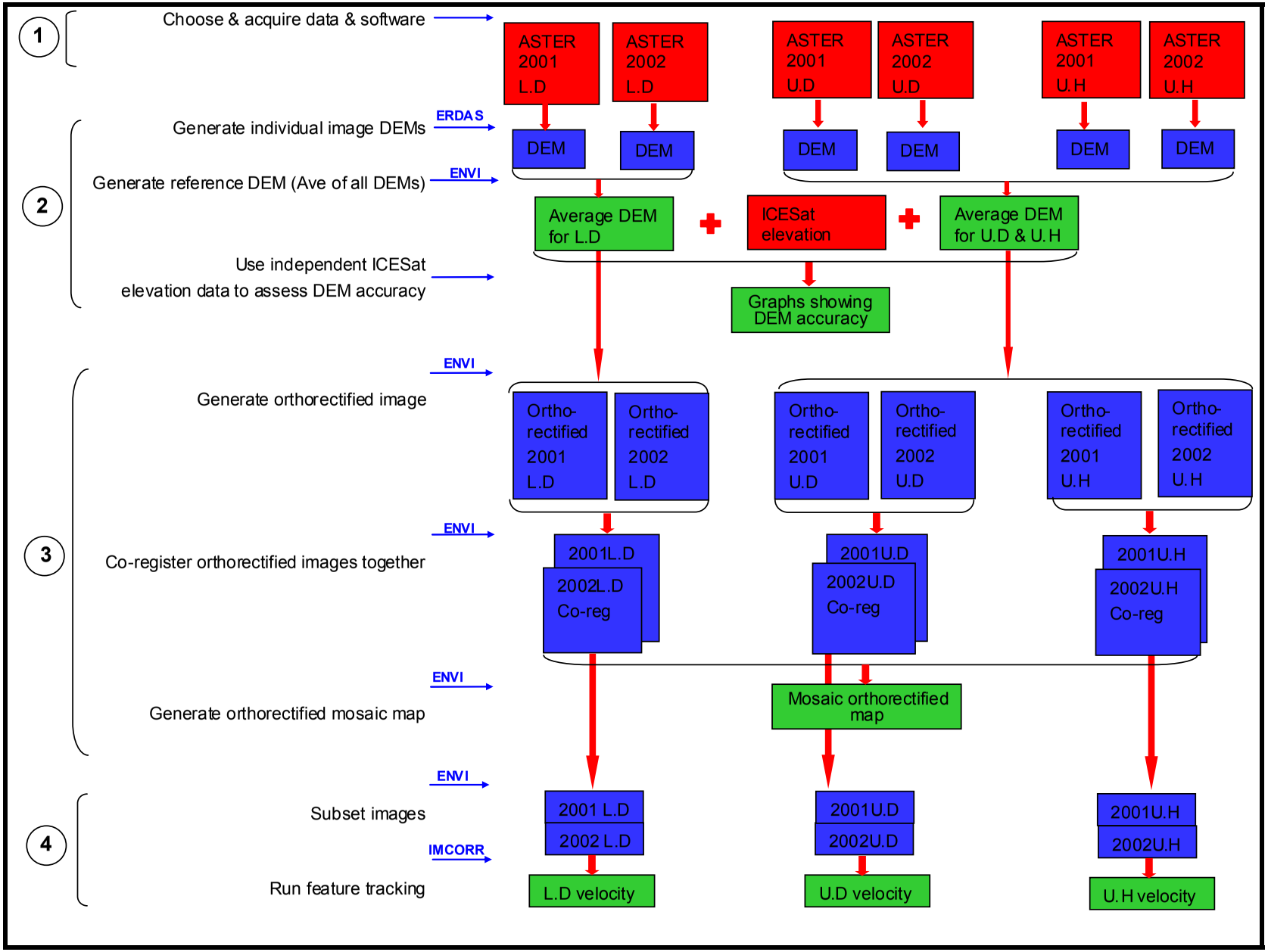

Figure 4.1: Schematic flow diagram showing progression of steps required to produce a DEM, a velocity contour map and an accurate map of the Darwin/Hatherton glacial system using remote sensing .For simplicity, only data sets, 2001 and 2002 are shown in this diagram.
Red = Data source, Blue = Processing step, Green = Result, L.D = lower Darwin, U.D = upper Darwin, U.H = upper Hatherton

4.2 Data sources and acquisition.

4.2.1 ASTER data

Satellite imagery data from the Advanced Spaceborne Thermal Emission and Reflection Radiometer (ASTER) sensor were used. The ASTER sensor is aboard the Terra Satellite and is run co-operatively by NASA and Japan's Ministry of Economic Industry (Elachi and van ZYL, 2006). Terra was launched on 18 December 1999 (Richards and Jia, 2006). The Terra Satellite has a near polar orbit and is sun-synchronous. The images are acquired by a multispectral imager that operates by pushbroom line scanning in the along track direction (Figure 4.2b) with three telescopes, covering 15 bands from the visible to the thermal infrared spectral region (Table 4.2). Of the 15 bands, the 3n and 3b bands (Table 4.2) acquire images with slightly different look directions (Figure 4.2a) and by combining the two slightly different bands, stereoscopy can be used to create a DEM (Elachi and van ZYL, 2006). ASTER data have been used successfully used to create DEMs for many applications and have been successfully used to determine ice velocity from feature tracking (Stearns and Hamilton 2005, Stearns et al. 2005, Mayer et al. 2006).

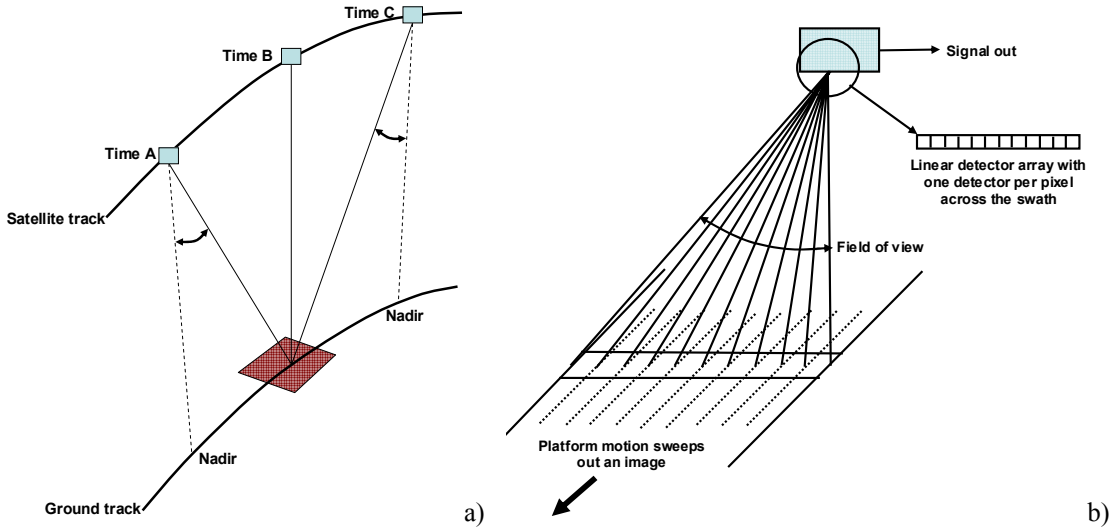

Figure 4.2: a) Along-tack stereo satellite configuration showing both forward and backward (3n and 3b) band look angles, which are acquired during one overflight with a time difference of seconds to minutes (modified from Kaab, 2005). b) Pushbroom line scanning in the along-track direction (Richards and Jia, 2006)

Table 4.2: ASTER characteristics (modified from Elachi and van ZYL, 2006 and Richards and Jia, 2006)

Subsystem	Band no.	Spectral range (μm)	Spatial resolution(m)	Swath (km)	Quantization levels (bits)	
VNIR	1	0.52-0.60	15	60	8	
	2	0.63-0.69	15	60	8	
	3n	0.78-0.86	15	60	8	Stereo Pair
	3b	0.78-0.86	15	60	8	
SWIR	4	1.60-1.70	30	60	8	
	5	2.145-2.185	30	60	8	
	6	2.185-2.225	30	60	8	
	7	2.235-2.285	30	60	8	
	8	2.295-2.365	30	60	8	
	9	2.360-2.430	30	60	8	
TIR	10	8.125-8.475	90	60	12	
	11	8.475-8.825	90	60	12	
	12	8.925-9.275	90	60	12	
	13	10.25-10.95	90	60	12	
	14	10.95-11.65	90	60	12	

Eleven ASTER images were chosen from three different times; December 2001, 2002, and 2005 (Figure 4.3 and Table 4.3). Data time periods were chosen to provide the most up to date DEM, satellite map, and ice velocity measurements as well as choosing a time separation designed to balance out two factors when attempting feature tracking; a long enough time period to reduce the proportion of pre-processing error, and b) a short enough time period to reduce the distortion of identifiable features for feature tracking. Images acquired at similar times of year reduce seasonality issues such as snow cover and sun illumination angle. Choosing a similar time of day was considered in order to reduce illumination differences. Due to the small set of good quality images, this level of selection was not possible. The range in quality of ASTER images is primarily due to cloud cover. Therefore images were chosen and acquired with less than 10 % cloud cover.

Image data were acquired through the USGS NASA Land Processes Distributed Active Archive Centre (LPDAAC) website (www.LPDAAC.usgs.gov, 2007). The images were in LIA format, which is the raw and unprocessed format that has no projection information requiring a DEM in order to correct for topographic error. For this research the given projection was UTM, spheroid and datum WGS84, and zone 57 south. Image codes for three images from 2001, six from 2002 and two from 2005 can be seen in table 4.3. The location with 5 images covering the lower Darwin Glacier and 6 images covering the upper Darwin and Hatherton Glaciers can be seen in figure 4.3.

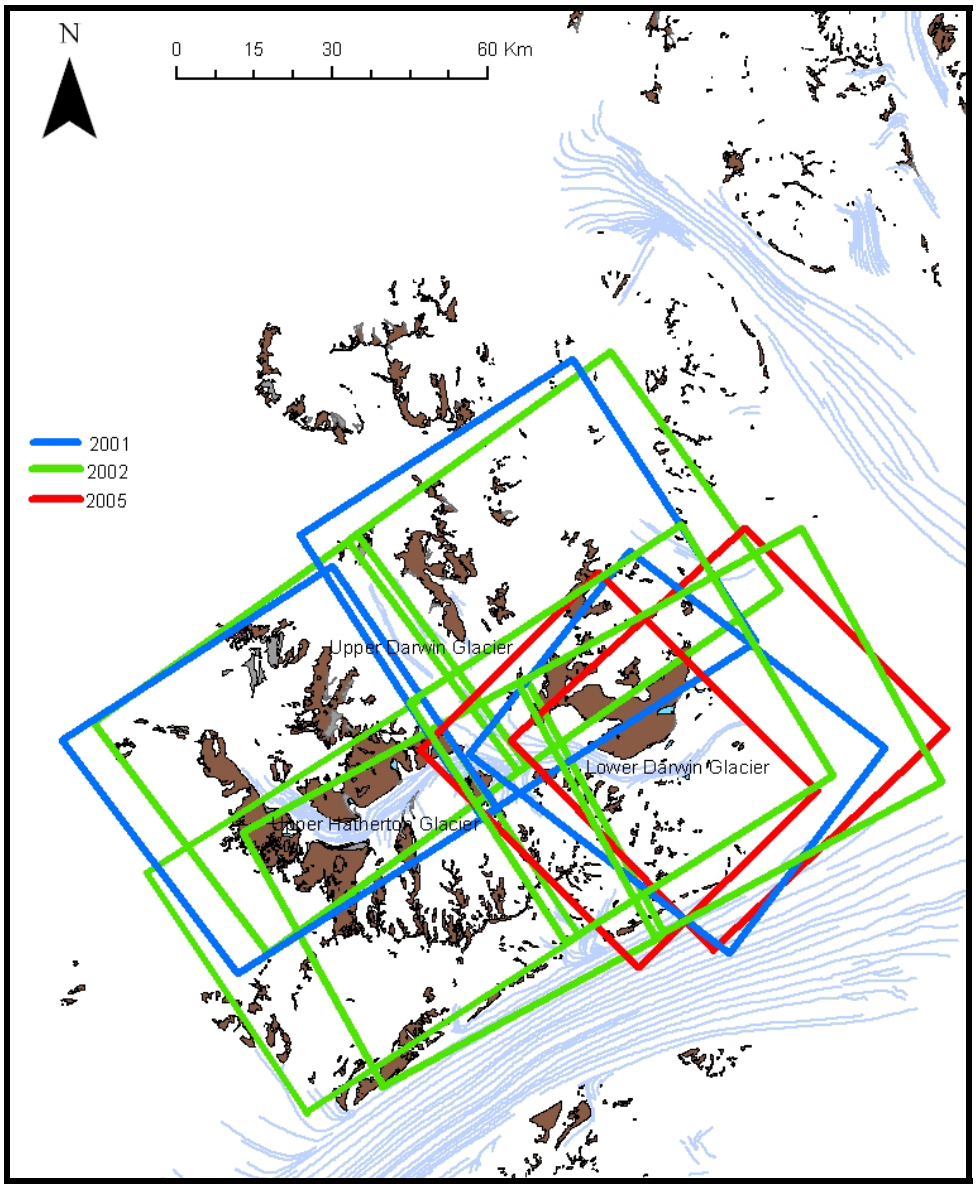

Figure 4.3: Reference map for locations of ASTER images, with colour indicating year of acquisition

Table 4.3: ASTER L1A reconstructed unprocessed instrument V003 data for imagery used in this research. First two numbers of the code = the acquisition year, LD = Lower Darwin, UD = Upper Darwin, UH = Upper Hatherton

Image Data Code	Code	Date	Time	Latitude (South)	Longitude
SC:AST_L1A:003:2006010384	01UD	22 Dec 2001	20:11:00	79.89	155.63
SC:AST_L1A:003:2006010385	01UH	22 Dec 2001	20:11:09	79.61	158.24
SC:AST_L1A:003:2008836878	01LD	29 Dec 2001	15:23:47	79.85	159.91
SC:AST_L1A:003:2010110024	02LDa	04 Dec 2002	19:51:01	79.83	160.08
SC:AST_L1A:003:2009693791	02LDb	09 Dec 2002	20:09:27	79.83	159.05
SC:AST_L1A:003:2010110023	02UHa	04 Dec 2002	19:51:09	80.09	157.36
SC:AST_L1A:003:2009629930	02UHb	07 Dec 2002	20:21:48	79.84	155.97
SC:AST_L1A:003:2009693792	02UHc	09 Dec 2002	20:09:36	80.12	156.41
SC:AST_L1A:003:2009629920	02UD	07 Dec 2002	20:21:39	79.54	158.46
SC:AST_L1A:003:2032605958	05LDa	05 Dec 2005	14:49:16	79.88	159.35
SC:AST_L1A:003:2032304483	05LDb	18 Dec 2005	20:49:46	79.83	160.01

4.2.2 ICESat satellite data

Data from the geoscience laser altimeter system (GLAS) on the NASA ice, cloud and land elevation satellite (ICESat) were used to validate the quality of the ASTER generated DEM. ICESat has been used in Antarctica to study elevation changes of ice sheets, outlet glaciers and ice streams (Baek et al. 2005, Csatho et al. 2005, Nguyen and Herring 2005, Schenk et al. 2005) and to validate DEMs generated from other data (Baek et al. 2005, Bamber and Gomez-Dans, 2005). The laser altimeter pulses energy with a wavelength of 1064 nm at 40 Hz, and the echo pulse is received by a telescope with a 1 m diameter (Schutz et al., 2005). The laser illuminating footprint on the earth surface is ~65 m in diameter and each elevation measurement spot has a successive along-track spacing of 172 m (Schutz et al., 2005).

The ICESat mission was launched in 2003 with a primary purpose of providing data to analyse polar ice sheet volume change with an accuracy of greater than 2 $cmyr^{-1}$ (Schutz et al., 2005) to be combined with mass balance and sea level rise research. ICESat accuracy studies using ground based GPS surveys in Bolivia (Fricker et al., 2005), and independent terrain models from the NASA airborne terrain mapper in the USA and Dry Valleys of Antarctica (Martin et al., 2005), give an absolute accuracy in elevation of ~2 cm. Timing accuracy has been validated to microsecond level (Magruder et al., 2005).

The Antarctic and Greenland ice sheet data product (GLA12) from Laser 2a was used in this research. The GLA12 data were acquired between October and November, 2003 (Figure 4.4) and obtained through the National Snow and Ice Data Centre (NSIDC) at the University of Boulder, Colorado. The accuracy of GLA12 data over the Antarctic and Greenland ice sheets has been shown to have a systematic error of 9.6 cm and a standard deviation corresponding to the residual error of $\pm$ 4.9 cm (Brenner et al., 2007).

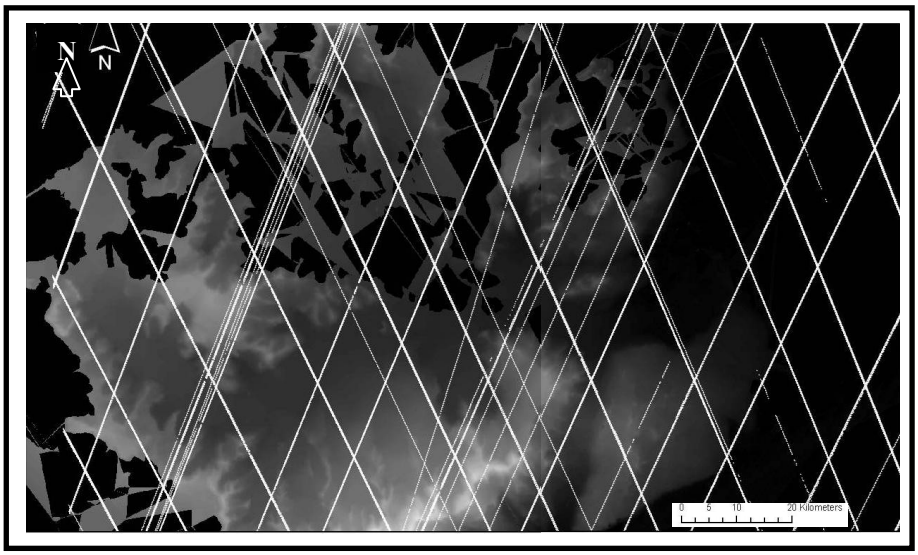

Figure 4.4: ICESat laser altimeter data points available for the Darwin-Hatherton glacial system (shown by white points that make the white lines), overlaid on an ASTER DEM of the area.

4.2.3 Ground control point data

Ground control points (GCPs) were determined in order to create a DEM and to orthorectify the ASTER images. To provide satellite imagery over the entire Darwin-Hatherton glacial system, at least three ASTER images with a 60 km x 60 km area were required. Therefore at least one GCP was required to use for each image. The Darwin-Hatherton glacial system is remote and there is a lack of GCPs available.

GCPs were acquired in two different ways, both using the datum WGS84. In the lower Darwin Glacier, GPS points were taken in the field in January 2007 using a Garmin 72 GPS, and WGS84 datum. One GPS point was at a site near the terminus of the Foggydog Glacier (Figure 4.5) and was able to be located on the ASTER images with an estimated accuracy of $\pm$ 3 pixels (45 m). The GPS point had a horizontal accuracy of $\pm$ 11.4 m and was not differentially corrected. In the upper Darwin and upper Hatherton Glaciers, GCPs were obtained from a digitised version of the 1963 ST 57-60/13* topographic map from the Antarctica 1:250,000 Reconnaissance Series (USGS, 1963). The digitised maps had point elevation data available for high points in ice free areas (Figure 4.5). These points were approximately located onto the ASTER images by assuming that the points corresponded to the highest point in the area of which they were extracted from on the digitised map. The elevation data were extracted from the USGS maps and located onto the ASTER images using ArcGIS.

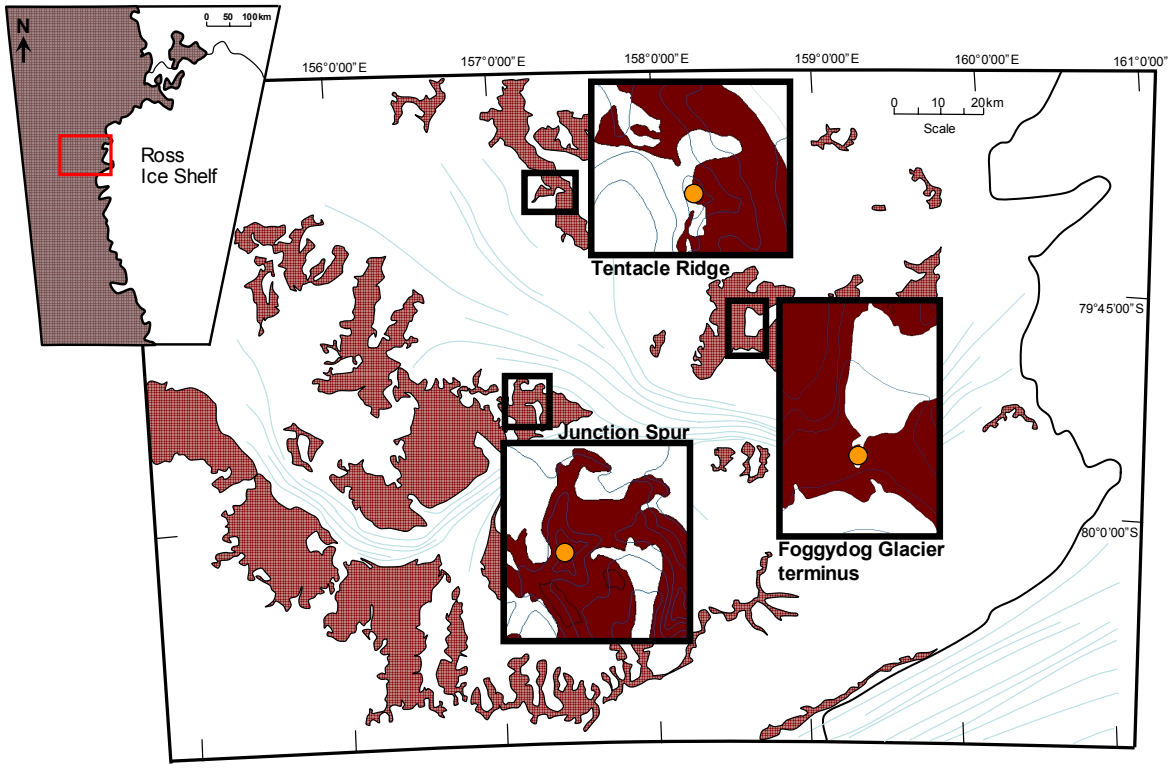

Figure 4.5: Location of GCPs used in this research. Yellow dots indicate approximate location of GCP. Foggydog Glacier terminus GCP was acquired from hand held GPS measurement. Junction Spur and Tentacle Ridge GCPs were acquired from the digitised ST 57-60/13* Antarctica 1:250,000 Reconnaissance Series map (USGS, 1963).

4.3 Digital elevation model generation and accuracy validation

4.3.1 Generation of DEMs

Stereoscopy techniques were used to construct DEMs for each raw ASTER image using the ERDAS Lieca Photogrammetry Suite. Each ASTER multispectral image contained a stereo image pair in the visible near infra red (VNIR) spectral range. The stereo image pair was of near identical image areas acquired from slightly different look angles and was used along with GCP to construct a DEM. Images covering the lower Darwin Glacier used one GPS GCP (Figure 4.5), and images covering the upper Darwin and Hatherton Glaciers used a USGS topographical map GCP (Figure 4.5). The DEM resolution was 45 m due to the limitations of the software requiring the minimum pixel size to be three times the resolution of the original image pixel size. This is due to the number of GCPs available. A one pixel (15 m) resolution DEM has previously been created from ASTER imagery (San and Suzen, 2005), but 30 to 60 GCPs were used.

For each stereo image pair, GCPs and tie points were located so that triangulation could be achieved. Once the GCPs were located, 5 - 10 tie points were manually located allowed automatic tie point generation to run, producing 350 - 1000 tie points. The automated tie point selection process concentrated in the highly-featured ice free areas with very few tie points on the relatively feature-free glacial ice. The feature point density within the tie point generation parameters was changed from the default. This caused the total spatial distribution to be more evenly spread. The tie points were triangulated to give each point a latitude, longitude and elevation allowing a DEM to be generated. As a product of the remaining low tie point density areas within the image, sections of the image were given zero values by the DEM generation as the data were too sparse in these areas to be of sufficient quality and appear as blank sections.

4.3.2 Extracting ICESat and ASTER point data for accuracy validation.

GLAS ICESat laser altimeter elevation data from the GLA12 product were used to determined the systematic and residual error for the ASTER DEMs. The ICESat data were acquired in 2003, and the ASTER data were acquired between 2001 and 2005. For accuracy validation purposes the ICESat data were assumed to have true elevation values (ICESat accuracy is outlined in section 4.1.2). Extracting the point data required the DEMs to be displayed as raster files in ArcGIS and the ICESat data to be overlaid as a vector layer. The ICESat data format came with x,y co-ordinates and elevation data. Therefore the DEM elevation data corresponding to the x,y co-ordinates was extracted from the DEM using ArcGIS and exported to a compatible format. Due to the large amount of ICESat data available (Figure 4.4), accuracy assessments were undertaken in two ways.

1. To assess the total accuracy, for the lower Darwin Glacier ASTER DEM and the upper Darwin and Hatherton Glacier's ASTER DEM, approximately 10,000 and 20,000 ICESat elevation points respectively were available. A random smaller subset of elevation points was extracted to produce for both the DEMs. Both the systematic error and the residual error were calculated for the total data.

2. Along two different profiles. The individual ASTER DEMs and the averaged ASTER DEMs were compared against ICESat elevation points. In order to create profile graphs, ICESat point data along a linear track were chosen to generate a profile for each averaged ASTER DEM. The profiles were chosen based on the covering an area containing both low gradient glacial areas and high gradient ice free areas. The residual error was calculated for the profile data and the profile slope and elevation were used to validate correlations with the residual error.

4.3.3 Adjusting and averaging DEMs to increase accuracy

The systematic error was determined for all the ASTER DEMs by calculating the mean elevation difference between the ASTER and ICESat data (Figure 4.6). The ASTER DEMs were adjusted to remove the systematic error by adding the mean elevation difference to the entire DEM using the bandmath function in ENVI 4.3. Once the DEMs were adjusted to remove the systematic error the DEMs for each ASTER satellite image were stacked and averaged to increase the precision of an overall DEM.

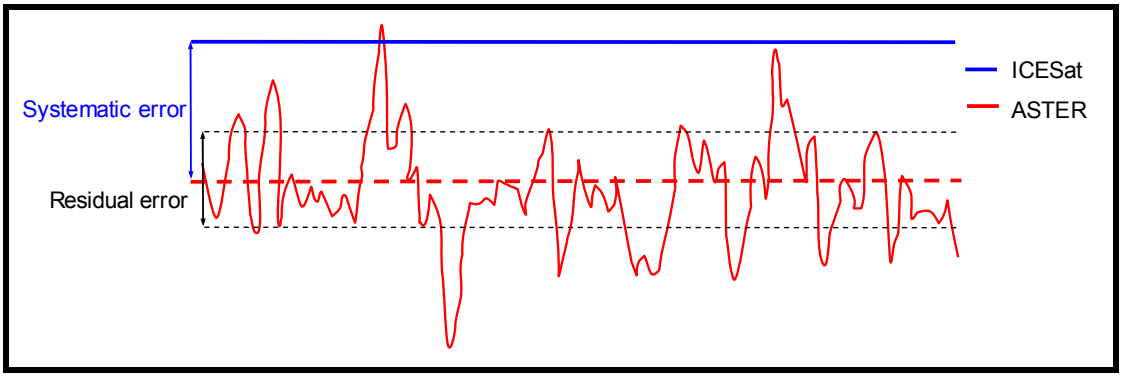

Figure 4.6: Schematic diagram showing systematic error (mean elevation difference) and residual error (elevation difference standard deviation) calculated from elevation difference between ASTER and ICESat elevation data.

By stacking and averaging the DEMs this reduced the residual error, providing that the errors were statistically indendent, hence increasing the accuracy. Each individual DEM covered a slightly different area due to the image acquisition (Figure 4.3), and blank sections produced due to lack of tie points. An average DEM was calculated for both the lower Darwin Glacier and the upper Darwin and Hatherton Glaciers. Zero values due to blank sections and areas not fully overlapped were eliminated from the averaging calculation to prevent zero values from affecting the average. An average DEM was calculated by layer-stacking individual DEMs and applying an ENVI 4.3 bandmath function to process and produce a resulting average DEM. To easily assess the areas with potentially the greatest precision due to different stack sizes within the average DEM, an overlap map was produced indicating the number of individual DEMs used in different areas of the average DEM.

4.3.4: Validating the accuracy of the averaged ASTER DEMs

The residual error was calculated for the profile and total data (Figure 4.6) by calculating the standard deviation of the elevation differences between the ICESat and ASTER DEM elevation points. This was done for both the individual DEMs (after adjustment) and the averaged DEMs.

Graphical analysis included plotting: a) histograms for the averaged DEM data to show the distribution of the elevation differences, b) profile elevation graphs to compare individual ASTER DEMs to averaged ASTER DEMs, c) profile elevation graphs to compare ASTER, RAMPv2 and ICESat data, d) profile elevation difference graphs, and e) correlation plots assessing whether the elevation difference was a function of slope and/or elevation.

4.4 Satellite map generation

Raw ASTER images were orthorectified using the two averaged DEMs. Because multiple ASTER images were required to cover the entire research area, co-registration of these images was used to finely align the images to one base image. Once finely aligned the images were mosaiced to create a true colour 15 m resolution satellite map of the Darwin-Hatherton glacial system.

4.4.1 Orthorectification of images

The original ASTER images (Figure 4.3) were orthorectified to a) to remove the topographic distortion due to the oblique look angle of the satellite, and b) to place the ASTER images into a projection, giving each pixel a geographic location. The DEM was required to remove the topographic distortion. Orthorectification required the raw LIA images to be distorted from the original format and geometrically corrected to the orthorectified format by resampling. There were three resampling options; nearest neighbour, bilinear interpolation and cubic convolution. Bilinear interpolation (Figure 4.7b) is a resampling technique that produces output pixel values by calculating the weighted average of the four nearest pixels based on the distance from the output pixel (Campbell, 1996). Bilinear interpolation was used for orthorectification.

4.3.2 Co-registration and mosaicing of images

Errors between individual orthorectified images occurred offsetting each orthorectified image by 1 - 4 pixels. To finely align all the orthorectified images to remove this offset, the images were co-registered. Co-registration finely aligned all images, allowing a smooth image mosaic and reducing extra potential error from the feature tracking process. This extra error was because the total ice movement was predicted to be between 50 – 250 m (3-16 pixels) over a one year time span (Hughes and Fastook, 1981) and without co-registration, the features were already offset due to processing error rather than ice flow.

ENVI 4.3 was used to co-registering all images (warp images) to a base image. A minimum of 3 manually selected tie points was required on areas that were stationary over the 4 year study period (e.g. ice free areas). However, between 6 and 10 tie points were collected per image with good spatial coverage from the ice free areas (Figure 4.7a). In order to simultaneously align all the tie points, a polynomial warp function, combining translation, rotation, change in size and types of skew (Rees, 2001) was applied to every pixel. The original image required resampling because each pixel in the new warped image did not corresponding directly to one pixel in the base image (Figure 4.7b). Bilinear interpolation resampling assigned new pixel values by calculating the weighted average of the four closest pixels (Campbell, 1996).

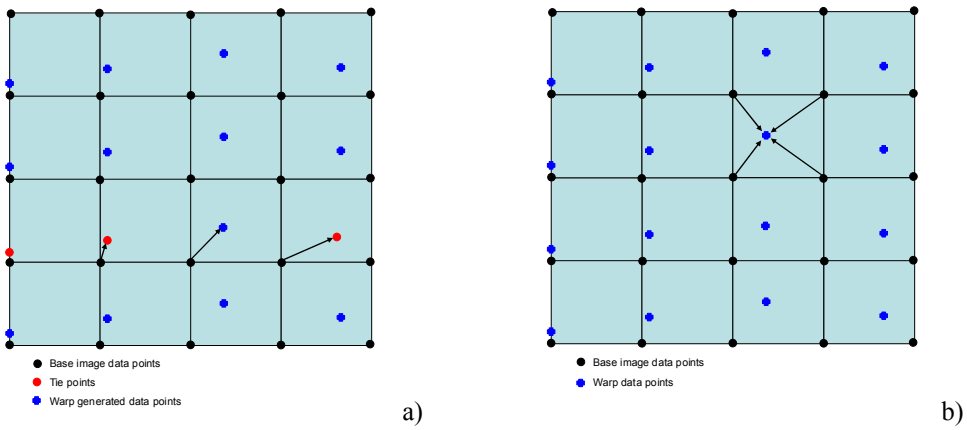

Figure 4.7: Principle of co-registration. a) Shows how tie points are used by the warp function to establish translation and rotation (in this example) and how this warp is projected to all other data points. b) Shows the bilinear interpolation method used to resample new data point values by averaging the four closest original pixel values (modified from Campbell, 1996).

Lastly the co-registered images were mosaiced to create a true colour, 15 m resolution ASTER satellite map of the entire Darwin-Hatherton glacial system area.

4.5 Feature tracking

The orthorectified and co-registered images were then used to assess feature tracking as a method for measuring ice velocity. The images required further pre-processing, which was followed by automated feature tracking.

4.5.1 Pre-processing of image files

For feature tracking, the areas of interest were the glacier surface, with a focus on small areas that had obvious features such as crevasses. Image pairs were selected for this purpose by subsetting the original orthorectified and co-registered images. Feature tracking required the image pairs to be in binary format, requiring a file conversion from the format used in orthorectification and co-registration. Therefore each subset image pair had to be exactly the same size (same number of samples and lines) and have the same upper left start pixel. This was paramount so that when the image was converted to binary format, the digital numbers for all pixels aligned (Figure 4.8). Subsetting was done in ENVI with nearest neighbour resampling, where pixels in the subsetted image receive their values from the closest pixel in the original image (Campbell, 1996). The final step was to convert the files from ENVI files to generic binary format.

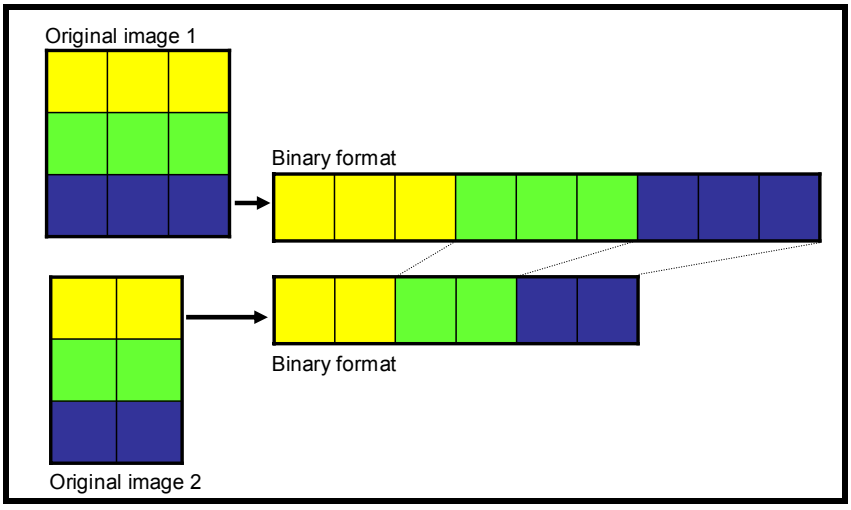

Figure 4.8: Example of offset that can occur if subsetting is not done correctly and images are not the same size. If the original images are of different sizes or of different areas, the binary formatting will cause the data to be offset. If this occurs, all feature tracking results will be incorrect.

4.5.2 Automated feature tracking

IMCORR software was used to undertake automated feature tracking by tracking the displacement of small grids of pixels between two images. The IMCORR programme uses a fast fourier transform-based version of a normalised cross-co-variance method (Bernstein, 1983). This method was initially designed to co-register images but if an independent co-registration method was used, this method could be used to track moving features. In order to run IMCORR, search parameters were specified using both the default values and specifically chosen values based on the expected displacement of the features. The parameters included a search and reference chip size, grid spacing of the chip, and x and y co-ordinate offset and subset pixel values (www.NSIDC.org, 2007).

The resulting IMCORR output determines displacement values, correlation strength and error values for every reference chip. The quality of the results was determined by the correlation strength (www.NSIDC.org, 2007). This was calculated by the IMCORR software and a result flag was given for chips that had acceptable correlation strengths. The correlation strength was calculated by:

$$\left[\frac{\text{peak correlation value} - \text{mean background value}}{\text{std.dev. of background values} + 0.2 \times (\text{no. of ``large'' values} > 3 \text{ pixels away from peak} - 1.0)}\right].$$

Chips with invalid result flags and with abnormally high error values above were removed as well as chips with displacement values greater than one pixel and less than 16 pixels per year. To visualise chip displacements, successful displacement vectors were projected onto an orthorectified, co-registered, subsetted satellite image using line arrows to show the direction of flow as well as the velocity in pixels per year.

Feature tracking on the Darwin-Hatherton glacial system as a method for measuring surface velocity was unsuccessful. IMCORR did produce pixel chips that had correlation strengths which partly satisfied the program, resulting in success flags. However when the successful chips were displayed as velocity arrows indicated flow direction and displacement, there were obvious errors showing an almost random display of flow direction and an unlikely magnitude in displacement.

4.5.3 Limitations causing feature tracking to fail

In order for feature tracking to work, patterns of pixels over features needed to be identified and be displaced over a period of time. Therefore the ultimate limitation causing feature tracking to fail using ASTER satellite images of the Darwin-Hatherton glacial system is that there is a lack of trackable features at 15 m resolution that.

The Darwin-Hatherton glacial system has less identifiable features compared to other glaciers that have been feature tracked using 15 m ASTER satellite imagery (Mayer et al. 2006, Berthier et al. 2003, Stearns et al. 2005, Stearns and Hamilton 2005). Certain features pose problems for feature tracking. Melt water ponds and streams are inadequate features because they are not accurate indicators of ice flow. Medial moraines, which are aligned parallel to flow, are accurate indicators of ice flow. However on the Darwin-Hatherton glacial system and at 15 m resolution while they are identifiable to the eye, they are not crisp enough to provide enough detail to be automaticaly feature tracked. Crevasses that are on grounded ice pose the question of the accuracy of the velocity measurements, as areas of crevasses tend to always occur in the same place on a glacier due to the stresses that are acting on that particular area. Crevasses can also distort due to the surrounding stresses with the potential to cause the crevasses to be unidentifiable over the time period. However transverse crevasses on ungrounded ice can be good features to track (Lucchitta and Ferguson, 1986). These crevasses are possibly produced due to tidal flexure, and flow with the surrounding ice which makes them accurate indicators of ice flow.

There are a number of possible reasons why the features that could be identified by the eye didn't work. Firstly the ice velocity was not fast enough to displace the features far enough within the time period to be distinguished from the pre-processing displacement error that exists (approx $\pm$ 4 pixels), or the features distorted too much within this time period to be identifiable. Secondly the features were suitable, but the differences in illumination of the images due to the change in sun angle caused the features pixel values to alter. This could have caused enough of a pixel value change that the feature could not be identified by the automated feature tracking software. A combination of all these reasons could have also been possible.

Chapter 5: DEM generation and a satellite image of the Darwin-Hatherton glacial system.

5.1 ASTER DEM generation by stacking and averaging.

5.1.1 Individual ASTER DEMS

For each ASTER image (Table 4.3) a 45 m resolution DEM is generated (Figure 5.3 and 5.4) by stereoscopy using the ERDAS Leica Photogrammetry Suite. The ASTER DEMs are divided into DEMs covering the lower Darwin Glacier (Figure 5.1) and DEMs covering the upper Darwin and Hatherton Glaciers (Figure 5.2) and are kept separate for further DEM processing and analysis.

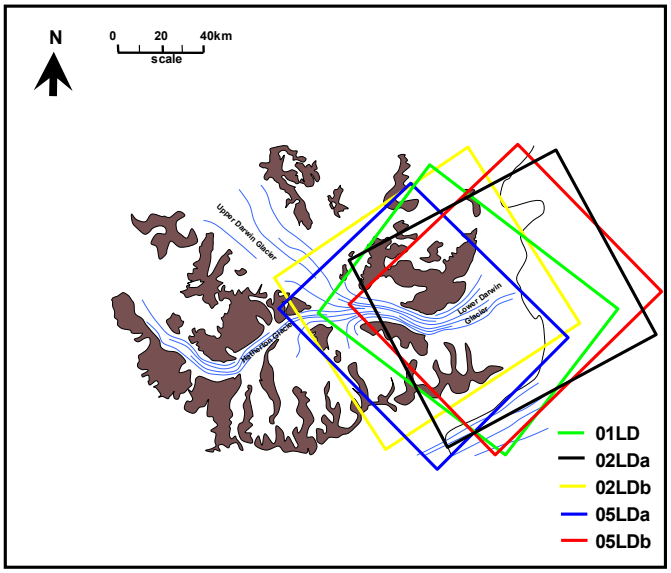

Figure 5.1: Location of the individual lower Darwin Glacier DEMs.

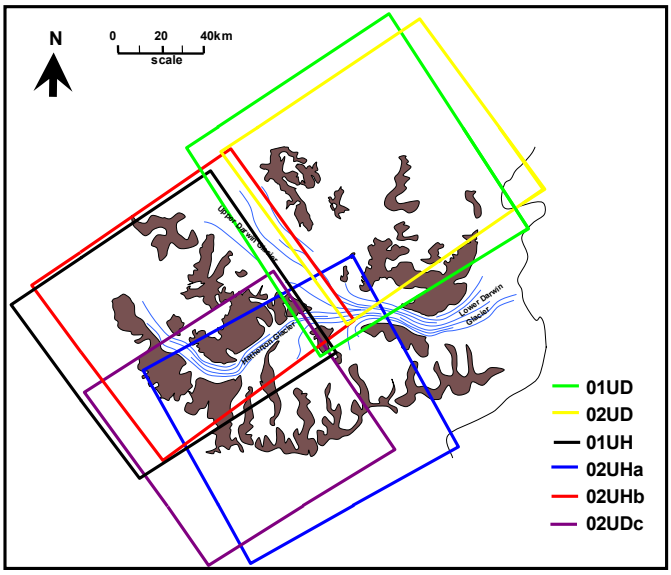

Figure 5.2: Location of the individual upper Darwin and Hatherton Glacier DEMs

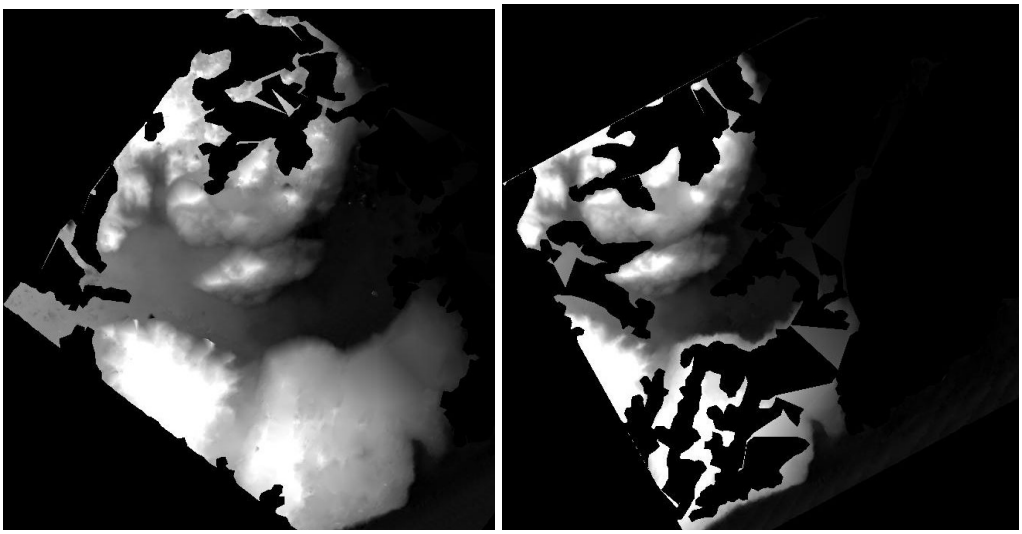

01LD 02LDa

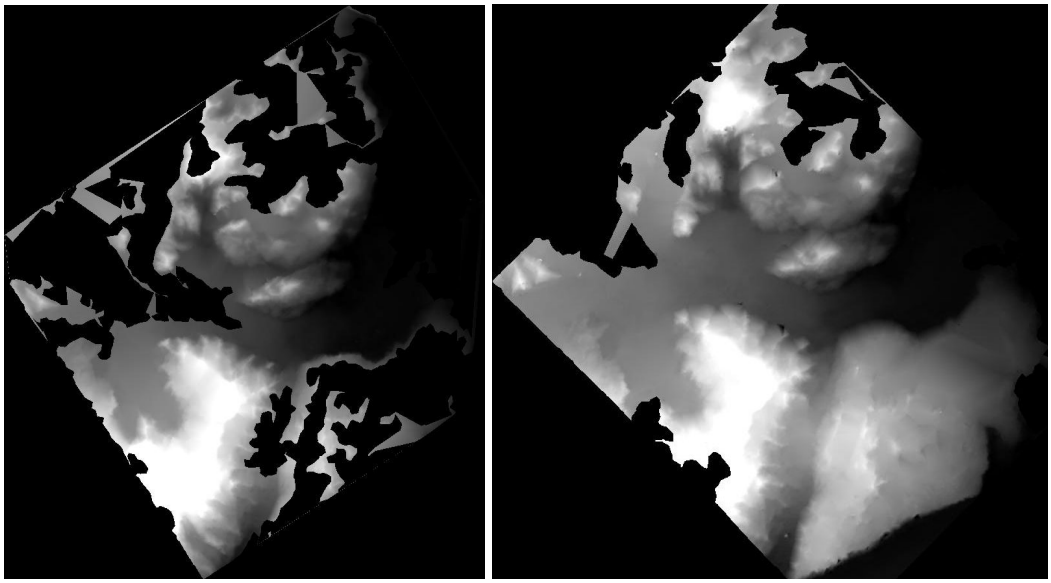

02LDb 05LDa

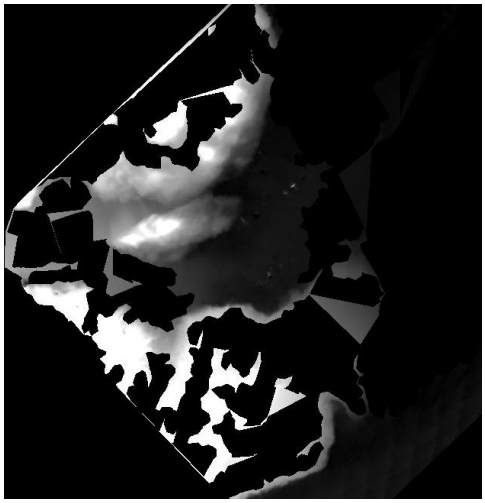

05LDb

Figure 5.3: Raw individual DEMs for the lower Darwin Glacier ASTER satellite images .

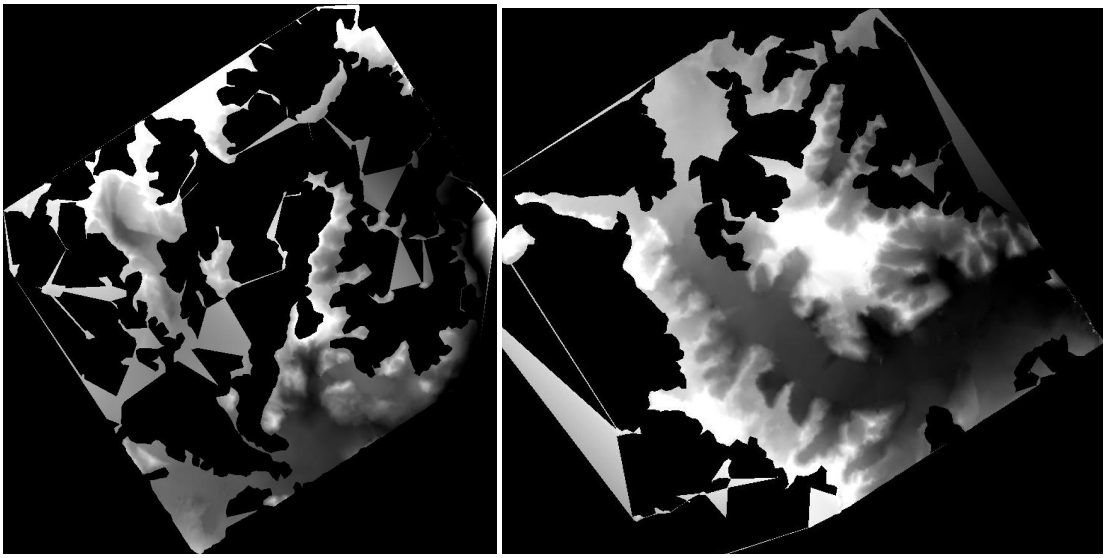

01UD 01UH

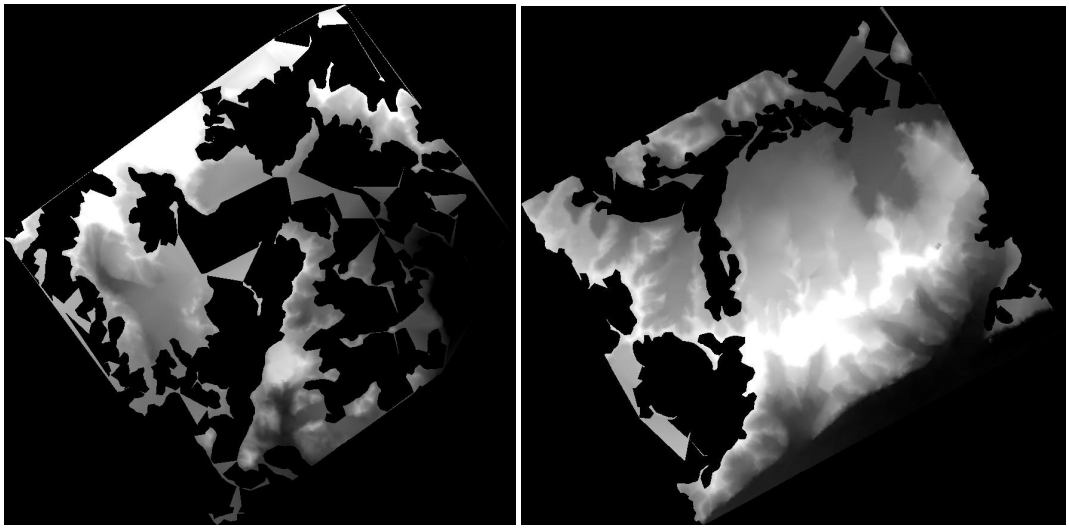

02UD 02UHa

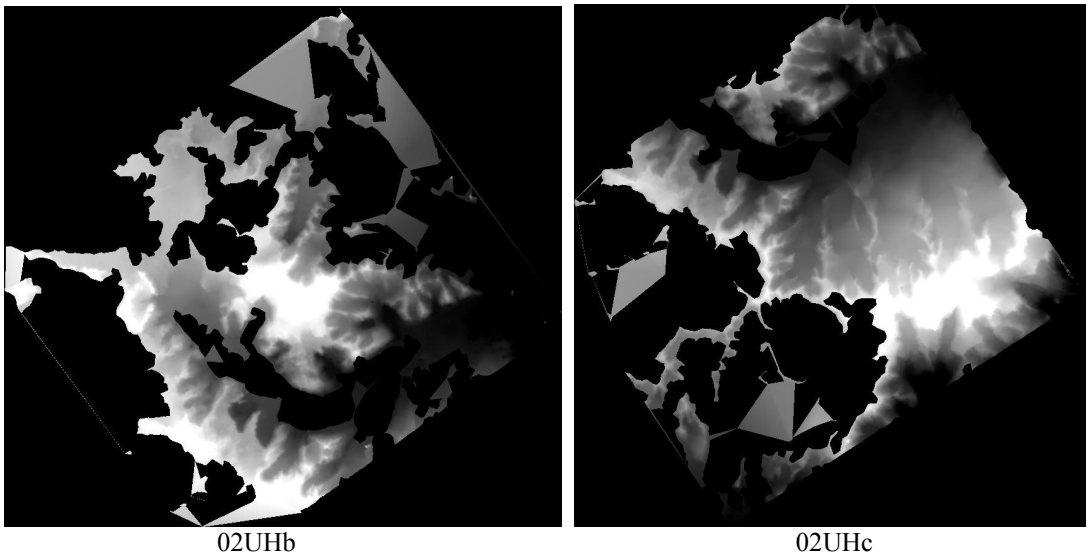

02UHb 02UHc

Figure 5.4: Raw individual DEMs for the upper Darwin and Hatherton Glaciers ASTER satellite images.

The 45 m resolution ASTER DEMs show considerable variation in blank areas. In general the lower Darwin Glacier DEMs (Figure 5.4) have fewer blanks than the upper Darwin and Hatherton Glaciers DEMs. Reasons for the location, and distribution of the blank areas produced in DEM generation are due to the quality of the ASTER satellite image e.g. cloud cover, image contrast (image contrast is very poor over snow-covered areas), and location and distribution of GCPs and tie points.

In the lower Darwin Glacier the DEMs with the least blanks areas are 01LD and 05LD. The DEMs with high areas of blanks are 02LDa, 02LDb, and 05LDb. On visual inspection of the true colour ASTER satellite images (Appendix 1), the images with high areas of blanks have small areas of cloud in the ASTER image which reduced the amount of surface area that was available for tie point generation. All images used the same GCP located at the Foggydog Glacier terminus (Figure 4.5). In the upper Darwin and Hatherton Glaciers there are no DEMs with few areas of blanks or images with any cloud cover. However the DEMs that cover the upper Darwin Glacier have more blank areas than the DEMs that cover the upper Hatherton Glacier. The GCPs used for these areas came from the same topographic map source (USGS, 1963) but were from different areas, with the upper Darwin Glacier GCP located on Tentacle Ridge (Figure 4.5) and the upper Hatherton Glacier GCP located on Junction Spur (Figure 4.5).

5.1.2 Systematic error

The systematic error (Figure 4.6) can partially be used to validate the accuracy of the ASTER DEMs along with the residual error (Figure 4.6). The DEMs are adjusted to remove the systematic error, increasing the accuracy of the ASTER DEMs. The systematic error is determined by calculating the mean elevation difference between the ASTER DEM and ICESat elevation data (Table 5.1). When calculating the systematic error, outlying elevation differences due to artifacts of the remote sensing processing are removed. The threshold to determine and remove outliers is $\pm$ 300 m elevation difference. This is chosen as a logical threshold value based on observations of elevation differences and precious research on ASTER DEMs.

Table 5.1: Systematic error for individual DEMs derived from mean elevation differences between the ASTER and ICESat data.

Individual DEMs: Lower Darwin Glacier	Systematic error (m)		Individual DEMs: Upper Darwin and Hatherton Glaciers	Systematic error (m)
01LD	-8		01UD	62
02LDa	24		02UD	-9
02LDb	4		01UH	30
05LDa	-31		02UHa	49
05LDb	-45		02UHb	<1
			02UHc	12

The DEMs that cover the lower Darwin Glacier have positive and negative systematic errors and vary by 69 m (Table 5.1). The DEMs from 2002 have positive systematic error and the DEMs from 2001 and 2005 have negative systematic errors. The DEMs from 2001 and 2002 have smaller systematic errors than the DEMs from 2005. The DEMs that cover the upper Darwin and Hatherton Glaciers have positive and negative systematic errors and vary by 61 m (Table 5.1) The DEMs are all from 2001 and 2002. Overall the systematic error can be generalised to be within $\pm$ 100 m.

The reason for the systematic error and the variation in systematic error is due GCP acquisition. The GCP used for the lower Darwin Glacier DEM (Figure 4.5) was acquired with a hand held Garmin 72 GPS which had a horizontal error of $\pm$ 11.4 m. The GCPs used for upper Darwin and Hatherton Glaciers DEM (Figure 4.5) were acquired from the digitized version of the ST 57-60/13* topographic map from the Antarctica 1:250,000 Reconnaissance Series (USGS, 1963). Due to the resolution of this map, locating the GCPs onto the ASTER satellite images produces error. The errors produced from the accuracy of GCPs in both the lower Darwin Glacier and the upper Darwin and Hatherton Glaciers have the potential to produce the magnitude of errors that are measured as systematic error (Table 5.1). The systematic error is also due to the quality of the DEM generation and the number of GCPs used. Due to availability and quality, only one GCP was used for each individual DEM. The quality of the DEM has a direct relationship with the number of GCPs used (San and Suzen, 2005).

5.1.3 Stacked and averaged ASTER DEMs

The adjusted DEMs are used to calculate two averaged DEMs (Figure 5.5) which are the final DEM product and can be used in further research studies. The Darwin-Hatherton glacial system is divided to create an averaged DEM for the lower Darwin Glacier (Figure 5.6), and an averaged DEM of the upper Darwin and Hatherton Glaciers (Figure 5.7). The DEM coverage slightly overlaps (Figure 5.5) but the division of the research area is based on having two different sources of GCPs which are kept separate so as not to introduce further error due to differences in the GCP accuracy (Figure 4.5). The averaging of individual DEMs reduces the residual error. The reduction of the residual error is a function of how many DEMs overlap allowing averaging providing that the errors are statistically independent between the individual DEMs. The amount of overlap is primarily due to the footprint of each ASTER satellite image (Figure 5.1 and 5.2), but is also determined by the amount of blanks present in each individual DEM (Figure 5.3 and 5.4). The overlap can be seen by a corresponding overlap map (Figure 5.7 and 5.9).

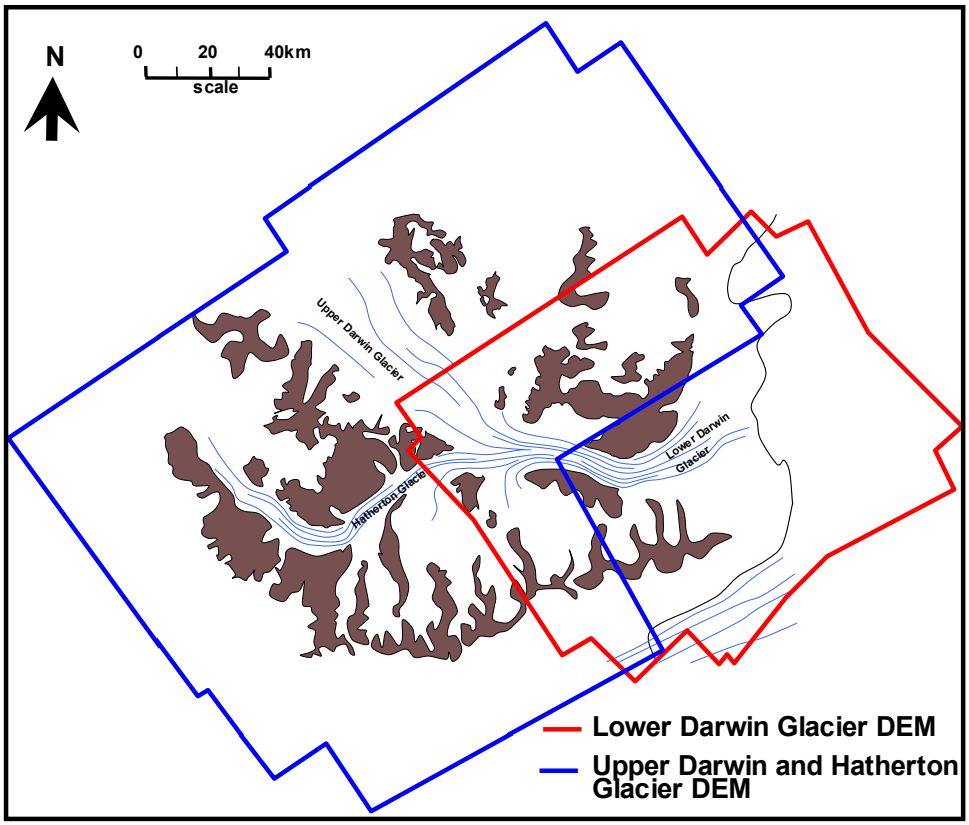

Figure 5.5: Location of the averaged DEMs

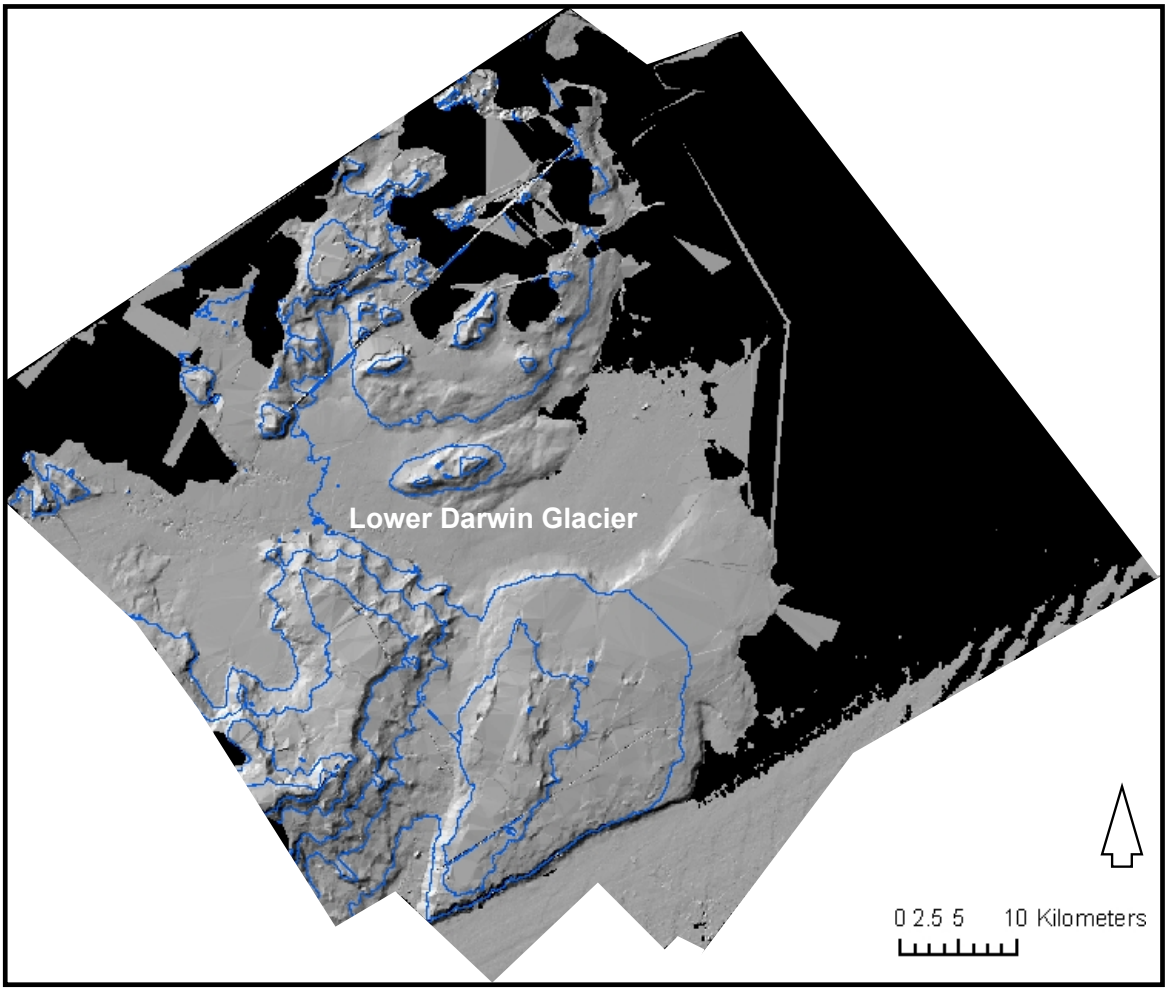

Figure 5.6: DEM of the lower Darwin Glacier at 45 m resolution. Averaged from five individual ASTER DEMs. Hill-shade version with 500 m interval topographic contours.

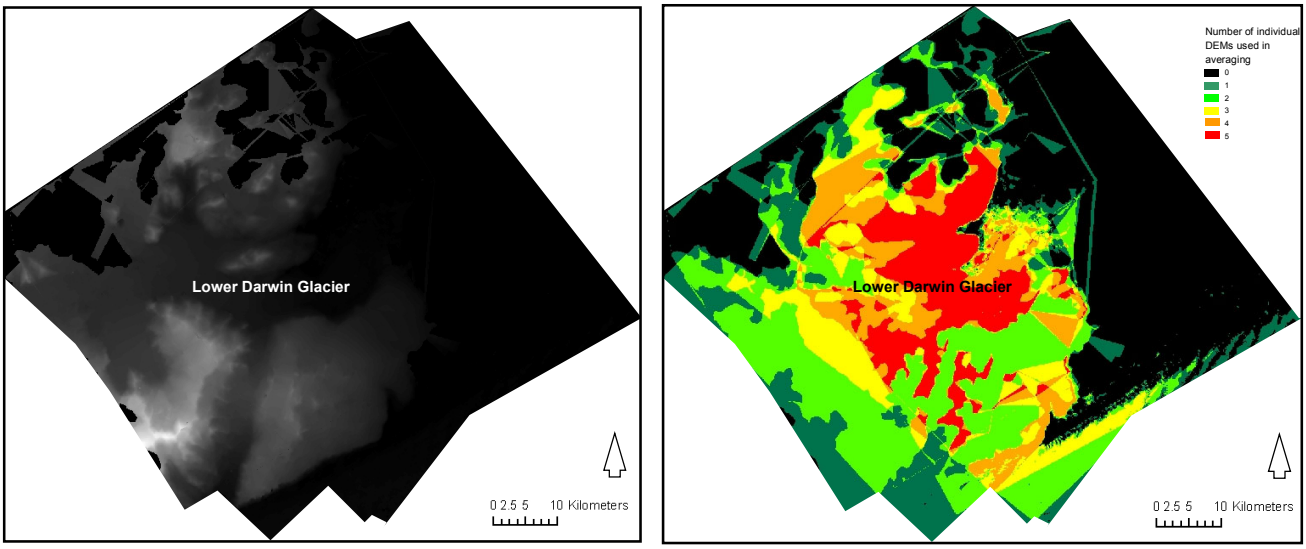

Figure 5.7: Raw DEM (left) and overlap map for lower Darwin Glacier DEM (right).

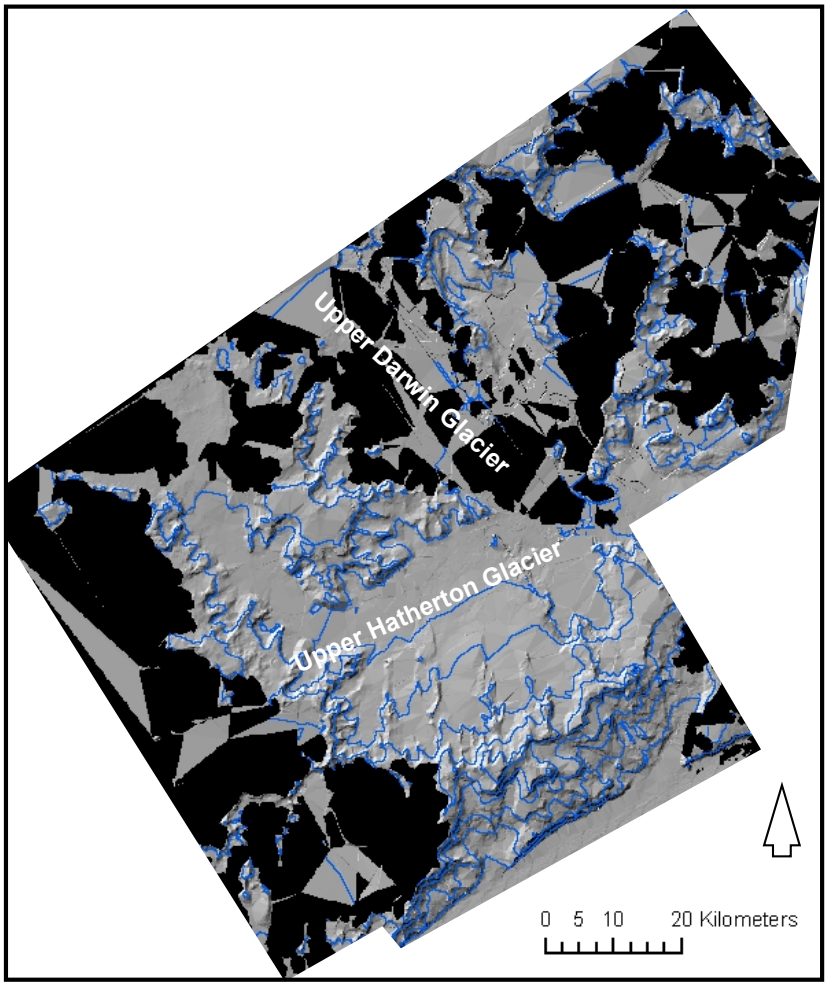

Figure 5.8: DEM of the upper Darwin and Hatherton Glaciers at 45 m resolution. Averaged from six individual ASTER DEMs. Hill-shade version with 500 m interval topographic contours.

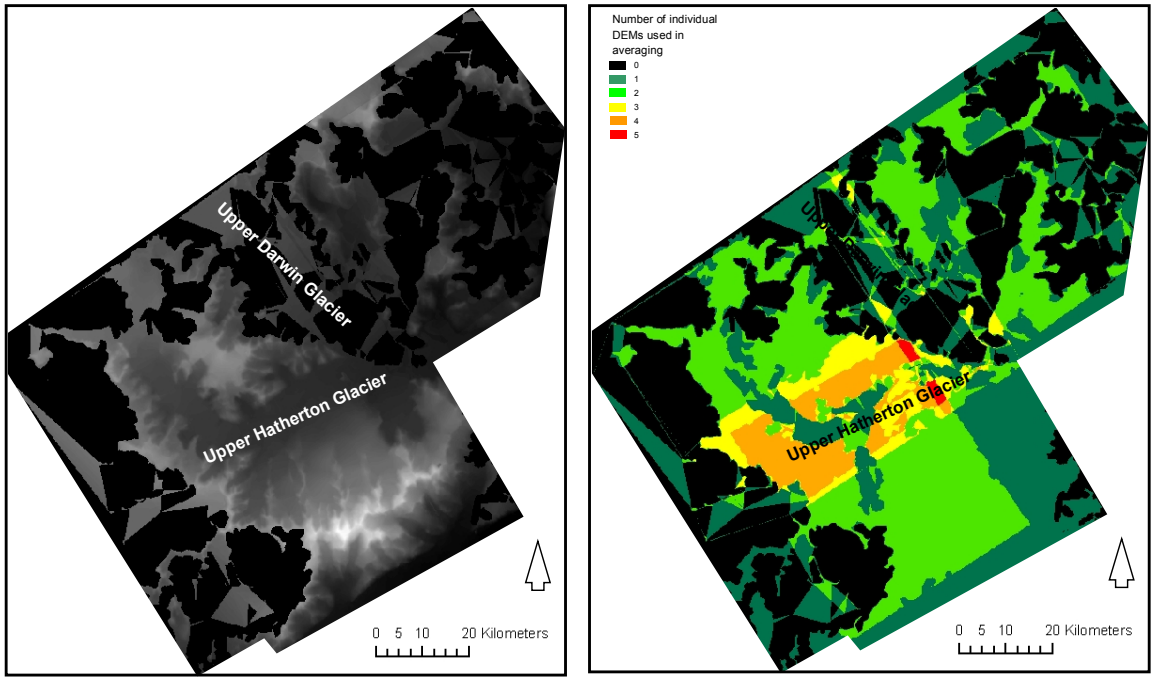

Figure 5.9: Raw DEM (left) and overlap map for upper Darwin and Hatherton Glacier DEM (right).

The lower Darwin Glacier 45 m resolution DEM provides a total coverage of the area, and almost total coverage of the glacier surface (Figure 5.6). The average DEM is derived from 5 individual DEMs with high overlap, seen by the large areas of red, orange and yellow on the overlap map (Figure 5.7). The upper Darwin and Hatherton Glacier 45 m resolution DEM provides a moderate total coverage of the area, with good coverage over the upper Hatherton Glacier and moderate coverage over the upper Darwin Glacier (Figure 5.8). The average DEM is derived from 6 individual DEMs with moderated overlap, seen by the few areas of red, orange and yellow in the overlap map (Figure 5.9). Despite having 6 individual DEMs, the maximum overlap in the upper Darwin and Hatherton was 5. For both averaged DEMs there are areas that are not covered by any individual DEMs. These areas remain blank/black on the average DEMs.

By projecting the DEMs as hill-shades we can see that both DEM surfaces are smooth without any major spikes, troughs or steps indicating the high quality of the averaged DEMs. The adjustment of individual DEMs to remove systematic error before averaging helps to smooth the DEM surface. Without the removal of systematic error, steps in the DEM surface would have been visible indicating where the overlap of the individual DEMs changes.

5.2 Validating the ASTER DEM accuracy

In order to validate the ASTER DEM accuracy, independent elevation data from the GLAS sensor aboard ICESat is used (Figure 4.4). ICESat is assumed to be correct for purposes of this research due to having considerably higher accuracy than both the ASTER and RAMPv2 DEMs, with a systematic error of 9.6 cm and a residual error of $\pm$ 4.9 cm (Brenner et al., 2007). ICESat data provides approximately 10,000 elevation points over the lower Darwin Glacier DEM (Figure 5.10a) and 20,000 for the upper Darwin and Hatherton Glacier DEM (Figure 5.11a). From the data set a smaller random subset is extracted and a profile for each DEM is also extracted (Figure 5.10b and 5.11b).

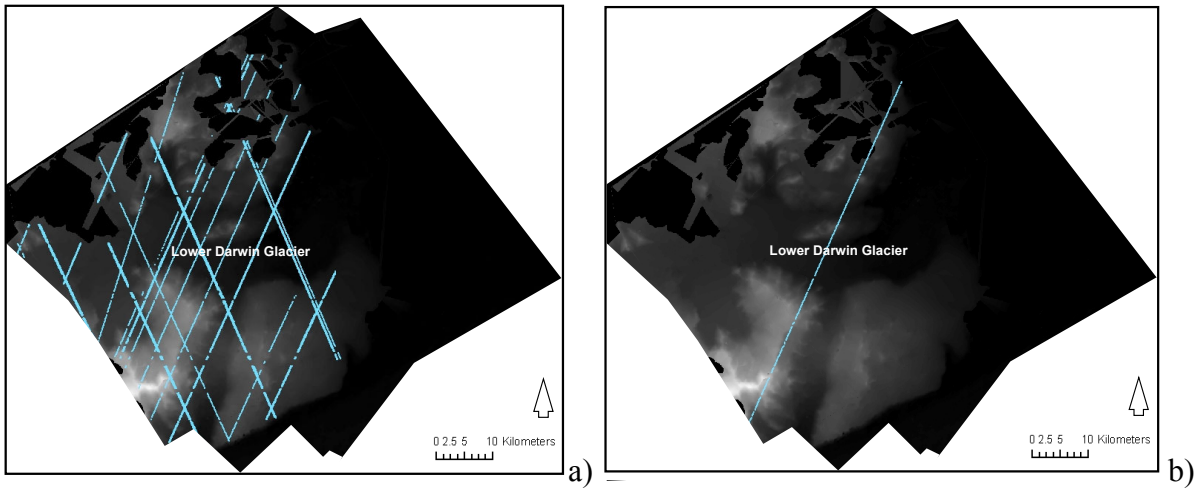

Figure 5.10: Averaged ASTER DEM of the lower Darwin Glacier showing location of a) total ICESat points used for comparison and b) profile ICESat points.

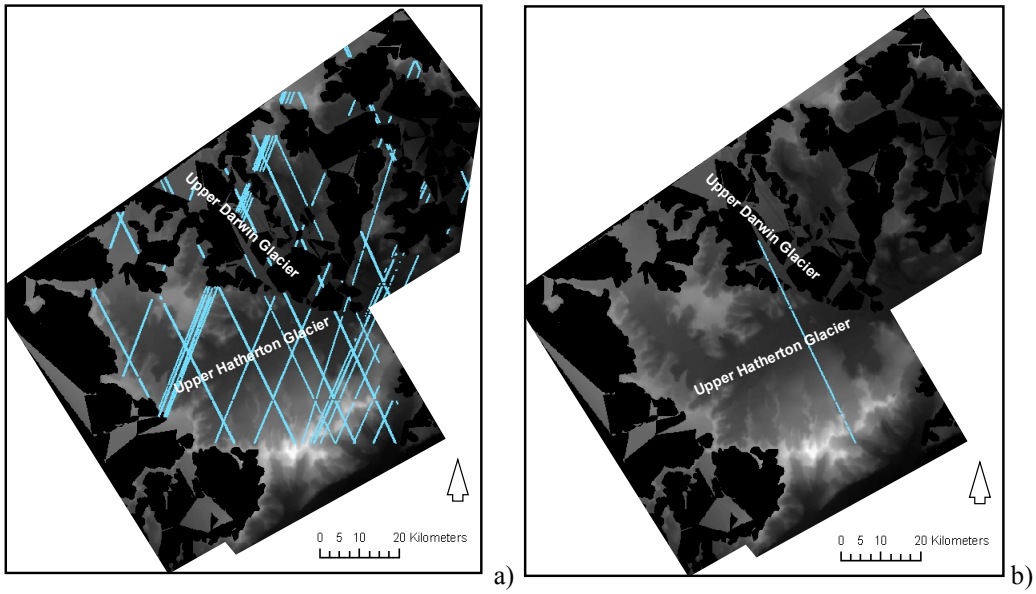

Figure 5.11: Averaged ASTER DEM of the upper Darwin and Hatherton Glaciers showing location of a) total ICESat points used for comparison and b) profile ICESat points.

When using the profile data to compare the individual DEMs to the stacked and averaged DEMs (Figure 5.12 and 5.13), the averaging process is shown to be successful because the averaged DEM is plotted centrally within the individual DEM profiles. There are obvious random errors in some of the individual DEMs e.g. between 55 and 60 km in Figure 5.12 and between 34 and 36 km in Figure 5.13. The averaged DEM profile in these areas shows a smoothed profile reducing this error. IN some areas of the profile the averaged DEM is a product of the stacking and averaging of up to 5 individual DEMs, but in other areas the average DEM is the same as the single individual DEM available for that area.

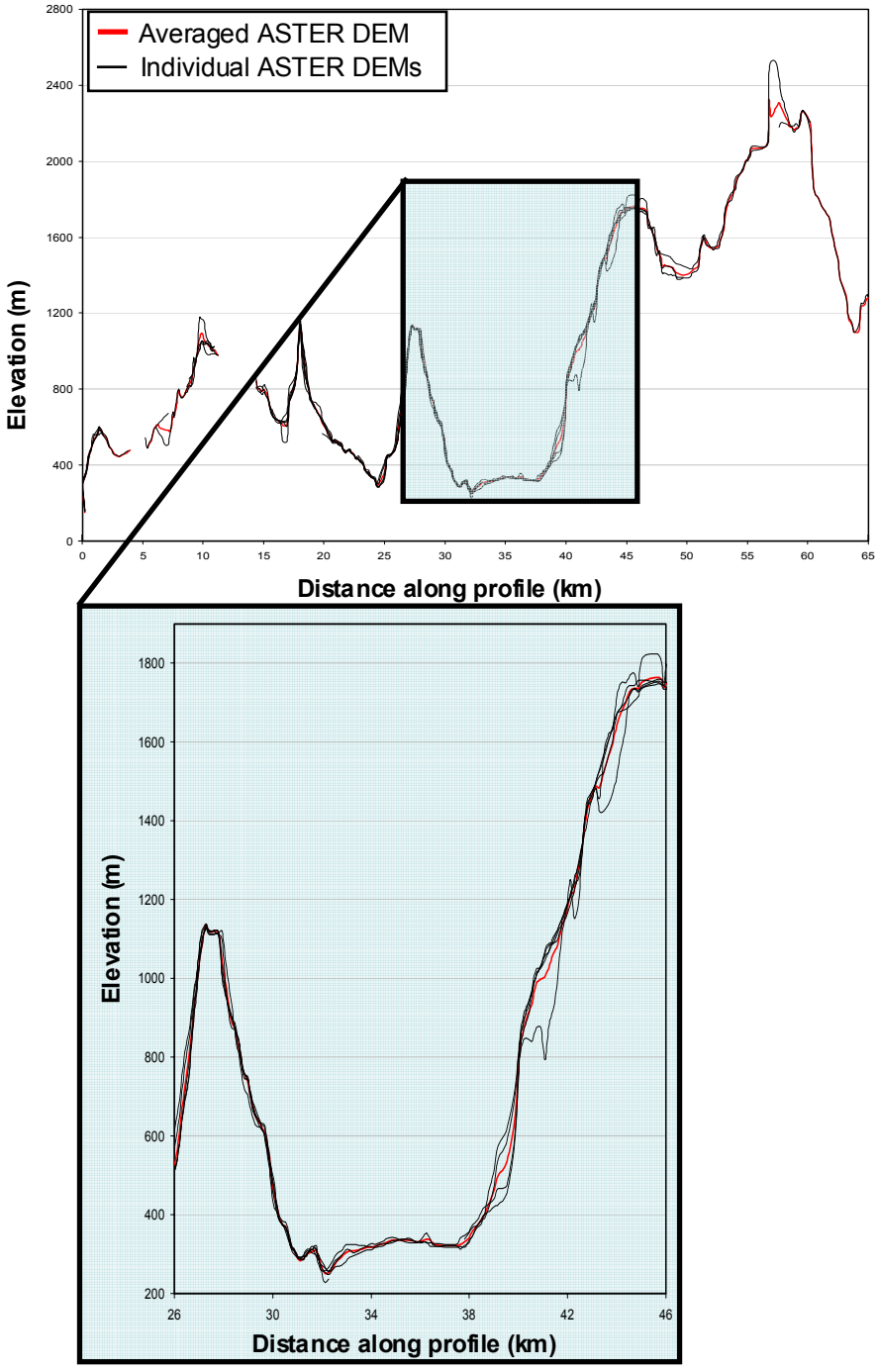

Figure 5.12: Lower Darwin Glacier DEM profile. Comparison between the individual and averaged ASTER DEMs.

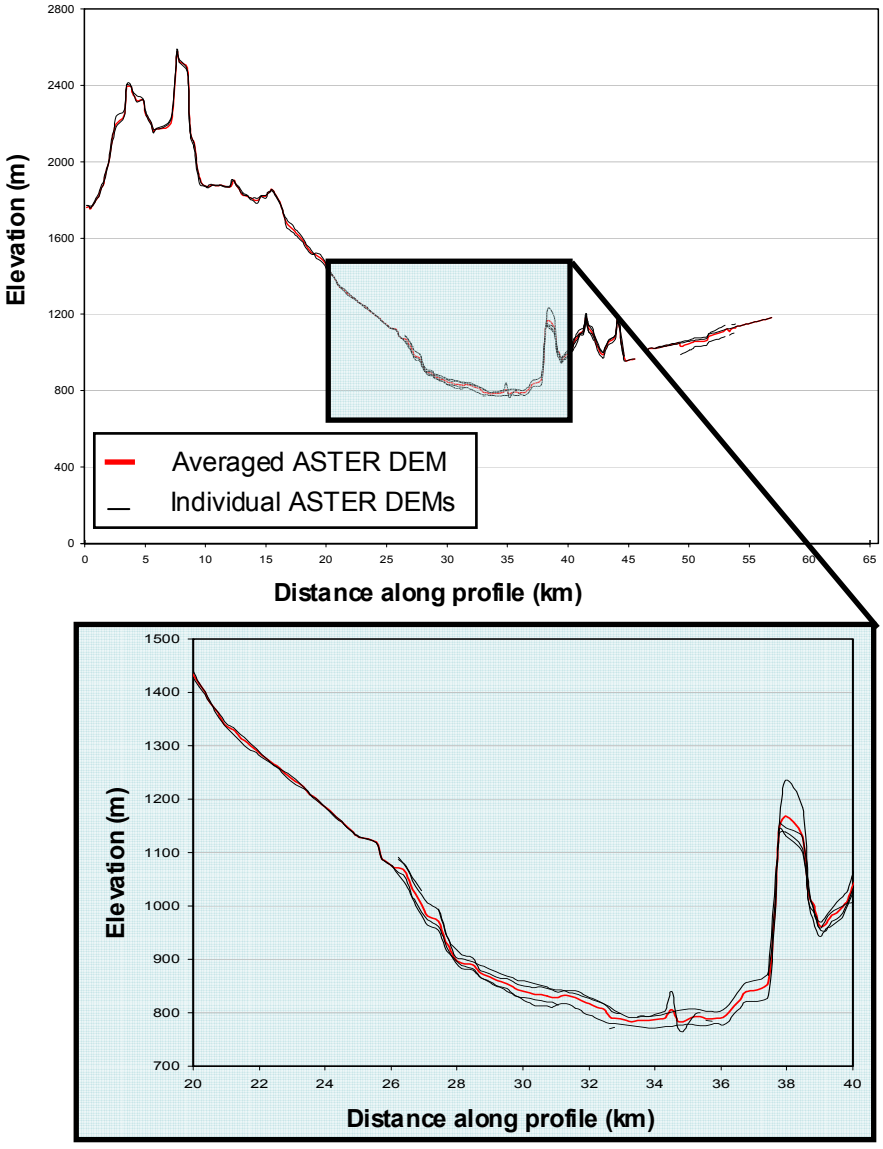

Figure 5.13: Upper Darwin and Hatherton Glaciers DEM profile. Comparison between the individual and averaged ASTER DEMs.

5.2.2 Residual error

The residual error can be used to validate the accuracy of the ASTER DEM and is determined for both the total data and profile data by calculating the elevation difference standard deviation between the ASTER and ICESat data (Table 5.2). Histograms of the elevation difference are plotted to visually show the elevation difference distribution (Figure 5.14 and 5.15). The residual error is used for a number of accuracy comparisons: a) between the individual DEMs, b) between the two averaged ASTER DEMs, c) between the averaged ASTER DEMs and the existing RAMPv2 DEM, and d) between ASTER DEMs of the Darwin-Hatherton glacial system and for an area of similar terrain of the Swiss Alps (Kaab, 2005).

Table 5.2: Residual error for ASTER DEMs. Residual error is determined by calculating the elevation difference standard deviation between the ASTER DEM and ICESat laser altimeter elevation. Note that the profile did not overlap one of the individual DEMs in the upper Darwin Glacier, which is allocated as N/A.

Lower Darwin Glacier	Residual error (m)	Upper Darwin and Hatherton Glacier	Residual error (m)
Total		**Total**	
Averaged DEM	**± 9**	**Averaged DEM**	**± 37**
Individual DEM : 01LD	± 26	Individual DEM : 01UD	± 13
Individual DEM : 02LDa	± 17	Individual DEM : 02UD	± 29
Individual DEM : 02LDb	± 16	Individual DEM : 01UH	± 14
Individual DEM : 05LDa	± 20	Individual DEM : 02UHa	± 14
Individual DEM : 05LDb	± 22	Individual DEM : 02UHb	± 13
		Individual DEM : 02UHc	± 14
Profile		**Profile**	
Averaged DEM	**± 37**	**Averaged DEM**	**± 33**
Individual DEM : 01LD	± 40	Individual DEM : 01UD	± 22
Individual DEM : 02LDa	± 23	Individual DEM : 02UD	N/A
Individual DEM : 02LDb	± 23	Individual DEM : 01UH	± 21
Individual DEM : 05LDa	± 41	Individual DEM : 02UHa	± 42
Individual DEM : 05LDb	± 51	Individual DEM : 02UHb	± 24
		Individual DEM : 02UHc	± 37

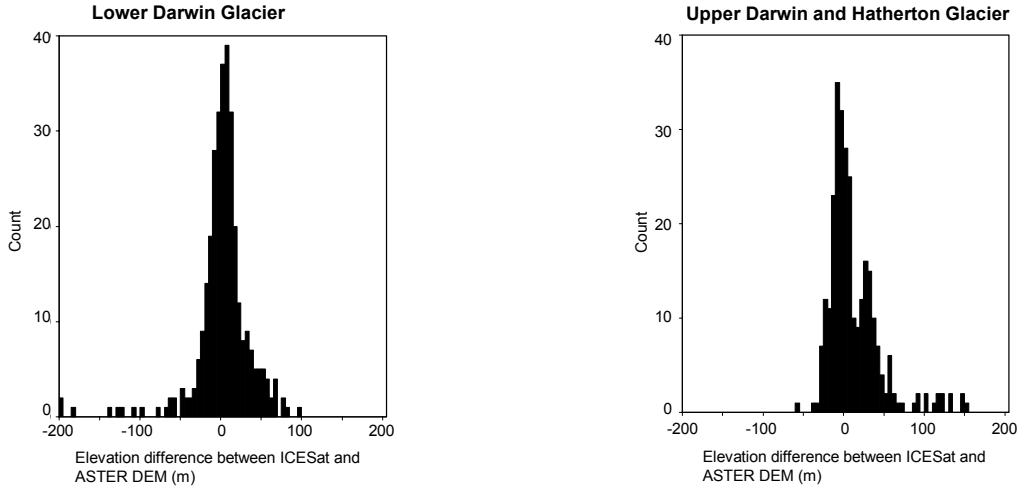

Figure 5.14: Histograms showing distribution of elevation difference for the profile data.

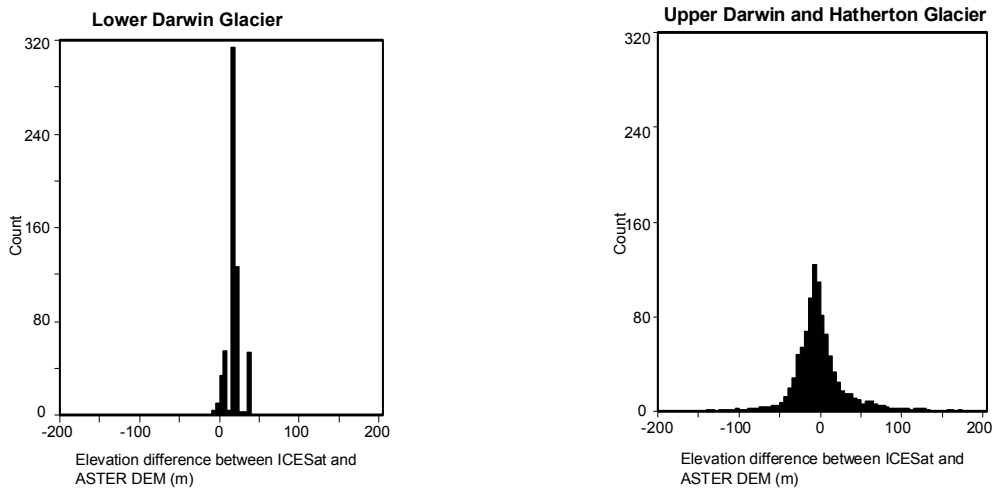

Figure 5.15: Histograms showing distribution of elevation difference for the total data.

In the lower Darwin Glacier DEM, the residual error for the averaged DEM total data is $\pm$ 9 m (Table 5.2). This is less than the residual errors for of the individual DEMs. This suggests that the stacking and averaging process was very successful in increasing the accuracy by decreasing the residual error. The residual error for the averaged DEM profile data is $\pm$ 37 m (Table 5.2). The profile has a greater residual error than the total, which suggests that there is spatial variation in the residual error over the lower Darwin Glacier DEM. This is to be expected because there is difference in residual error for each individual DEM (with a variation of 10 m for the total data), and the stacked and averaged DEM has a difference in overlap by the individual DEMs (Figure 5.7). The histogram for the total data of the lower Darwin Glacier DEM (Figure 5.15) shows a small systematic error remaining, which suggests that the method of adjusting all the individual DEMs before stacking and averaging does not completely remove the systematic error for the averaged DEM.

In the upper Darwin and Hatherton Glaciers DEM, the residual error for the averaged DEM total data is $\pm$ 37 m (Table 5.2). This is slightly more than the all of the residual errors of the individual DEMs. However the residual error for the averaged DEM profile is less than two of the individual DEMs. This suggests that the stacking and averaging process was not as successful for the upper Darwin and Hatherton Glaciers DEM as is was for the lower Darwin Glacier DEM. This also suggests that there is spatial variation within the DEM with some areas being more successfully averaged than others. This is possibly because some areas in the individual DEMs were statistically correlated. This means that instead of the averaging process reducing the residual errors (if they were statistically independent), the averaging process instead increased the residual errors.

5.2.2 Accuracy as a function of slope and elevation

The accuracy of remotely sensed elevation has been shown to be a function of slope (Bamber and Gomez-Dans 2005, Brenner et al. 2007). To assess whether the accuracy of the Darwin-Hatherton glacial system ASTER DEMs are a function of slope or elevation, the elevation difference between ASTER and ICESat profile data are tested against profile slope and elevation (Figure 5.16). By applying a linear coefficient, R^2 values are used to validate the correlation between elevation difference and slope/elevation.

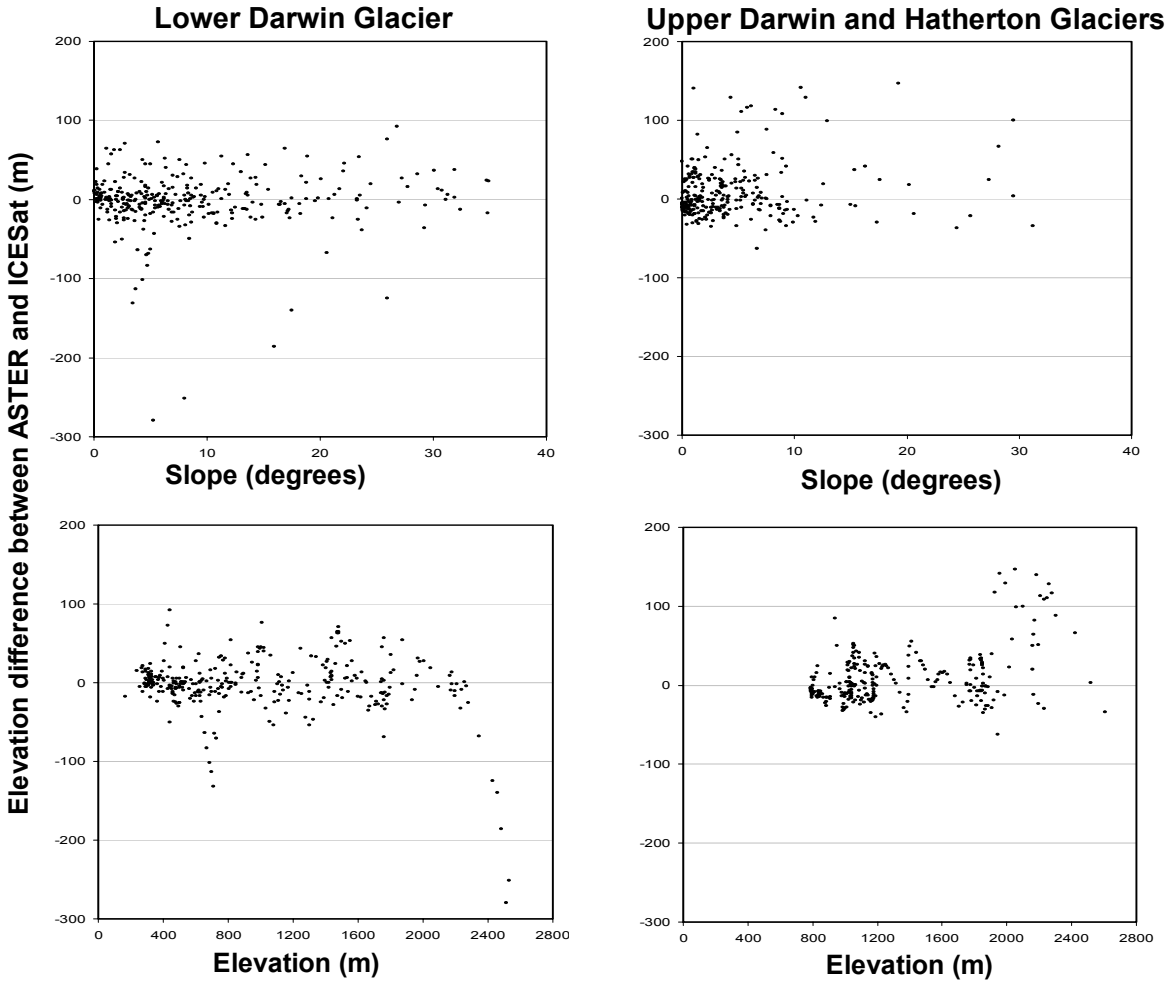

Figure 5.16: Correlation plots comparing profile slope and profile elevation against elevation difference.

Weak R^2 values suggest that there is no significant correlation for slope or elevation (Figure 5.16) with R^2 values of <0.01 (slope), and 0.04 (elevation) for the lower Darwin Glacier DEM and 0.02 (slope), and 0.16 (elevation) for the upper Darwin and Hatherton Glaciers DEM. Visual analysis of the correlation plots shows an auto-correlation within the elevation plots in both the lower Darwin Glacier and the upper Darwin and Hatherton Glaciers DEMs (Figure 5.16). Both show an auto correlation with amplitude of approximately 50 m (elevation difference) and a frequency of approximately 200 m (elevation).

The reason for this auto correlation is due to surface undulations that occur with an approximate frequency of every 200 m in elevation. The reason for the surface undulations is not known but is likely to be a product of glacial ice flow mechanisms. The undulations are accepted as true (and not due to the measurement error) due to the high accuracy observed by the ICESat data which has been shown to have a systematic error of 9.6 cm and a residual error of $\pm$ 4.9 cm (Brenner et al., 2007). The reason the undulations cause an auto-correlation is because the ICESat data is accurate enough to observe the undulations but the ASTER DEM generation partially tends to average out the surfaces that undulate with this amplitude and wavelength (Figure 5.20 – enlargement).

5.2.3 Comparison of the ASTER DEM with an existing DEM.

An existing RAMPv2 200 m resolution DEM (www.nsidc.org, 2007) covers the Darwin-Hatherton glacial system (Figure 5.17b and 5.18b). This RAMPv2 DEM has been validated to show vertical errors to be greater than 100 m (Bamber and Gomez-Dans, 2005). Therefore the new 45 m ASTER DEMs (Figure 5.17a and 5.18a) provide improved DEMs for the Darwin-Hatherton glacial system. In order to compare the existing DEM with the new DEM, a difference image (Figure 5.17c and 5.18c) is generated by subtracting the RAMPv2 DEM from the ASTER DEM, and profile graphs visually show the difference between ICESat, ASTER and RAMPv2 elevation data (Figure 5.19 and 5.20). The residual error (Table 5.3) is calculated for the ASTER and RAMPv2 DEMs from ICESat elevation data and histograms plot the elevation difference data (Figure 5.17d and 5.18d).

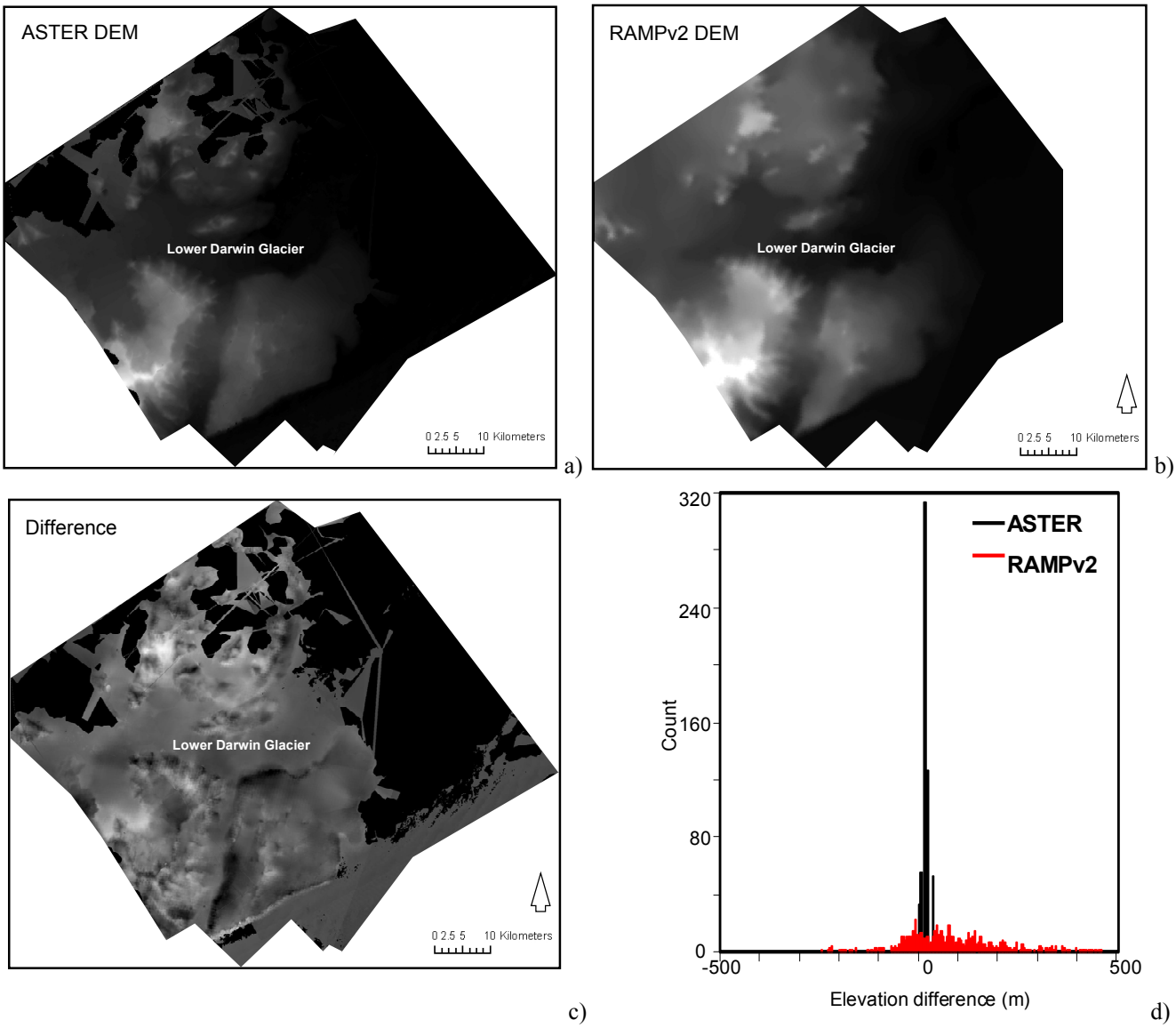

Figure 5.17: Comparison between the ASTER and RAMPv2 DEM in the lower Darwin Glacier. a) ASTER DEM. b) RAMPv2 DEM, c) Difference between ASTER and RAMPv2 DEMs, d) Histogram of elevation difference from ICESat data for both ASTER (black) and RAMPv2 (red).

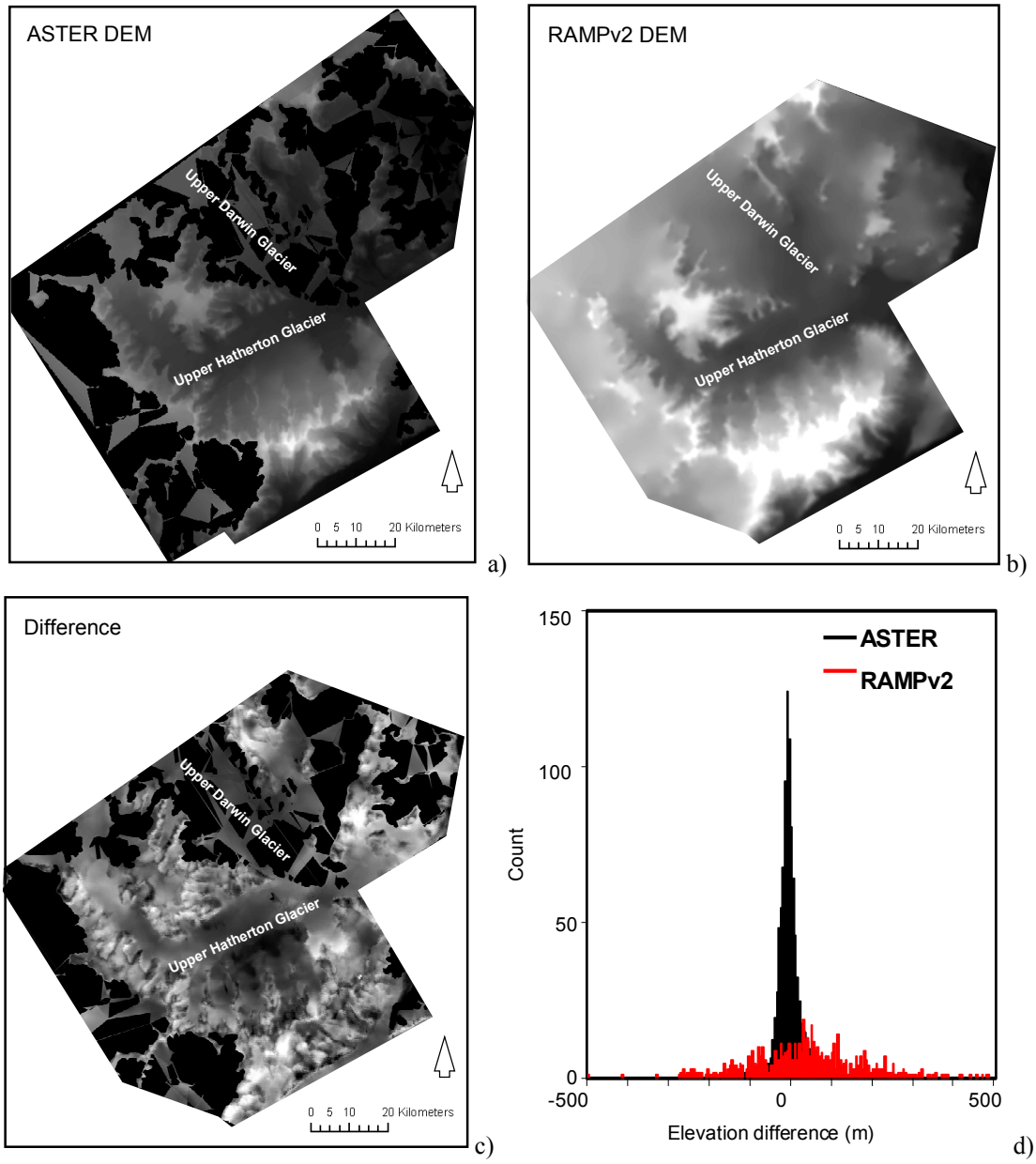

Figure 5.18: Comparison between the ASTER and RAMPv2 DEM in the upper Darwin and Hatherton Glaciers. a) ASTER DEM. b) RAMPv2 DEM, c) Difference between ASTER and RAMPv2 DEMs, d) Histogram of elevation difference from ICESat data for both ASTER (black) and RAMPv2 (red).

The difference between DEMs is shown in the difference images (Figure 5.17c and 5.18c). Dark areas indicate that the RAMPv2 DEM has higher elevations than the ASTER DEM and light areas indicate the RAMPv2 DEM has lower elevations than the ASTER DEM. Dark areas tend to be steep slopes and light areas tend to be flat elevated areas. The glacier surface is generally a mid grey colour indicating that the RAMPv2 and ASTER DEM values are similar in these areas relative to the rougher terrain.

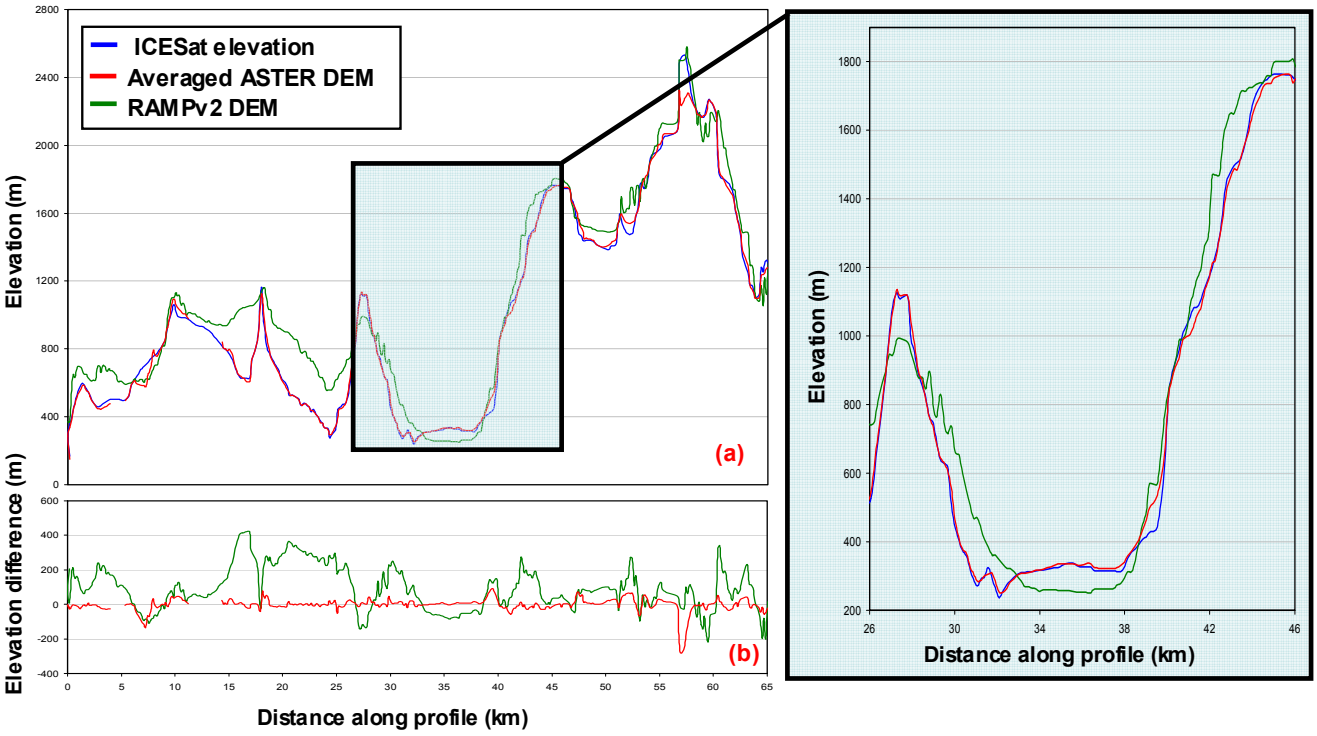

Figure 5.19: Lower Darwin Glacier profile a) Comparison between the averaged ASTER DEM, RAMPv2 DEM and the ICESat elevation data. b) Elevation difference from ICESat (assumed true elevation) for the averaged ASTER and RAMPv2 DEMs.

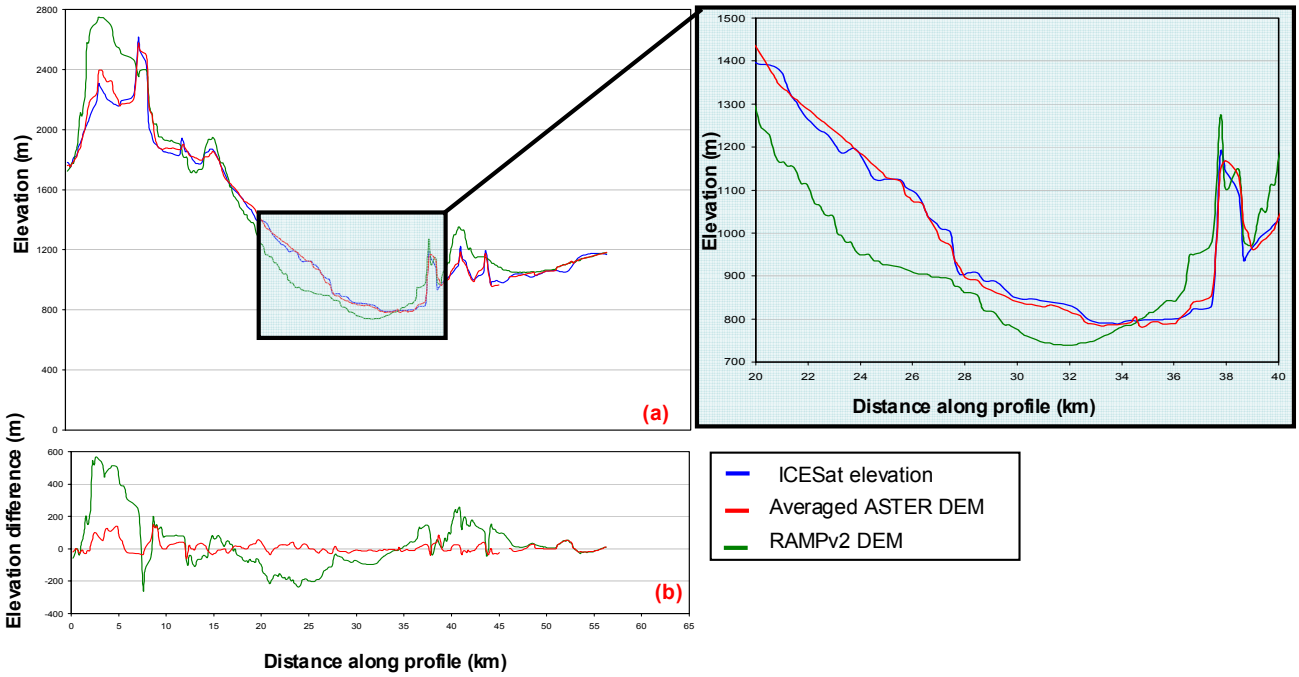

Figure 5.20: Upper Darwin and Hatherton Glacier profile a) Comparison between the averaged ASTER DEM, RAMPv2 DEM and the ICESat elevation data. b) Elevation difference from ICESat (assumed true elevation) for the averaged ASTER and RAMPv2

The increase in accuracy between the existing RAMPv2 DEM and the new ASTER DEM can best be visually seen in the profile graphs (Figure 5.19 and 5.20) with the ASTER DEM elevation data closely matching the ICESat elevation data and the RAMPv2 DEM elevation data loosely matching the ICESat elevation data (Figure 5.19a and 5.20a). The ASTER DEM elevation data correlates well with the ICESat data with R^2 values of 0.99 for both the lower Darwin Glacier and upper Darwin and Hatherton Glaciers DEMs. The RAMPv2 DEM elevation data does not correlate as well as the ASTER DEM and has R^2 values of 0.95 and 0.93. Figure 5.19b and 5.20b show the elevation difference which also immediately gives a visual indication of the increase in accuracy of the ASTER DEM over the RAMPv2 DEM.

The 45 m ASTER DEMs higher accuracy compared to the RAMPv2 DEM is quantified by the residual errors (Table 5.3). In the lower Darwin Glacier the total residual error decreases from ± 138 m for the RAMPv2 DEM to ± 9 m for the ASTER DEM (Table 5.3). The upper Darwin and Hatherton Glaciers the total residual error shows a decrease from ± 152 to ± 37 m (Table 5.3). Both of these decreases in residual error indicate major improvements in the accuracy. The histograms visually show the decrease in residual error between the RAMPv2 and ASTER DEM data.

Table 5.3: Residual error indicating accuracy for profile data of ASTER and RAMPv2 DEMs

	Residual error (m)	
	Lower Darwin Glacier	Upper Darwin and Hatherton Glaciers
ASTER total	± 9	± 37
ASTER profile	± 37	± 33
RAMPv2 total	± 138	± 152
RAMPv2 profile	± 126	± 151

The increase in resolution of the new DEMs, from 200 m in the RAMPv2 DEM to 45 m in the ASTER DEM is shown when comparing the ASTER and RAMPv2 DEMs (Figure 5.17a,b and 5.18a,b). The increase in resolution causes more topographic detail and sharper topographic detail to be observed in the ASTER DEM. While the existing 200 m resolution RAMPv2 DEM is useful for ice sheet scale applications, the new higher resolution 45 m ASTER DEM allows for more focused outlet glacier and ice stream scale applications.

5.3 DEM summary

5.3.1 ASTER DEM accuracy

The accuracy of the lower Darwin Glacier DEM can be quantified by a residual error of ± 9 m and the accuracy of the upper Darwin and Hatherton Glacier DEM can be quantified by a residual error of ± 37 m (Table 5.2). The error on the accuracy values can determined from the ICESat elevation error. The ICESat accuracy in Antarctica has a systematic error of 9.6 cm and a residual error of ± 4.9 cm standard deviation (Brenner et al., 2007). The upper Darwin and Hatherton Glacier DEM has a lower accuracy than the lower Darwin Glacier DEM. The stacking and averaging process successfully provided the most spatial coverage possible for both the lower Darwin Glacier and the upper Darwin and Hatherton Glaciers. The averaging process successfully reduces the residual error for the lower Darwin Glacier DEM, but increases the residual error slightly in the upper Darwin and Hatherton Glaciers DEM. The difference in accuracy can be attributed to; a) the quality and the overlap of the individual DEMs in the stacking and averaging process, b) the amount of error between the individual DEMs that is statistically correlated, and c) the accuracy and number of GCPs and tie points used in DEM generation which was outlined in section 4.1.3 and discussed further in section 5.3.2.

The accuracy of the new 45 m ASTER DEMs is compared to the existing 200 m RAMPv2 DEM. The new ASTER DEM improves the accuracy from a residual error of ± 138 m to a residual error of ± 9 m for the lower Darwin Glacier, and improves the accuracy from a residual error of ± 152 m to a residual error of ± 37 m for the upper Darwin and Hatherton Glacier (Table 5.3).

The accuracy of this ASTER DEM can be compared to the accuracy of a DEM created for an area of similar rough terrain in the Gruben area of the Swiss Alps, and a similar area of smoother terrain over the Gries Glacier (Section 2.1.1), which have residual errors of ± 78 m and ± 35 m respectively (Kaab, 2005). The lower Darwin Glacier DEM and the upper Darwin and Hatherton DEM have residual errors of ± 9 m and ± 37 m (Table 5.2, 5.3) which can be compared. The accuracy for both DEMs in the Darwin-Hatherton glacial system has higher accuracy than the Gruben area DEM and similar accuracies to the Gries Glacier. It is important to note that the two Swiss Alp DEMs have a resolution of 30 m (2 pixel) compared to a resolution of 45 m (3 pixel) for the Darwin-Hatherton glacial system DEMs. For the Gruben area DEM a 60 m (4 pixel) resolution DEM was also made and for elevation

differences less than 100 m (approximately 90 % of sample) the 30 m DEM had greater accuracy than the 60 m DEM (Kaab, 2005). From this we can infer that if more GCPs were available, a higher resolution ASTER DEM could be generated for the Darwin-Hatherton glacial system and the accuracy of the DEM would increase.

5.3.2 Limitations

The fundamental limitation of the ASTER DEMs is the accuracy and quantity of GCPs available (Figure 4.5). This causes error in the DEM, blank areas within the DEM with no data. Using the limited amount of GCPs, the software used limits the resolution of the DEMs to 45 m, which with more GCPs could be as high as 15 m resolution.

The quality of GCPs and tie points induces a residual error of $\pm$ 9 m for the lower Darwin Glacier DEM and $\pm$ 37 m for the upper Darwin and Hatherton Glacier DEM. The quality of the GCPs is determined by; the error associated with the acquisition of GCPs in the field, and the error associated with extraction and accurate location of GCPs onto the ASTER satellite image. The quantity of GCPs reduces the potential resolution of the DEM. Using 15 m ASTER imagery the highest DEM resolution that has been obtained in other research is 15 m (San and Suzen, 2005), however between 30 and 60 GCPs were used. By having a low number of GCPs, tie point generation is limited and this limitation causes the areas of the DEM that remain blank due to lack of sufficient data in these areas.

A minor limitation reducing the quality of the overall averaged DEM is the difference in illumination of the ASTER satellite images. Due to the small amount of satellite data available not all images could be obtained with similar illumination. Therefore the difference in illumination reduces the consistency between different ASTER images when locating GCPs onto the images.

5.4 An ASTER satellite map of the Darwin-Hatherton glacial system

A true colour, 15 m resolution orthorectified image is generated for each individual ASTER image using either the averaged lower Darwin Glacier DEM or the averaged upper Darwin and Hatherton Glacier DEM (Section 4.3.1). Before the individual images are mosaiced, the images are co-registered to fine tune and match the images (Section 4.3.2). The individual orthorectified images are mosaiced to produce a satellite map for the total area (Figure 5.21). After co-registration the remaining horizontal error is between 1 and 4 pixels (15 – 50 m) and can be used to give an overall accuracy of the mosaiced satellite image. It is important to note that the software used to orthorectify each individual ASTER DEM does not leave blank areas to correspond with the blank areas in the DEM. Therefore the areas that correspond to blank areas of the DEMs potentially have higher error than the rest of the image. No radiometric correction was applied to the mosaiced image (Figure 5.21).

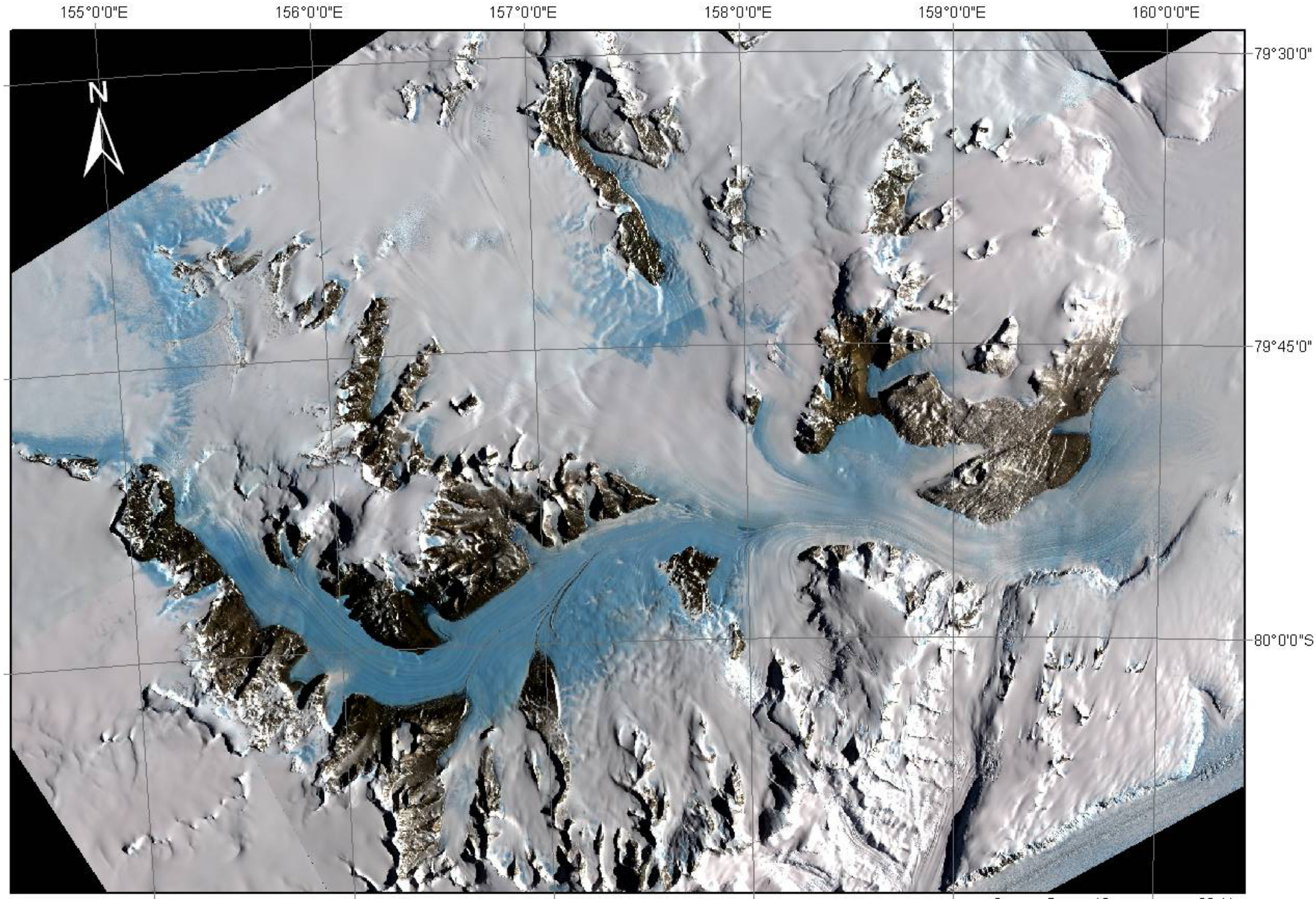

Figure 5.21: Orthorectified, true colour, 15 m ASTER satellite map of the Darwin-Hatherton glacial system, Transantarctic Mountains.

Chapter 6: Conclusion

6.1 Applications of thesis data.

Two new 45 m resolution ASTER DEMs for the Darwin-Hatherton glacial system provide surface elevation for the time period 2001 to 2005 with high accuracy compared to previous DEMs of the area. The lower Darwin Glacier DEM has a residual error $\pm$ 9 m and the upper Darwin and Hatherton Glaciers DEM has a residual error of $\pm$ 37 m. For mass balance and response time studies of the Darwin-Hatherton glacial system, this DEM data set can be used in conjunction with either; DEMs created from past aerial photographs or satellite images, and/or future DEMs created from satellite imagery to be acquired in the future. By gaining a better understanding of the Darwin-Hatherton glacial system, as well as other outlet glaciers along the Transantarctic Mountains, this data can be used in mass balance and response time modeling for the Ross Ice Shelf, the WAIS and the EAIS.

A true colour, 15 m resolution and accurately orthorectified ASTER image can be used to accurately plan field activities, use as a location map for field work, and provides a suitable map for geomorphic mapping in conjunction with field geomorphic mapping.

The limitations of the feature tracking on the Darwin-Hatherton glacial system provide essential information that can be used when assessing the suitability of feature tracking as a ice velocity measuring method for use on other glaciers, including both information about the suitability of the type, size and number of glacial features that are present, as well as information about the suitability of the satellite imagery including the image time separation, and image illumination limitations, especially with applications to polar regions.

6.2 Recommended future research

6.2.1 Recommendations for future research for DEMs

As described in section 5.3.2, the major limitation of the ASTER DEM for the Darwin-Hatherton glacial system is the availability of high quality GCPs in this area. The lack of quantity and quality GCPs causes errors in the DEM and causes the areas to remain blank due to lack of suitable data. To improve this, a ground survey is required with high precision GPS equipment to survey a large quantity of suitable GCPs. The main issue that remains despite a high precision ground survey is the issue of precisely locating the GCPs onto the ASTER satellite images. This issue could be reduced by using higher resolution satellite imagery which would allow finer features to be used as GCPs, increasing the precision in GCP location.

ICESat data has only been used to validate the accuracy of the ASTER DEM in this thesis. However the ICESat data may be able to be used as seed data when generating the DEM. Seed data is used after GCPs and tie points have been located and triangulation has been undertaken (Section 4.3.1), and is used to provide extra elevation information which improves the accuracy of the DEM (Schenk et al. 2005, Baek et al. 2005).

To improve coverage of the DEM and remove the blanks without regenerating the DEM and obtaining more GCPs, the blanks can be interpolated to create an elevation value for the area. This potentially will have errors larger than the non blank areas of the DEM, but depending on the application and the area that the blank area covers e.g. rough terrain versus smooth terrain, an interpolated surface may be sufficient. Another option to remove the blanks that would have greater accuracy than interpolation without obtaining more GCPs is by acquiring more satellite images from years other than 2001, 2002 and 2005. More satellite images would provide a larger data set to use for DEM averaging (Section 4.3.2) which would cause greater overlap and less blank areas. Currently the greatest number of DEM overlap and averaging in one area is five DEMs over the lower Darwin Glacier.

In future as more satellite data becomes available at lower resolution e.g. ALOS for the Darwin-Hatherton glacial system, DEMs can be made with higher resolution. Higher resolution satellite data has the potential to have less error due to more precise GCP location. Therefore a DEM with higher resolution will have more applications.

6.2.2 Recommendations for future measurements of ice velocity

It has been shown that currently suitable satellite imagery is not available for measuring ice velocity remotely in the Darwin-Hatherton glacial system area. Feature tracking is a useful technique used to establish ice velocity of glaciers. However it is important to apply feature tracking to glaciers with the correct resolution to enable suitable features to be identified. Ideal features for tracking would be features that retain their original pixel values over a long time period and are not prone to distortion, features that either create a point or lie perpendicular to the ice flow direction, and features that create a high contrast on the surrounding area. Therefore an ideal situation would require large stable boulders scattered supra-glacially which are approximately the size of the image resolution. The ice would need to displace a minimum distance of four times the image resolution in order to be greater than the pre-processing error, unless the pre-processing error can be reduced (for ASTER imagery the minimum ice displacement would be 60 m). However the larger the displacement the greater the overall ice velocity accuracy. Acquiring all images from the same or similar time of day would eliminate all potential for features to appear distorted due to differences in illumination.

In order to use feature tracking on the Darwin-Hatherton glacial system, higher resolution data are required to identify and track finer features. Now that a high resolution and high accuracy DEM exists for the Darwin-Hatherton glacial system area, a variety of satellite data can be orthorectified and used for feature tracking. Current satellite imagery that could be used includes the advanced land-observing satellite (ALOS) which was launched in January 2006. The VNIR sensor aboard the ALOS has a resolution of 10 m (www.eorc.jaxa.jp, 2007).

Other ice velocity measuring methods could be used if higher resolution satellite imagery still doesn't provide suitable features to be tracked. Firstly field based ice velocity surveys have been used successfully on many glaciers around the world including the Darwin-Hatherton glacial system (Hughes and Fastook, 1981). Field based surveys do not provide the spatial coverage that remote sensing can produce but are useful in validating remotely sensed ice velocity measurements. InSAR can be used in areas with few features. However a specific satellite image type is required and currently there is no data available for the Darwin-Hatherton glacial system.

6.3 Final conclusion

In conclusion, the results from this research successfully complete the aims. Aim 1 is to produce a new DEM for the Darwin-Hatherton Glacial system to provide improved resolution and accuracy from the existing DEM that covers the area and aim 2 is to validate the accuracy of the DEM to give an accurate indication of the total accuracy. Aim 3 is to produce a high resolution satellite image of the Darwin-Hatherton glacial system and aim 4 is to investigate remote sensing as a method to measure the surface ice velocity.

The final product for aim 1 is two new improved DEMs generated from ASTER satellite data, with a resolution of 45 m to cover the lower Darwin Glacier and the upper Darwin and Hatherton Glaciers. The resolution increases from 200 m to 45 m between the existing RAMPv2 DEM and the new ASTER DEMs. The accuracy is validated using independent ICESat laser altimetry elevation data and shows significant accuracy improvement between the existing RAMPv2 DEM and the new ASTER DEM. The improvement in accuracy is shown be a reduction in the remaining error from $\pm$ 138 m to $\pm$ 9 m in the lower Darwin Glacier and from $\pm$ 152 m to $\pm$ 37 m in the upper Darwin and Hatherton Glaciers. The process of adjusting the individual DEMs, followed by the stacking and averaging of the individual DEMs is successful in generating the two high accuracy final DEMs that cover the entire Darwin-Hatherton glacial system. The individual DEM adjustment prior to averaging successfully removed artificial steps in the surface elevation that would have otherwise been present in the final DEM. The averaging of the individual DEMs produced two DEMs with the minimum amount of blank areas. The stacking and averaging also increased the accuracy by reducing the residual error for the lower Darwin Glacier. The final product for aim 3 is a 15 m resolution, true colour, orthorectified ASTER satellite image of the Darwin-Hatherton glacial system. Feature tracking is determined to not be suitable as a method for measuring surface ice velocity on the Darwin-Hatherton glacial system using 15 m resolution imagery. This is due to the unsuitability of the features present at 15 m resolution including the feature crispness and the total displacement of the features over the 1 to 4 year time period.

The new higher resolution and accuracy DEMs, and the satellite image allow more accurate research to be undertaken at outlet glacier scale. This is particularly useful for glacial modeling research of the Darwin-Hatherton glacial system. Recommendations for the use of feature tracking can be used when assessing the suitability of glaciers for measuring ice flow.

Acknowledgements

Firstly I would like to thank my supervisors, Dr Wendy Lawson for giving me the opportunity to do this project and glaciology and thesis writing support and encouragement, and Dr Wolfgang Rack for remote sensing support and guidance. Without both, this project would not have happened. Secondly I would like to thank NZ Post and Antarctica New Zealand for awarding me an Antarctic postgraduate scholarship, which has helped me greatly financially and has introduced me to many interesting people at Antarctica New Zealand and Scott Base.

Thanks to everyone in the Geography department and Gateway Antarctica who has listened to my challenges and given their advice and encouragement, especially to Simon Allen, Joel Thomas, Ifron Jones, Amy Whitehead, Paul Bealing and John Tyne for their technical help. It has also been great to have the daily support of Canterbury University students and staff to bounce ideas around with. And lastly thanks to all my friends, family and teachers who have always encouraged and supported me throughout my life, school and university education. Thanks to Mum, Dad, Hamish and the rest of my family and friends for bringing me up to love the outdoors and mountains.

References

Anderson, B.M., R.C.A. Hindmarsh, W.J. Lawson. (2004). "A modelling study of the response of Hatherton Glacier to Ross Ice Sheet grounding line retreat." Global and Planetary Change 42(1-4): 143-153.

Baek, S., O. Kwoun, A. Braun, Z. Lu, C.K. Shum. (2005). "Digital Elevation Model of King Edward VII Peninsula, West Antarctica, From SAR Interferometry and ICESat Laser Altimetry." IEEE Geoscience and Remote Sensing Letters 2(4): 413-417.

Bamber, J.L., J.L. Gomez-dans. (2005). "The accuracy of digital elevation models of the Antarctic continent." Earth and Planetary Science Letters 237: 516-523.

Bamber, J.L., R.A. Bindschadler. (1997). "An improved elevation dataset for climate and ice-sheet modeling: validation with satellite imagery." Annals of Glaciology 25: 438-444.

Bamber, J.L., S. Ekholm, W.B. Krabill. (2001). "A new high-resolution digital elevation model of Greenland fully validated with airborne laser altimeter data." Journal of Geophysical Research 106(B4): 6733-6745.

Berthier, E., B. Raup, T. Scambos. (2003). "New velocity map and mass-balance estimate of Mertz Glacier, East Antarctica, derived from Landsat sequential imagery." Journal of Glaciology 49(167): 503-511.

Bernstein, R. (1983). Image geometry and rectification. in Colwell, R.N (ed.). "Manual of Remote Sensing." Americal Society of Photogrammetry. Falls Church V.A.: 881-884.

Bhang, K.J., F.W. Schwartz, A. Braun. (2007). "Verification of the Vertical Error in C-Band SRTM DEM using ICESat and Landsat-7, Otter Tail County, MN." IEEE Transactions on Geoscience and Remote Sensing 45(1): 36-44.

Bindschadler. R.A., T.A. Scambos. (1991). "Satellite-image-derived velocity field of an Antarctic ice stream". Science 52(5003): 252-245.

Bindschadler, R.A. (1998a). "Future of the West Antarctic ice sheet." Science 282(5388): 428-429.

Brenner, A.C., J.P. DiMarzio, H.J. Zwally. (2007). "Precision and accuracy of satellite radar and laser altimeter data over the continental ice sheets." IEEE Transactions on Geoscience and Remote Sensing 45(2): 321-331.

Bockheim, J. G., S. C. Wilson, G. H. Denton, B. G. Andersen, M. Stuiver. (1989). "Late Quaternary ice-surface fluctuations of Hatherton Glacier, Transantarctic Mountains." Quaternary Research 31(2): 229-254.

Bockheim, J.G., S.C. Wilson. (1979). "Pedology of the Darwin Glacier area." Antarctic Journal of the United States 14(5): 58-59.

Brecher, H.H. (1982). "Photogrammetric determination of surface velocities and elevations on Byrd Glacier". Antarctic Journal of the United States 17(5): 79-81.

Campbell, J.B. (1996). "Introduction to Remote Sensing, second edition". The Guilford Press. New York. USA

Conway, H., B.L. Hall, G.H. Denton, A.M. Gades, E.D. Waddington. (1999). "Past and future grounding-line retreat of the West Antarctic Ice Sheet." Science 286(5438): 280-283.

Csatho, B.Y., Y. Ahn, T. Yoon, C.J. van der Veen, G. Hamilton, D. Morse, B. Smith, V.B. Spikes. (2005). "ICESat measurements reveal complex pattern of elevation changes on Siple Coast ice streams, Antarctica." Geophysical Research Letters 32(L2S04).

Davis, C.H., Y. Li, J.R. McConnell, M.M. Frey, E. Hanna. (2005). "Snowfall-Driven Growth in East Antarctic Ice Sheet Mitigates Recent Sea-Level Rise." Science 308(5730): 1898-1902.

Denton, G.H. (1979). "Glacial history of the Byrd-Darwin Glacier area, Transantarctic Mountains". Antarctic Journal of the United States 14(5): 57-58.

Denton, G.H., T.J. Hughes. (2000). "Reconstruction of the Ross ice drainage system, Antarctica, at the last glacial maximum." Geografiska Annaler 82A: 143-166.

Elachi C., J. van ZYL. (2006). "Introduction to the Physics and Techniques of Remote Sensing, 2nd edition." Wiley. N.J. USA.

Fricker, H.A., A. Borsa, B. Minster, C. Carabajal, K. Quinn, B. Bills. (2005). "Assessment of ICESat performance at the salar de Uyuni, Bolivia." Geophysical Research Letters 32(LS1S06).

Hindmarsh, R.C.A. (1999). "On the numerical computation of temperature in an ice sheet". Journal of Glaciology 45(151): 568-574.

Hughes, T., J.L. Fastook. (1981). "Byrd Glacier: 1978-1979 field results." Antarctic Journal of the United States 16(5): 86-89.

IPCC. (2007) "Fourth assessment report of the IPCC." Geneva, Switzerland.

Kaab, A. (2001). "Photogrammetric reconstruction of glacier mass balance using a kinematic ice-flow model: a 20-year time series on Grubengletscher, Swiss Alps." Annals of Glaciology 31: 45-52.

Kaab. A. (2005). "Remote sensing of mountain glaciers and permafrost creep." Geographisches Institut der Universitat Zurich, Germany.

Lucchitta, B.K. H.M. Ferguson. (1986). "Antarctica: measuring glacier velocity from satellite images." Science 234(4780): 1105-1108.

Magruder, L., E. Silverberg, C. Webb, B. Schutz. (2005). "In situ timing and pointing verification of the ICESat altimeter using a ground-based system." Geophysical Research Letters 32(L21S04).

Martin, C.F., R.H. Thomas, W.B. Krabill, S.S. Manizade. (2005). "ICESat range and mounting bias estimation over precisely-surveyed terrain." Geophysical Research Letters 32(L2S07).

Massom, R., D. Lubin. (2006). "Polar Remote Sensing, Volume II: Ice Sheet". Praxis Publishing Ltd. Chester. UK.

Mayer, C., A. Lambrecht, M. Belo, C. Smiraglia, G. Diolaiuti. (2006) "Glaciological characteristics of the ablation zone of Baltoro Glacier, Karakoram, Pakistan." Annals of Glaciology 43: 123-131.

Nguyen, A.T., T.A. Herring. (2005). "Analysis of ICESat data using Kalman filter and kriging to study height changes in East Antarctica." Geophysical Research Letters 32(L23S04).

Rack, W., H. Rott, A. Siegel, P. Skvarca. (1999). "The motion field of northern Larsen Ice Shelf, Antarctic Peninsular derived form satellite imagery." Annals of Glaciology 29: 261-266.

Ramillien, G., A. Lombard, A. Cazenave, E.R. Ivins, M. Llubes, F. Remy, R. Biancale.(2006). "Interannual variations of the mass balance of the Antarctica and Greenland ice sheets from GRACE." Global Planetary Change 53(3): 198-208.

Rees, W.G. (2001). "Physical principles of remote sensing, second edition." Cambridge University Press. Cambridge. UK

Richards, J.A., X. Jia. (2006). "Remote Sensing Digital Image Analysis: An Introduction forth edition." Springer. Berlin.

Rignot, E., R.H. Thomas. (2002). "Mass balance of polar ice sheets." Science 297(5586): 1502-1506.

San, B.T., M.L. Suzen (2005). "Digital elevation model (DEM) generation and accuracy assessment from ASTER stereo data." International Journal of Remote Sensing 26(22): 5013-5027.

Schenk, T., B. Csatho, C.J. van der Veen, H. Brecher, Y. Ahn, T. Yoon. (2005). "Registering imagery to ICESat data for measuring elevation changes on Byrd Glacier, Antarctica." Geophysical Research Letters 32(L23S05).

Schutz, B.E., H.J. Zwally, C.A. Shuman, D. Hancock, J.P. Dimarzio. (2005). "Overview of the ICESat Mission." Geophysical Research Letters 32(L21S01).

Shepherd, A., D. Wingham. (2007). "Recent Sea-Level Contributions of the Antarctic and Greenland Ice Sheets." Science 315: 1529-1532.

Stearns, L.A., G.S. Hamilton (2005). "A new velocity map for Byrd Glacier, East Antarctica, from sequential ASTER satellite imagery." Annals of Glaciology 41: 71-76.

Stearns. L.A., G.S. Hamilton, N. Reeh. (2005). "Multi-decadal record f ice dynamics on Daugaard Jensen Gletscher, East Greenland, from satellite imagery and terrestrial measurements." Annals of Glaciology 42: 53-58.

Toutin, T. (2001). "Elevation modeling from satellite visible and infrared (VIR) data." International Journal of Remote Sensing 22(6): 1097-1125.

Toutin, T., P Cheng. (2001). "DEM generation with ASTER stereo data." Earth Observation Magazine 10(6): 10-13.

Toutin, T., P Cheng. (2002). "Comparison of automated digital elevation model extraction results using along-track ASTER and across-track SPOT stereo images." Optical Engineering 41(9): 2102-2106.

USGS. (1963). "Antarctica 1:250,000 Reconnaissance Series Map, ST 57-60/13*." USGS, USA

Wingham, J.D., A. Ridout, R. Scharroo, R. Arthern, C.K. Shum. (1998). "Antarctic elevation change from 1992 to 1996." Science 282(5388): 456-458.

Whillams, I.M., R.A. Bindschadler. (1988). "Mass balance of Ice Stream B." Annals of Glaciology 11: 187 – 193.

www.nsidc.org (10/06/2007). National Snow and Ice Data Center, Boulder University Colorado, USA

www.LPDAAC.usgs.gov (3/03/2007). NASA Land Processes Distributed Active Archive Centre, USA

www.eorc.jaxa.jp (14/11/2007). JAXA Earth Observation Research Centre, Japan

Zwally, H.J., M.B. Giovinetto, J. Li, H.G. Cornejo, M.A. Beckley, A.C. Brenner, J.L. Saba, D. Yi. (2006). "Mass changes of the Greenland and Antarctic ice sheets and shelves and contributions to sea-level rise: 1992-2002." Journal of Glaciology 51(175): 509-527.

Appendices

Appendix 1: Individual Orthorectified ASTER images

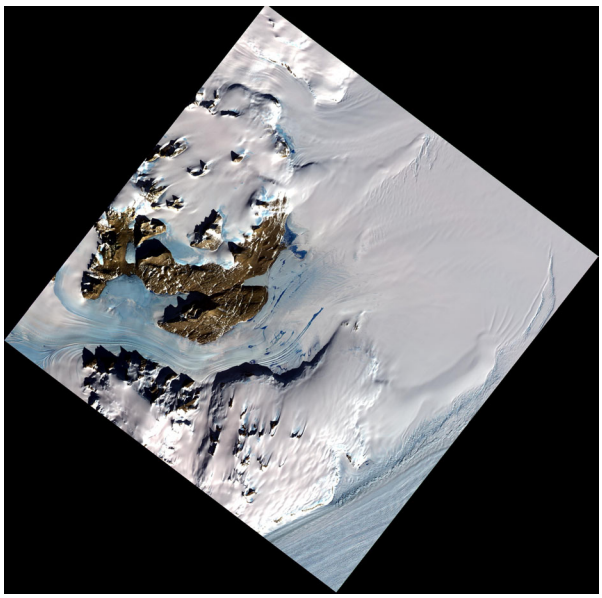

01LD: Orthorectified image of Lower Darwin, 2001

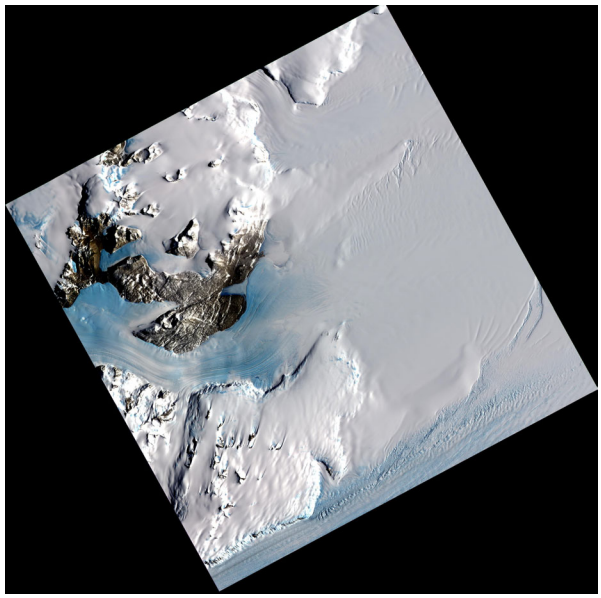

02LDa: Orthorectified image of Lower Darwin, 2002

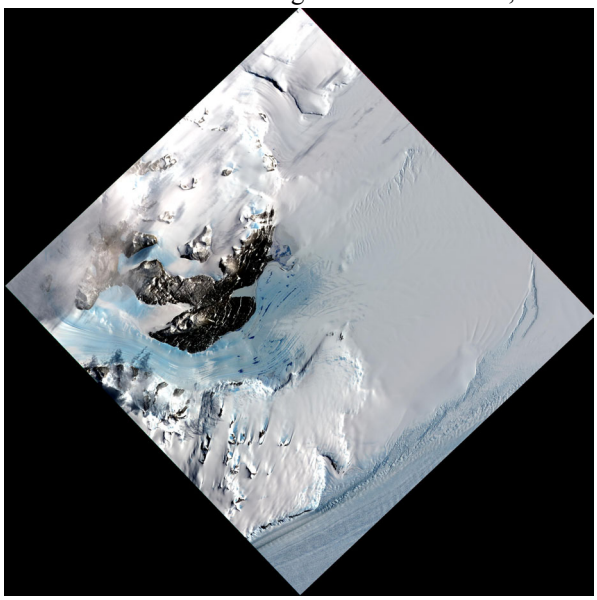

02LDb: Orthorectified image of Lower Darwin, 2002

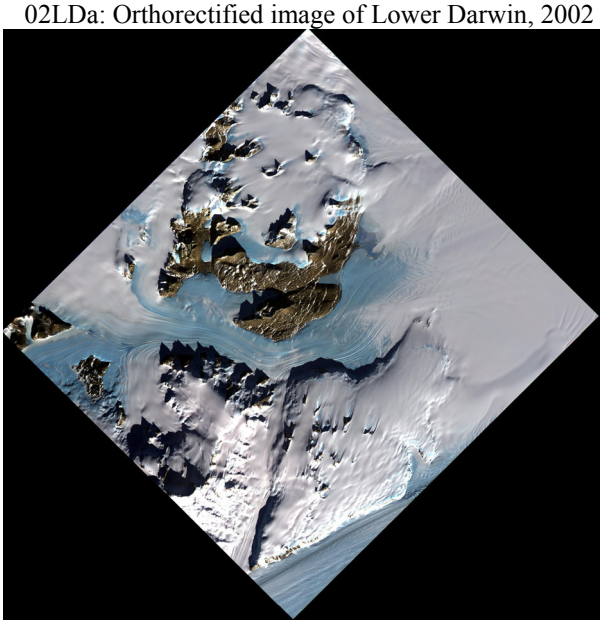

05LDa: Orthorectified image of Lower Darwin, 2005

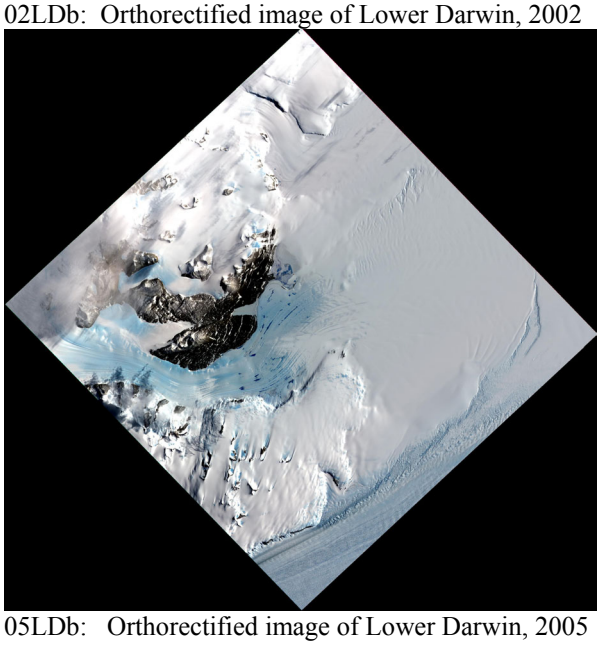

05LDb: Orthorectified image of Lower Darwin, 2005

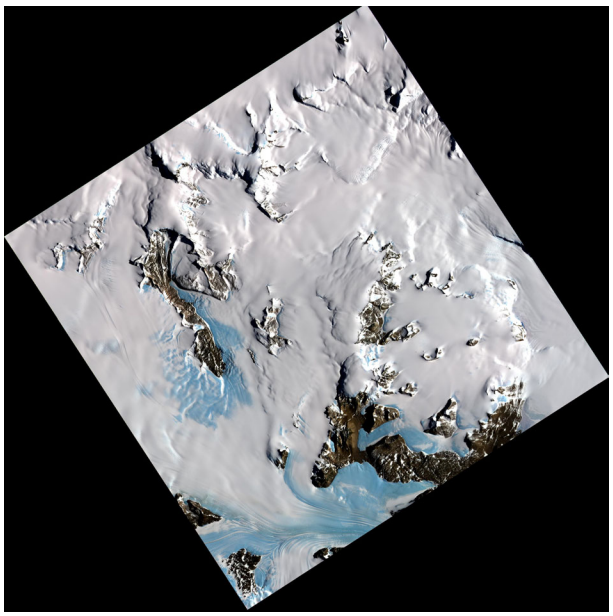

01UD: Orthorectified image of Upper Darwin, 2001

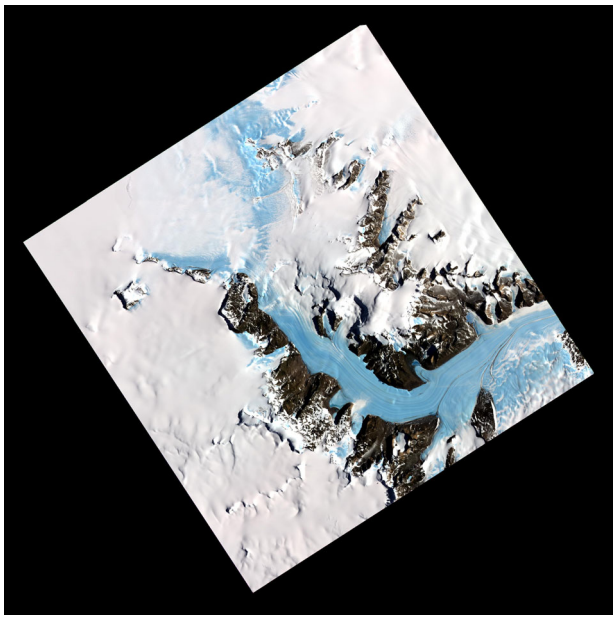

01UH: Orthorectified image of Upper Hatherton, 2001

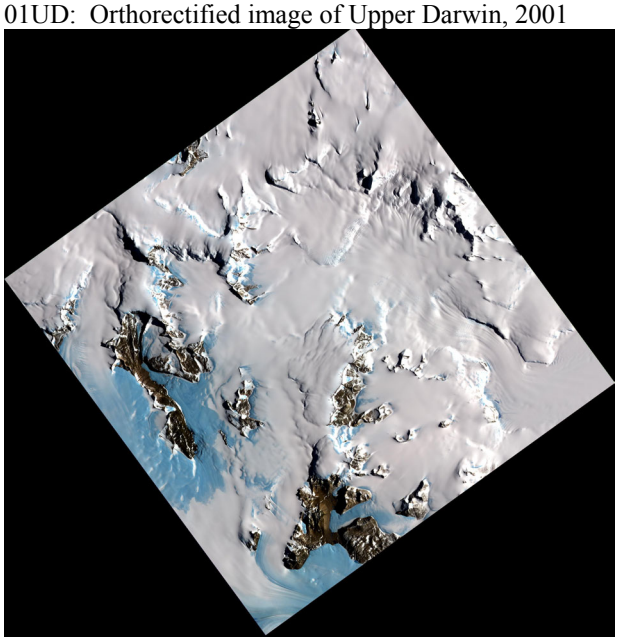

02UD: Orthorectified image of Upper Hatherton, 2002

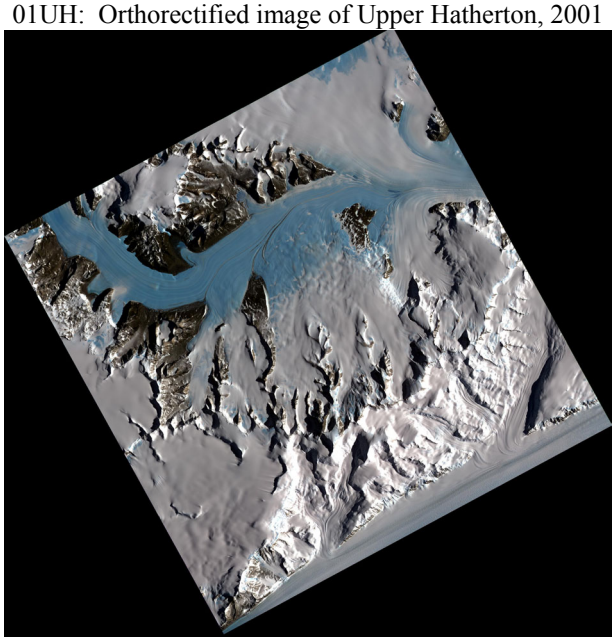

02UHa: Orthorectified image of Upper Hatherton, 2002

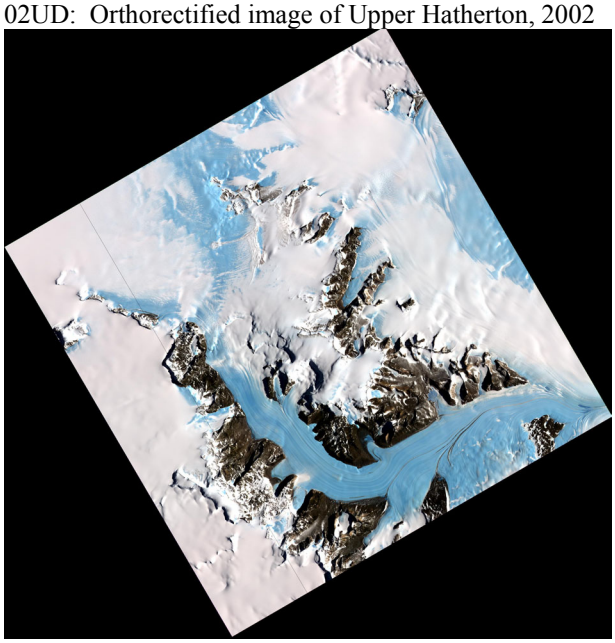

02UHb: Orthorectified image of Upper Hatherton, 2002

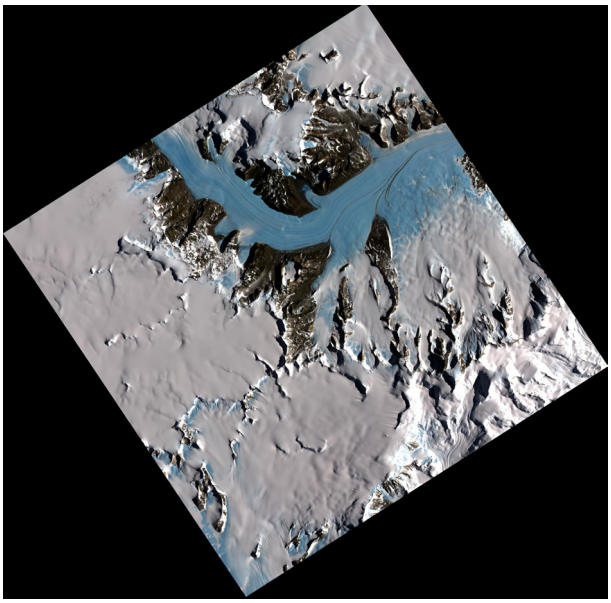

02UHc: Orthorectified image of Upper Hatherton, 2002

Appendix 2: DEM generation information

(c) Table of DEM generation properties and accuracy

	Mass Point Elevation			Mass Point Quality			
Image	**Min**	**Max**	**Mean**	**Excellent % (1-0.85)**	**Good % (0.85-0.7)**	**Suspicious %**	**Total Ref points used**
01LD	-198.4	2034.3	479.9	77.7	14.6	7.7	292
02LDa	-33.7	1960.8	362.2	81.7	11.4	6.9	356
02LDb	-39.3	2934.3	771.2	86.9	8.4	4.6	487
05LDa	-143.3	2380.7	653.4	77.1	13.0	9.8	281
05LDb	-152.0	1882.2	233.9	74.4	14.1	11.5	342
01UD	1.9	2547.6	997.2	89.2	6.5	4.3	560
01UH	766.9	2487.3	1472.4	88.7	6.0	5.3	619
02UD	-30.9	2788.5	1175.3	88.6	7.0	4.4	541
02UHa	26.6	3474.0	1354.2	80.8	13.7	5.5	784
02UHb	620.3	2457.2	1469.7	88.9	6.0	5.1	972
02UHc	327.9	3440.0	1566.0	87.2	8.3	4.5	471